THE SOLAR WIND KELVIN-HELMHOLTZ INSTABILITY OF THE MAGNETOPAUSE AND THE SEMIANNUAL VARIATION OF GEOMAGNETIC ACTIVITY

by

BRUCE R. BOLLER

A dissertation submitted to the Graduate Faculty in Physics in partial fulfillment of the requirements for the degree of Doctor of Philosophy, The City University of New York.

1970

This manuscript has been read and accepted for the Graduate Faculty in Physics in satisfaction of the dissertation requirement for the degree of Doctor of Philosophy.

May 12, 1970
date

Harold L. Stolov,
Chairman of Examining Committee

May 13, 1970
date

Harry Lustig, Executive Officer

Leon Cohen

David Shelupsky

Jerome Spar

Richard Stothers
Supervisory Committee

The City University of New York

ACKNOWLEDGEMENTS

The author wishes to express his gratitude to Harold L. Stolov for his guidance, patience, and, most of all, his friendship.

The unrewarding task of the typing of this thesis was courageously accepted by my wife, Sue, to whom I am indebted for a magnificent job. Her love and encouragement have been essential throughout the course of this work. Special thanks go to my son, John, for being good when his daddy had to work.

I wish to thank Drs. D. H. Fairfield and K. W. Ogilvie for their kind assistance in making available the magnetic field and plasma data from Explorer 34.

This research was supported in part by the National Aeronautics and Space Administration under contract NsG 197-62. I also wish to thank Dr. Robert Jastrow for his hospitality at the Institute for Space Studies.

I wish to dedicate this work to the memory of my father.

TABLE OF CONTENTS

LIST OF FIGURES

LIST OF TABLES

CHAPTER 1

INTRODUCTION

The magnetic field at the surface of the earth had been used for centuries as a means of navigating by its directional influence on small, supported magnets. In 1600 Sir William Gilbert in De Magnete attributed the earth's magnetic field to sources within the earth as a result of his experiments with small magnetized spheres of lodestone. Over 200 years later K. F. Gauss, in 1835, proved mathematically that the surface field was almost entirely due to sources below the surface. As early as 1635, however, Gellibrand discovered that the field was slowly changing. In addition to this secular change of the field certain regular and irregular changes, called transient variations of the direction of the field, on much smaller time scales were discovered and announced in 1722 by Graham. The regular ones occurred on a daily basis while the irregular ones possessed larger fluctuations which were superimposed on the regular changes. Celsius in Sweden and Graham in England, by comparing notes by letter, found in 1741 that the irregular variation or magnetic disturbance was often simultaneous in the two places, thus establishing the existence of the world wide phenomenon of the magnetic storm. In 1843 Schwabe made known the existence of the sunspot cycle and in 1852 Sabine announced that the same cycle was evident in the transient magnetic variations. The advent of the field of solar-terrestrial relationships was at hand. In 1882 Balfour Stewart presented

his arguments for the existence of electric currents flowing in the upper atmosphere producing the observed fluctuations. He attributed the currents to a dynamo type of mechanism in which the air of the upper atmosphere became ionized due to the influence of the sun's radiation. The presence of winds in this region would carry the ionized gases across the magnetic field lines thereby producing the electric currents (Chapman, 1964).

Another curious and more obvious phenomenon was soon shown to be intimately connected with solar-terrestrial relations, namely, the aurora. In 1770, Wilcke at Stockholm discovered that the auroral rays lie along the earth's magnetic field lines. A century later, in 1869, Elias Loomis published a paper showing the positions and heights of two of the greatest aurorae ever seen over North America. From data of stations around the earth he was able to draw the first auroral zone which had an oval form centered approximately about the geomagnetic pole and lying along lines of equal magnetic dip. In 1881 Goldstein offered the explanation that electric currents from the sun were responsible for much of the observed electric and magnetic phenomena on the earth (Chapman, 1964). Later on, in 1896, Birkeland was able to show by his famous cathode ray "terella" experiments that the aurora could be produced by electric rays from the sun impinging upon the earth's dipole field to form the auroral zones (Stormer, 1955). The trajectories of energetic particles impinging upon the earth's dipole field were mathematically calculated by Carl Stormer (1955). The intersection of these trajectories with the surface of the earth exactly coincided with the zones found experimentally by

Birkeland.

The main subject of this thesis had its beginning as early as 1912 when Cortie (1912) sought an explanation for the semiannual variation of geomagnetic activity with his "axial" hypothesis. In his paper, he proposed that the cause of the semiannual variation, whose maxima were around September and March, was due to the proximity of the earth's heliographic latitude to the average latitude of the centers of solar activity. Later, Bartels (1932) offered his "equinoctial" hypothesis as an explanation for the semiannual variation. McIntosh (1959) published evidence linking the orientation of the earth's dipole to the semiannual variation, thereby supporting the equinoctial hypothesis. Since then, several attempts have been made to support one or the other of these hypotheses (Priester and Cattaneo, 1962; Bartels, 1963; Currie, 1966; Meyer, 1966; Roosen, 1966; Shapiro, 1969).

In the following, a brief review of solar-terrestrial relationships is given. Geomagnetic activity and the index used to describe it will be briefly outlined. The characteristics of the solar wind and the magnetosphere will be mentioned. A mathematical model of the boundary between the interplanetary medium and the medium in the immediate vicinity of the earth will be developed with the ultimate intention of identifying the physical mechanism causing the semiannual variation of geomagnetic activity. Data from some geomagnetic stations will be used to demonstrate how the diurnal variation of geomagnetic activity supports the physical mechanism proposed. Illustrative quantitative estimates of the instability criterion developed will be made using satellite data.

CHAPTER 2

SOLAR-TERRESTRIAL RELATIONSHIPS

2.1 Introduction

This chapter is principally concerned with the disturbed conditions of the earth's magnetic field and some of the indices used to describe them. One set of indices will be used later in the data analysis. Disturbed conditions on the sun and their influence upon the earth will be surveyed before the main topic. No specific type of "solar-terrestrial" event is really sufficient to identify a certain effect on the earth with a disturbance occurring on the sun. It is felt, however, that the totality of events coupled with new and improved methods of observation and instrumentation will someday help to improve our understanding of the earth's environment in the interplanetary medium. The very large extent of disturbances and the large number of parameters involved make it difficult to identify an event with a specific cause.

2.2 Flares, M-Regions, and Other Disturbances

The phenomena occurring on the sun provide the solar system with spatial and temporal variations of electromagnetic radiation and corpuscular flux. The source of some of these variations has been traced to the solar flare. Some of the more intense flares release 10^{33} ergs within the first several minutes of their existence (Ellison, 1962). The sudden ionospheric disturbance (SID) is an enhancement of the electron density in the lower layers of the ionosphere during the daylight hours and is a direct consequence of the ionizing X-rays of the larger flares. The SID is detected

by the reflection and absorption effects the increased ionization has on certain radio waves (Collins and Herzberg, 1965). The SID is usually accompanied by the solar flare effect (SFE) which is a geomagnetic disturbance (called a "crochet") whose amplitude is about 25×10^{-5} gauss in the horizontal direction at the earth's surface and is believed to be due to flare-produced currents in the E and D regions of the ionosphere (Volland and Taubenheim, 1958).

In some cases the particle emissions from solar flares begin making their presence known within several hours of the peak of the solar flare in the form of polar cap absorption (PCA). The PCA is detected as increased absorption of extra-terrestrial radio sources by riometers due to the ionizing influence of energetic protons on the constituents of the lower ionosphere in the polar regions. The lack of geomagnetic disturbance during the early stages of PCA events indicates a low density of these energetic protons (Reid, 1965).

Approximately two days after the occurrence of some flares a high density, low energy plasma cloud intercepts the earth producing a geomagnetic storm (Hartz, 1965), to be described in more detail in the next section. It is hard to find a one to one correspondence between a solar flare and a geomagnetic storm since there are many more flares than storms (Paghis, 1965). The storms produced by flares can be termed "isolated" as opposed to the 27-day "recurring" geomagnetic storms produced by the M-regions hypothesized by Bartels (1932). These "magnetically" active regions were assumed by Bartels to be emitters of long lived solar corpuscular radiation lasting for periods of several solar rotations. At times

these recurrent storms could be associated with centers of activity on the sun (Mustel, 1961), but at other times, they could not be associated with any identifiable features. Babcock and Babcock (1955) have suggested that the M-regions of Bartels may actually be the unipolar magnetic (UM) regions which they have observed. These regions have magnetic fields $\lesssim$ 3 gauss and last for periods of several months.

The streams from the M-regions and the plasma clouds from the flares are imbedded in the ever present solar wind which is discussed in the next chapter. The continual presence of solar corpuscles interacting with the earth's magnetic field gives rise to a host of other phenomena such as ionospheric noise, geomagnetic micropulsations (Barrington and Fejer, 1965), aurora (Stormer, 1955; Montalbetti, 1965; Blevis and Collins, 1965; Hultqvist, 1969), and as will be seen, the semiannual variation of geomagnetic activity.

2.3 Geomagnetic Storms and Indices

Geomagnetic disturbance is measured and recorded by magnetometers at magnetic stations located at the surface of the earth. A local index K is assigned to each 3-hour interval of universal time corresponding to the component of magnetic field with the largest deviation at each station. These components are commonly the downward vertical component Z, the northward (geographic) component X, and the eastward component Y. Other magnetic elements include: F, the total magnetic field intensity; H, the horizontal component of magnetic field intensity; I, the angle below the horizontal of the direction of the magnetic field intensity F; δ(declination), the angle between H and geographic north. An appropriate set

of three of the following elements will be enough to specify $\vec{F}$:

F, H, X, Y, Z, I, δ.

If H, Z, and δ are the elements used at a station, then the components of the deviations would be in the H and Z directions and in the direction perpendicular to these two.

The disturbance field of a geomagnetic storm is called D and when it is used to represent a particular element of the magnetic field, say H for example, then it is denoted as D(H). This disturbance field depends upon θ, the colatitude; T, the storm time; and ϕ, the local time in angle measured east of the midnight meridian. Magnetic storms have irregularities associated with them so that there are no two alike, but there are some general similarities. The D field of a magnetic storm is separated into two parts, one that is azimuthally symmetric about the earth's spin axis and represents the mean value of D around a parallel of colatitude θ, and the other which represents the deviations of the disturbance field from its mean value and consequently has zero mean value around any particular colatitude. This division of D can be expressed in the following form for the element H:

$$D(H) = D_{st}(H; T, \theta) + DS(H; T, \theta, \phi).$$

The form of D_{st} as a function of T is shown in Figure (2.1), along with the four general phases of a magnetic storm.

Magnetic storms begin as sudden commencements (SC) or gradual commencements (GC), the main distinction being that the disturbed component in a SC has a rise time of less than 10 minutes. The

Figure 2.1

The form of D_{st} as a function of storm time showing the four general phases.

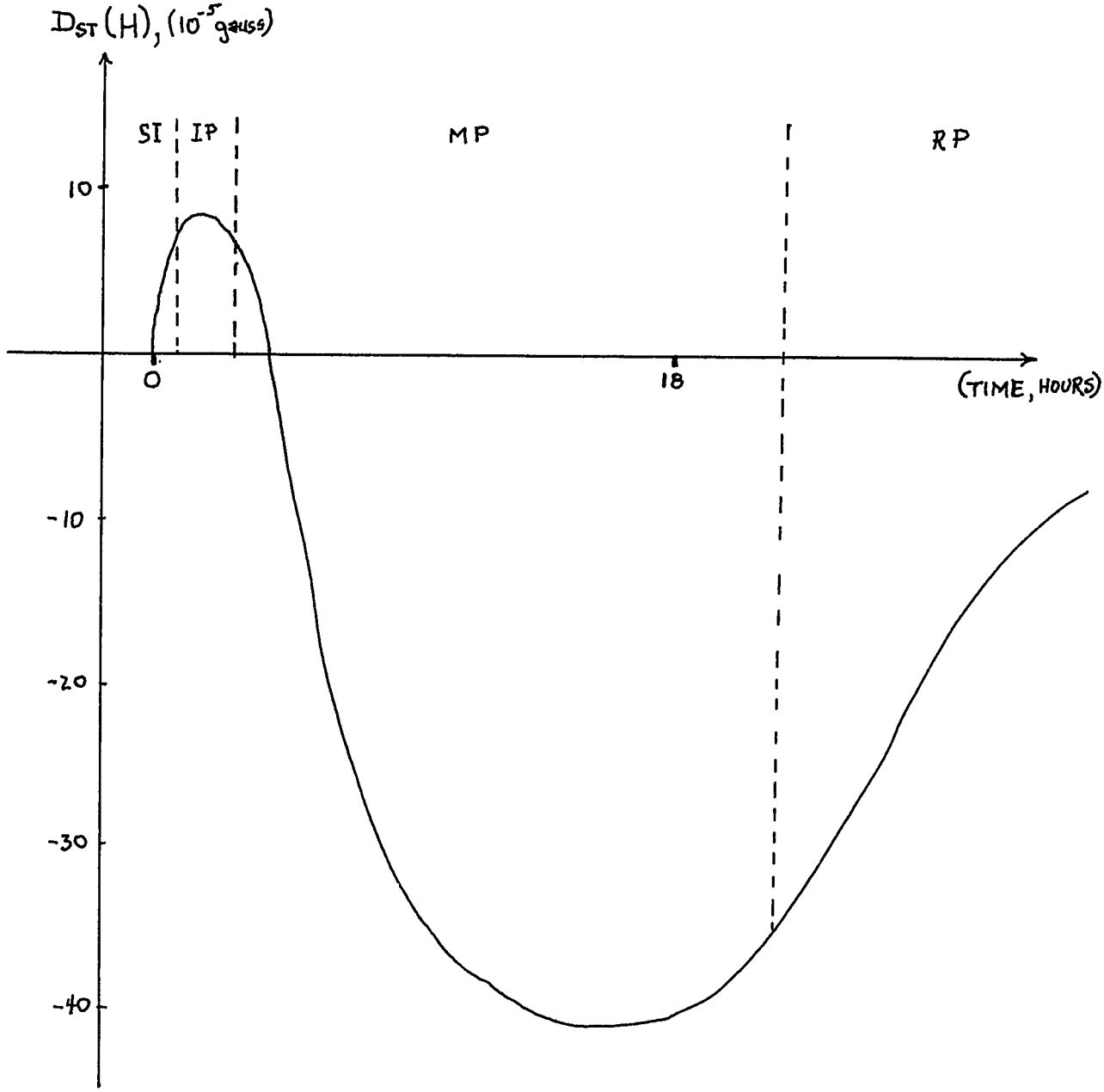
D_{ST} (H), (10^{-5} gauss)
SI
IP
MP
RP
10
-10
-20
-30
-40
0
18
(TIME, HOURS)

initial phase (IP) is characterized by an increase in the horizontal component of magnetic field having smaller amplitudes in the higher latitudes. This phase, however, is not clearly visible in the auroral and polar regions. The main phase (MP) consists of a depression of the horizontal component of the magnetic field and has larger amplitudes in the auroral zones. The recovery phase (RP) indicates that portion of the storm showing a gradual return to pre-storm conditions. For a [illegible] review of geomagnetic disturbances and storms see Matsushita (1967) and Akasofu and Chapman (1967).

The purpose of the K index is to measure the intensity of solar particle radiations by their effects on the geomagnetic field at the surface of the earth. Any other mechanisms disturbing the geomagnetic field are considered to be non-K variations and their effects are subtracted from the total deviation of the magnetic element in question leaving the range r. The non-K variations include the solar daily variation S_q, the lunar daily variation L, the solar flare effect, the post-perturbation effect, and the secular variation (Bartels et al., 1939; Bartels, 1957).

If the range r is in the unit γ, where $1\gamma = 10^{-5}$ gauss, then the following table indicates the lower limit of r corresponding to the index K for Maquarie Island at $60^{\circ}.7$ south geomagnetic latitude.

K =	0	1	2	3	4	5	6	7	8	9
r =	0	15	30	60	120	210	360	600	1000	1500

As an example, suppose that the range r for this station were equal to or greater than 30γ but less than 60γ for a particular 3-hour period, then the K-index would be 2.

Each station has a separate range set up according to the degree of disturbance it is most likely to experience. Stations at high latitudes have larger lower limits of r corresponding to K = 9 than stations at low latitudes. Since only the K indices are published and are readily available it is desirable to have a scaling set up in such a way that the given K indices can be converted into equivalent amplitudes for averaging purposes. The lower (K=9) limit of r for each station is published along with the K indices. An equivalent range called a_k is a standard scale which expresses approximately the center of the limiting ranges for a given K in the unit γ when multiplied by a certain factor which depends upon the station. This factor is obtained by dividing the lower limit of r for K = 9 for a station by 250. The relation between a_k and the K index is given below and is good for any station (Bartels, 1957).

K =	0	1	2	3	4	5	6	7	8	9
a_k =	0	3	7	15	27	48	80	140	240	400

As an illustration of this point, suppose the K index for Maquarie Island during a certain 3-hour interval is 2. The lower limit of the range r for K = 9 for this station is 1500. Dividing 1500 by 250 gives 6 for this station and means that the equivalent range a_k for Maquarie Island is expressed in the unit 6γ. Therefore K = 2 means an a_k of 7 units and an actual range of 42γ, which is approximately in the center of the limiting ranges for the K value at this station. The K indices from the participating observatories can be obtained from the International Union of Geodesy and Geophysics

IAGA Bulletin No. 12 series published annually (Price et al., 1966).

Each observatory assigns a K index to every one of the 3-hour intervals of universal time beginning with 0000 UT. The equivalent range a_k would be enough to know should the effect of the disturbance sought for be approximately proportional to a fixed percentage of the total range of a station. When an average over a number of stations is taken the effect would not be lessened to any degree as it would if the ranges r were used and some of the stations had smaller lower limits for K = 9. The original assumption, however, may not be correct and the range r may be more significant in an analysis of stations in a narrow range of geomagnetic latitude. The choice of r or a_k may therefore depend on the particular effect sought.

The planetary K_p index designed by Bartels (1949) is derived from the K indices of 12 stations at moderate geomagnetic latitudes. The K indices are first standardized for each station in such a way that the local time variation is removed. They are then averaged together to form K_p which is expressed in 28 grades from 0o, 0+, 1-, 1o, 1+,... to 9-, 9o. A K_p index is assigned to each 3-hour interval of universal time beginning at 0000 UT. It turns out that universal time variations are nearly absent from K_p (Michel, 1964).

Good reviews of the contents in this chapter and this section in particular may be found in Chapman and Bartels (1940), Hines et al. (1965), Chapman (1964), and Matsushita and Campbell (1967).

CHAPTER 3

THE SOLAR WIND

3.1 Early Predictions

Before the nature of the interplanetary medium was known, FitzGerald and Lodge at the turn of the century suggested that geomagnetic storms and the aurorae were respectively caused by clouds of charged atoms or ions and cathode ray constituents. In addition, they proposed that comet tails can be better explained by particle radiation emanating from the sun than solar electromagnetic radiation. They also believed that the earth had a minute tail directed away from the sun like that of a comet (Dessler, 1967). Later on, Chapman and Ferraro (1931, 1933) worked on the problem of an ionized neutral cloud of hydrogen gas emitted from the sun and intercepting the earth's magnetic field in an effort to explain the early stages of geomagnetic storms. They showed the first picture of the magnetic cavity formed by the earth's dipole imbedded within the cloud of gas flowing past the earth. The cavity was later to be called the magnetosphere.

By this time the idea of corpuscular streams flowing past the earth causing geomagnetic activity was firmly established among geomagneticians (Dessler, 1967). Bartels (1949) believed that the solar corpuscular radiation was nearly a continuous phenomenon because of the continual disturbance expressed by K_p. Further evidence for a continuous solar corpuscular radiation could be found in the continual occurrence of the aurora. In the meantime, exact calculations by Wurm (1943) showed that comet tails could

not be explained by photon pressure alone. Then, Biermann in a series of papers (1951, 1953, 1957) explained that the observed acceleration of gaseous comet tails was due to a continually expanding solar corpuscular radiation.

With the amount of evidence for a continual solar corpuscular radiation outlined above, Parker (1958a) gave this concept a theoretical foundation by his famous hydrodynamic expansion theory of the solar corona. He showed that a constant efflux of material from the solar corona was the natural consequence of the heating of the inner corona by shock waves from the photospheric surface. The predicted speeds were of the order of several hundred kilometers per second. In another paper that same year, Parker (1958b) had termed the continuous flow of gases from the sun the "solar wind."

The validity of using hydrodynamics for the solar corona was questioned at the time and a controversy arose between Parker on the one hand and Chamberlain on the other. Chamberlain (1960) questioned Parker's idea and proposed that the expansion of the solar corona was due to an evaporative model. This model assumed a type of coronal exosphere above some critical distance from the sun where the particles in this region moved on ballistic trajectories. As with the exosphere of the earth only a small number of particles in the high energy tail of the Maxwellian distribution can escape. The evaporative model did not lead to supersonic particle velocities as did Parker's hydrodynamic model. The hydrodynamic approximation assumes collisions which tend to move the corona as a whole while the solar gravity allows sonic velocity to be reached at some

specified distance from the sun. Beyond this distance the gases expand supersonically. (Dessler, 1967).

3.2 Experimental Confirmation

The first direct measurements of the solar corpuscular flux were reported in 1960 by Gringauz et al. (1960) using data from Lunik 2. The protons they detected had energies greater than 15 ev. or velocities greater than 54 km./sec. Gringauz (1961), using data from Lunik 3, estimated the velocity of the proton flux to be around 300 km./sec. while Gringauz et al. (1963), using data from a Venus probe, inferred a velocity of 400 km./sec. The flight of Explorer 10 enabled Bonetti et al. (1963) to estimate the velocity of the positive ions from the sun to be 280 ± 20 km./sec. They found that the solar flux formed a reasonably well collimated beam and that the thermal velocities of the ions were substantially smaller than the bulk velocity of the plasma. The data from these experiments, however, were only short term and it was at the end of 1962, when the first Mariner 2 results were reported by Neugebauer and Snyder (1962), that the solar wind theory of Parker was generally accepted. They reported that there was always a measurable flow of plasma from the sun and that the bulk velocities obtained from two spectra which they analyzed were 460 km./sec. and 810 km./sec. with respective particle densities of $2.5/cm^3$ and $4.5/cm^3$. Mariner 2 also carried a magnetic field experiment whose results were reported by Coleman et. al. (1962). They found that the magnitude of the interplanetary magnetic field stayed basically within the limits of 2 and 10γ (where $1\gamma = 10^{-5}$ gauss). The direction of the magnetic field was generally confined to the ecliptic plane along the predicted

Archimedes spiral angle (Coleman et al., 1960) with a fluctuating transverse component. The Archimedes spiral angle was first predicted by Chapman (1929) for the locus of particles in interplanetary space emitted radially from a source on the rotating sun. If these particles carry a "frozen-in" magnetic field with them then these magnetic field lines will be in the spiral direction.

3.3 Characteristics

More complete analyses of the Mariner 2 plasma data by Snyder et al. (1963) showed that the bulk velocity of the solar wind generally ranged between the limits of 350 km./sec. and 700 km./sec. They reported a good correlation between the velocity of the solar wind and the 24-hour sum of the K_p index. The relationship appeared to be linear and was best described by the following equation:

$$V_s(\text{km./sec.}) = (8.44 \pm 0.74)\sum K_p + (330 \pm 17) \quad . \qquad (3.1)$$

Extremely accurate interplanetary magnetic field measurements were reported by Ness et al. (1964) from the initial results obtained by IMP-1. They found the interplanetary field strengths to lie generally within the range of from 4 to 7γ, with values at times as low as 1 and as high as 10γ. The magnitudes were more steady than the direction which changed on time scales of several hours. Their results also confirmed the gross spiral structure of the interplanetary magnetic field associated with the rotation of the sun.

Wolfe et al. (1966a) reported, among other things, the compositional characteristics of the solar wind from Pioneer 6

data. They found the solar wind to be composed of 91.3% ionized hydrogen, 8.6% doubly ionixed helium, and 0.1% singly ionized helium. They noted a strong anisotropy in temperature where the highest temperature was found to be in the spiral direction of the interplanetary magnetic field lines. Defining the temperature in the magnetic field direction to be $T_{||}$ and the temperature perpendicular to this direction to be $T_{\perp}$, they found that $T_{||}/T_{\perp} > 5$ and that $T_{||}$ sometimes can be as much as an order of magnitude greater than $T_{\perp}$.

The magnetic field experiment on board IMP-1 (Wilcox and Ness, 1965) demonstrated a sectoring of the interplanetary magnetic field structure with the direction of the magnetic field either toward the sun or away from the sun along the Archimedes spiral angle. This sector structure corotates with the sun as the solar wind flows nearly radially at the orbit of the earth. Figure (3.1) shows the relative sizes of these structures, three taking up 2/7 of the total angle each in the ecliptic plane at the orbit of the earth and one taking up 1/7 of this angle. The structures had definite characteristics which repeated themselves within each sector. These characteristics were the magnitude of the interplanetary magnetic field, the plasma density, and the solar wind velocity. These characteristics are plotted as a function of position within a sector in Figures (3.2), (3,3), and (3.4). Figure (3.5) shows the daily sum of the K_p index also plotted as a function of position within a sector. The close correlation between $\sum K_p$ and V_s was pointed out by Wilcox and Ness (1965). Coleman et al. (1966) using data from Mariner 2, found that the

Figure 3.1

The sector structure of the interplanetary magnetic field. (After Wilcox and Ness (1965)).

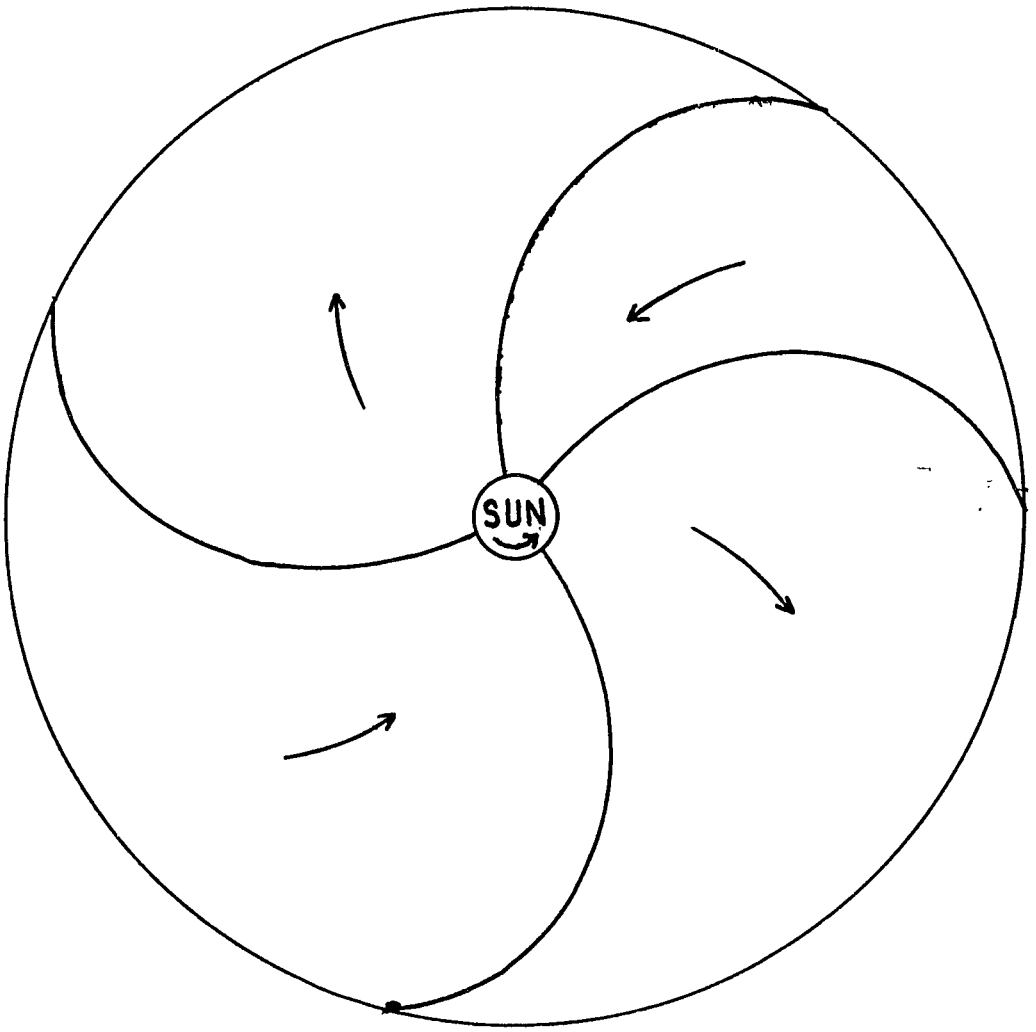
SUN

Figure 3.2

The interplanetary magnetic field plotted as a function of position (in days) within a sector, where (a) + indicates sectors with magnetic fields away from the sun and (b) - indicates sectors with magnetic fields toward the sun. (After Wilcox and Ness (1965)).

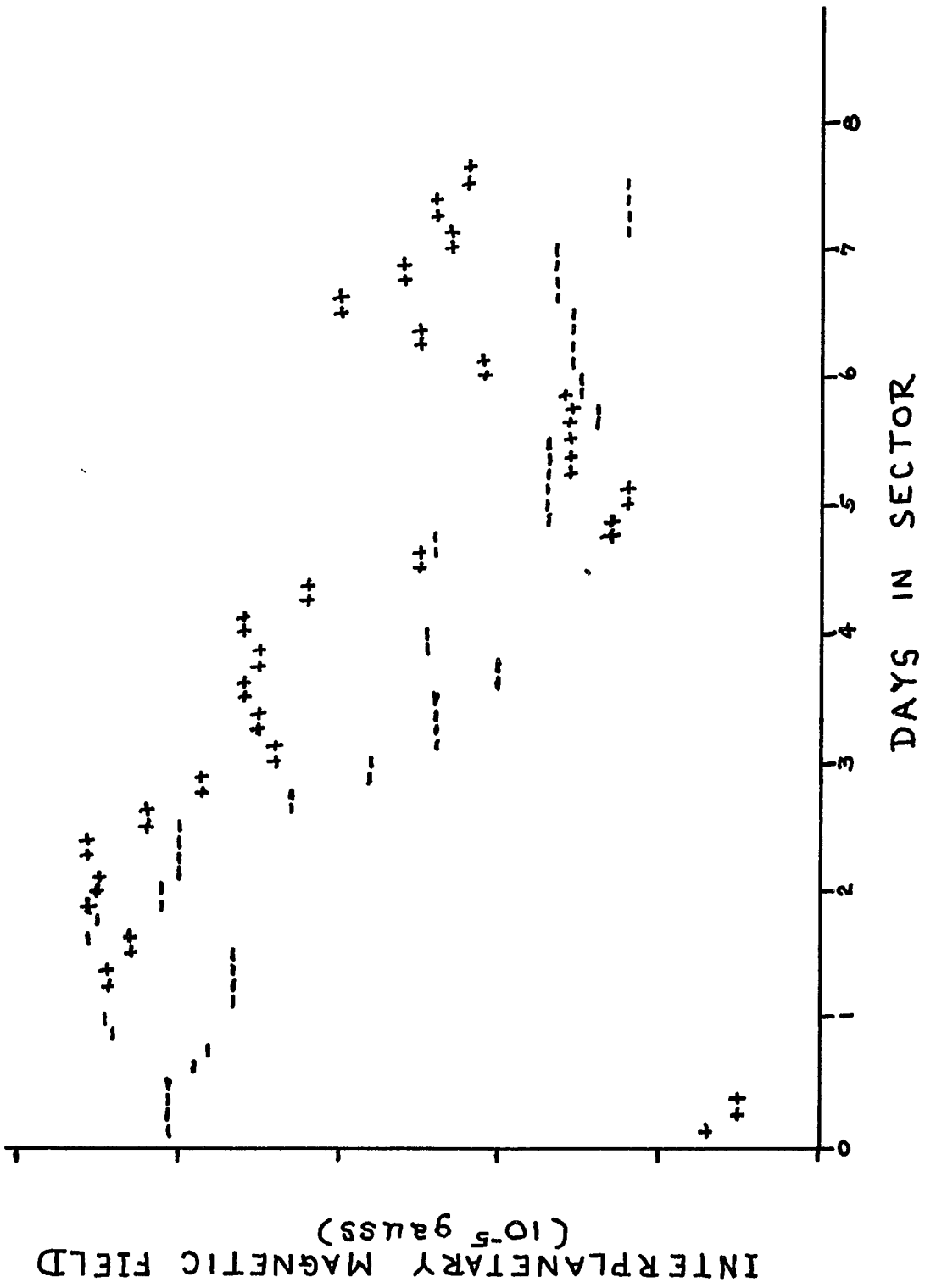
INTERPLANETARY MAGNETIC FIELD
(10⁻⁵ gauss)
DAYS IN SECTOR
0
1
2
3
4
5
6
7
8

Figure 3.3

The plasma density plotted as a function of position (in days) within a sector, where (a) + indicates sectors with magnetic fields away from the sun and (b) - indicates sectors with magnetic fields toward the sun. (After Wilcox and Ness (1965), but with revised M.I.T. solar wind data, Pai et al., 1967 (Wilcox, 1968)).

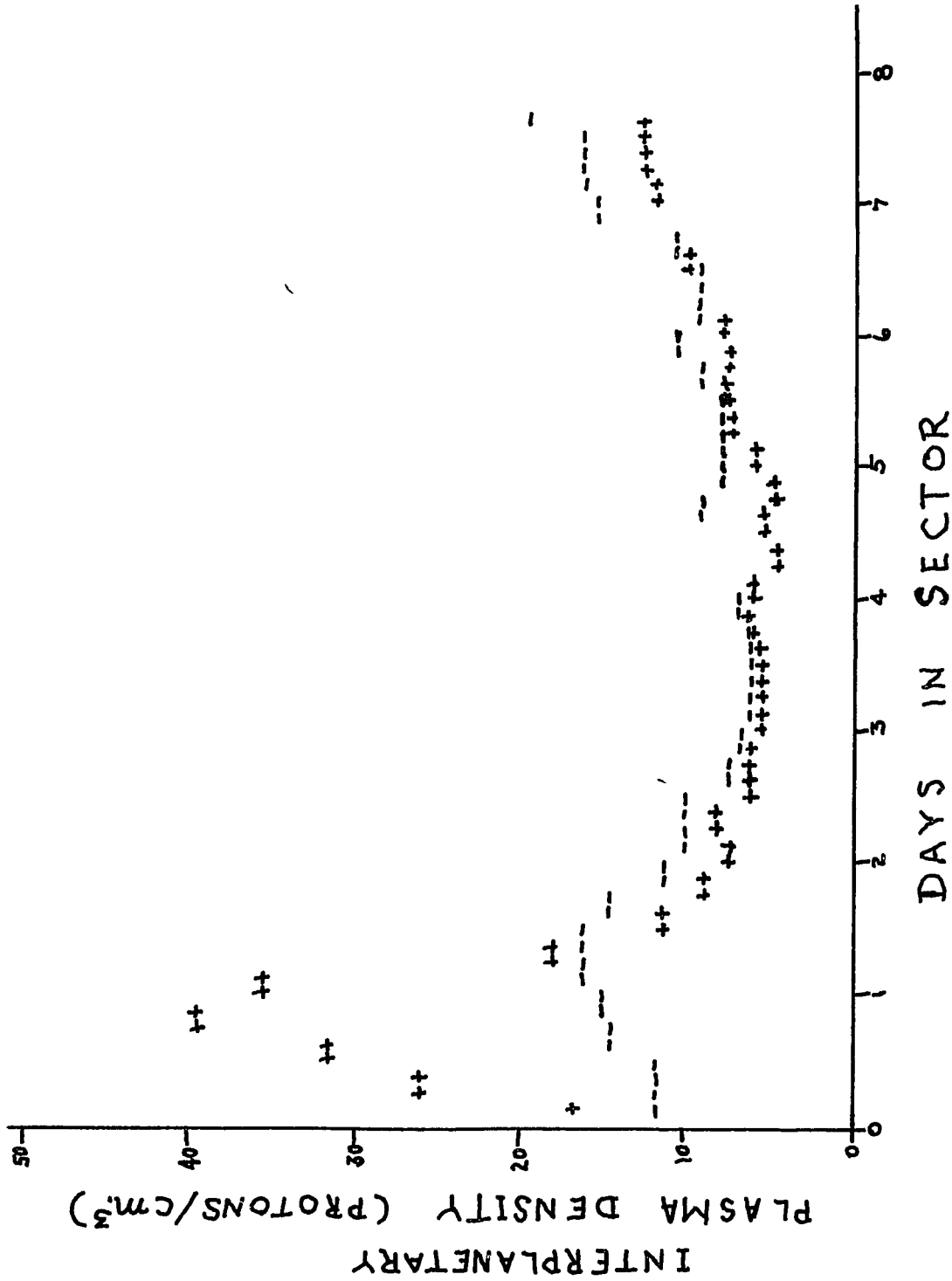
INTERPLANETARY
PLASMA DENSITY (PROTONS/cm.³)
50
40
30
20
10
0
0
1
2
3
4
5
6
7
8
DAYS IN SECTOR

Figure 3.4

The solar wind velocity plotted as a function of position (in days) within a sector, where (a) + indicates sectors with magnetic fields away from the sun and (b) - indicates sectors with magnetic fields toward the sun. (After Wilcox and Ness (1965), but with revised M.I.T. solar wind data, Pai et al., 1967 (Wilcox, 1968)).

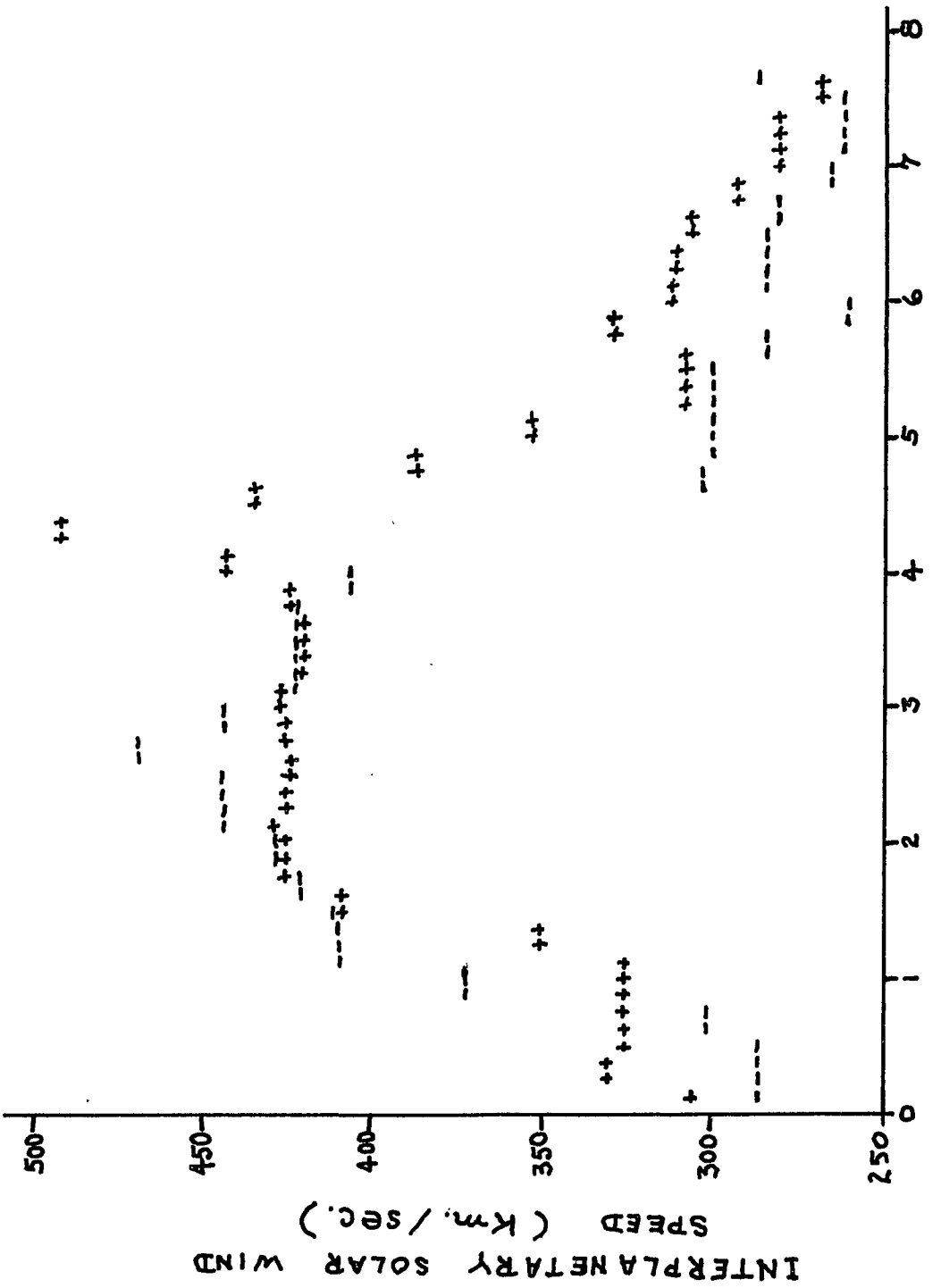
INTERPLANETARY SOLAR WIND
SPEED (km./sec.)
500
450
400
350
300
250
0
1
2
3
4
5
6
7
8
DAYS IN SECTOR

Figure 3.5

Daily sum of the K_p index as a function of position (in days) within a sector, where (a) + indicates sectors with magnetic fields away from the sun and (b) - indicates sectors with magnetic fields toward the sun. (After Wilcox and Ness (1965)).

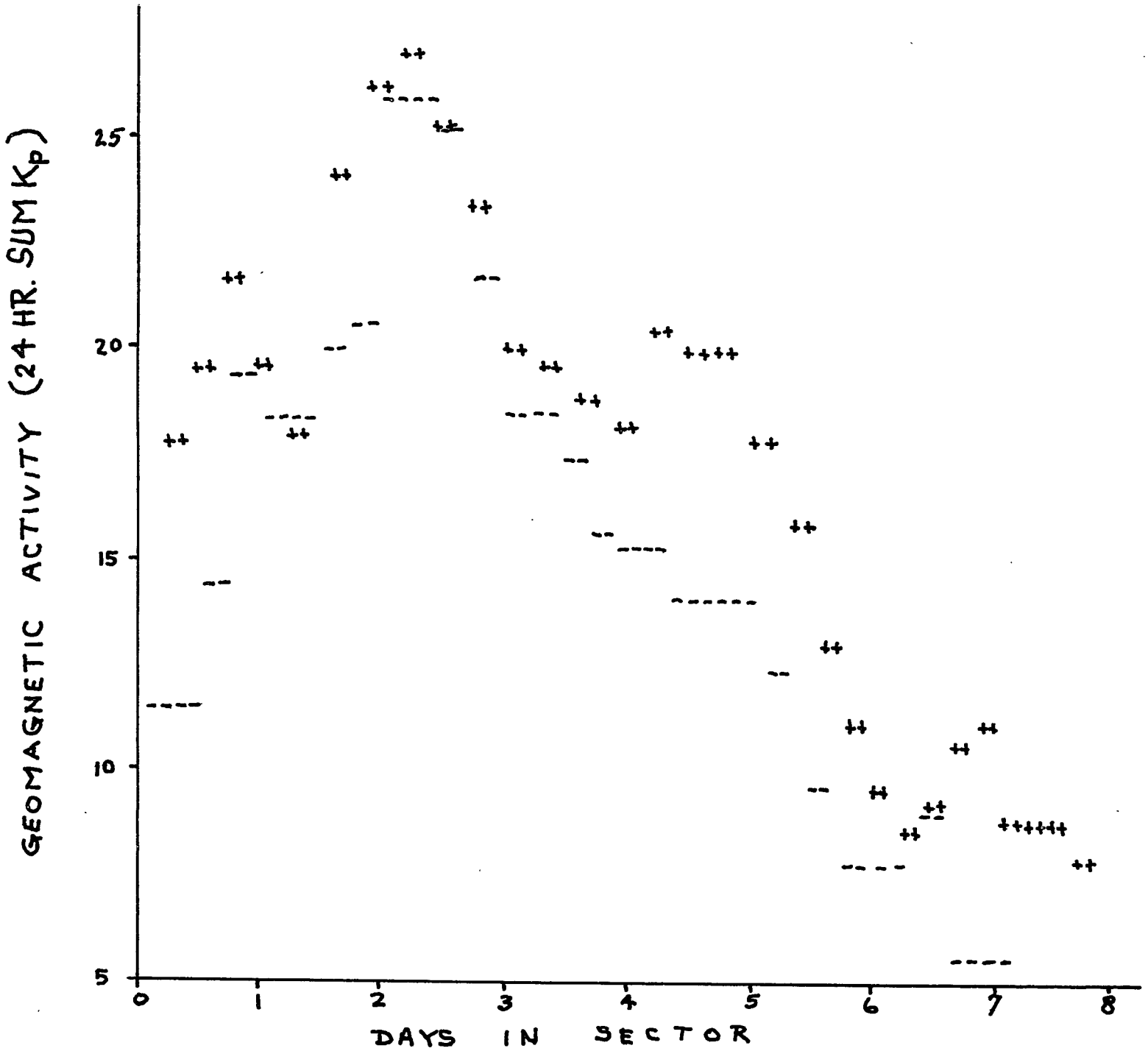
GEOMAGNETIC ACTIVITY (24 HR. SUM Kp)
25
20
15
10
5
0
1
2
3
4
5
6
7
8
DAYS IN SECTOR

interplanetary magnetic field was sectored as in the later flight of IMP-1. In addition they reported that the magnetometer experiments on Mariner 4 showed that the quasi-stationary corotating structure of the interplanetary field does not persist in the ascending cycle of solar activity.

The results of the Vela 3 plasma experiments reported by Hundhausen et. al. (1967) generally agreed with those of the Pioneer 6 data (Wolfe et. al., 1966a). The Vela 3 results yield a typical value of $T_{max.}/T_{av.} = 1.4$ whereas the value $T_{\parallel}/T_{\perp} = 5$ reported by Wolfe et al. (1966a) corresponds to $T_{max.}/T_{av.} = 2.6$. The average direction of the highest random energy of the ions was close to the average direction of the interplanetary magnetic field. They also found that the average velocity of the solar wind was about 345 km./sec.

Wilcox and Ness (1967) reported that the interplanetary sector structure observed on IMP-1 was most similar to the large scale magnetic structures on the sun at heliographic latitudes between about 10°N and 20°N. At the time of the observations of IMP-1, the earth was at a heliographic latitude of $3\frac{1}{2}\,^{\circ}$S. In addition, they found that the calcium plage regions between 10 and 20°N. heliographic latitude were densest one-quarter of the way into the observed sector structures. This coincides with the highest solar wind velocities and densities. The total calcium plage distribution was found by them to most closely resemble the solar wind velocity distribution within each sector. It appears, by the above observations, that the northern hemisphere of the sun somehow dominates the total solar wind flow so that the earth even

at $3\frac{1}{2}^{o}$S. heliographic latitude is in a sense connected to the northern hemisphere of the sun. This is exactly what Wilcox (1965) had predicted in 1965 after he reviewed the North-South asymmetry in the effectiveness of solar flares on geomagnetic activity reported by Bell (1961) and the asymmetry in solar magnetic fields published by Babcock (1959). Wilcox (1968) pointed out that the larger activity of the northern solar hemisphere would cause a greater coronal heating in the North as compared with the South and from Parker's (1963) analysis a greater efflux of solar wind would therefore be expected from the North. Figure (3.6) shows how the resulting imbalance in lateral pressure would place the earth within solar magnetic fields originating in the North.

3.4 A Simple Model of the Interplanetary Magnetic Field

Suppose a source of monoenergetic particles of the same mass was located on the equatorial plane of the sun at some distance b from the sun's center. Let the velocities be directed radially from the sun within the sun's own frame of reference, and let the sun's angular velocity be ω with respect to an inertial coordinate system. The problem is to find the locus of points formed by successively emitted particles or, equivalently, the trajectory of a particle emitted from the source in the sun's frame of reference. If the particles drag solar magnetic fields with them, these field lines will lie along the locus of points mentioned above. The gravitational force will be neglected.

Let particles corotate with the source until they are instantaneously projected out from the sun. In the inertial coordinate system at t = 0 the velocity of the particle is $\vec{V} = \vec{V}_{so} + \vec{V}_{\omega}$

Figure 3.6

An illustration of the earth within a plasma emanating from a hot northern hemisphere of the sun.

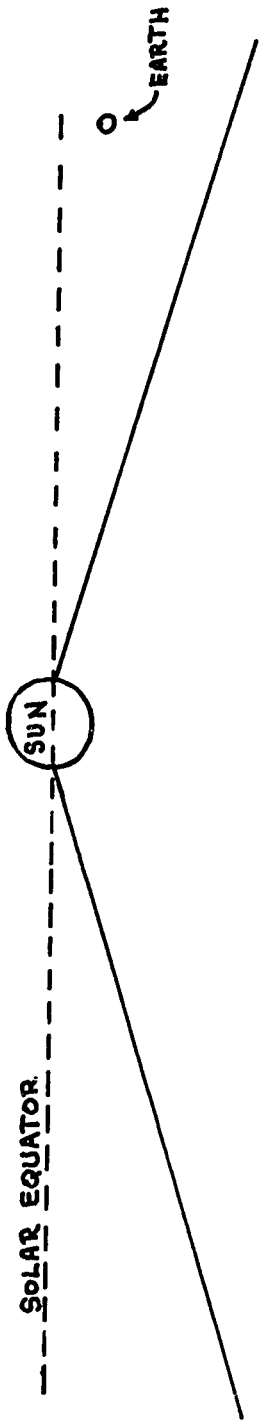
EARTH
SUN
SOLAR EQUATOR

where $\vec{V}_{so}$ is the component of the velocity directed along a radius and $\vec{V}_{\omega}$ is the angular component of the velocity. Since no external forces are assumed to act on the particle, its motion will be linear in the inertial frame of reference. The coordinates r,θ in Figure (3.7) will be used to describe the motion of this particle in the inertial coordinate system. The Lagrangian for this particle will be just T, the kinetic energy, since there are no forces acting on the particle once it is emitted. The kinetic energy is,

$$T = \frac{1}{2}m\dot{r}^2 + \frac{1}{2}mr^2\dot{\theta}^2 \quad ,$$

where a dot over a variable indicates a time derivative. Lagrange's equations then become,

$$\frac{d}{dt}\frac{\partial T}{\partial \dot{r}} - \frac{\partial T}{\partial r} = 0 \quad ,$$

$$\frac{d}{dt}\frac{\partial T}{\partial \dot{\theta}} - \frac{\partial T}{\partial \theta} = 0 \quad .$$

The equations of motion therefore are,

$$m\ddot{r} - mr\dot{\theta}^2 = 0 \quad ,$$

$$\frac{d}{dt}\left(\frac{1}{2}mr^2\dot{\theta}\right) = 0 \quad .$$

The second equation may be integrated to yield,

$$mr^2\dot{\theta} = \ell \qquad (3.2)$$

Figure 3.7

Definition of α, r and θ in the inertial coordinate system.

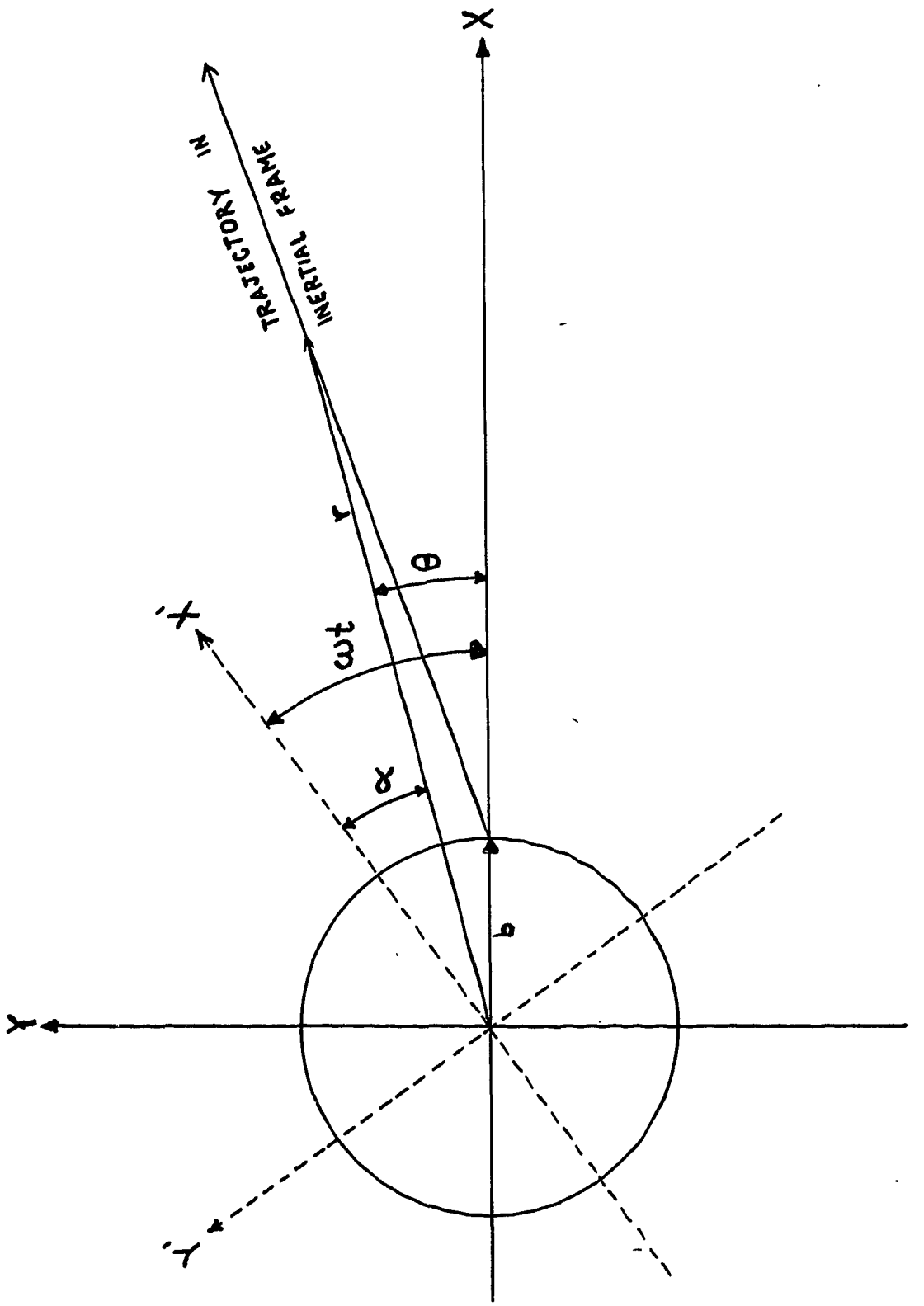
X
TRAJECTORY IN INERTIAL FRAME
r
θ
ωt
α
b
Y
X'
Y'

where ℓ is a constant. This is just a statement of the conservation of angular momentum. The first equation of motion may now be put into the following form,

$$m\ddot{r} = -\frac{\partial}{\partial r}\left(\frac{1}{2}\frac{\ell^2}{mr^2}\right) \quad .$$

By multiplying both sides of this equation by $\dot{r}$ the left hand side may be written as

$$\frac{d}{dt}\left(\frac{1}{2}m\dot{r}^2\right) \quad ,$$

while the right hand side may be put in the form

$$-\frac{d}{dt}\left(\frac{1}{2}\frac{\ell^2}{mr^2}\right) \quad .$$

The whole equation becomes,

$$\frac{d}{dt}\left(\frac{1}{2}m\dot{r}^2 + \frac{1}{2}\frac{\ell^2}{mr^2}\right) = 0 \quad ,$$

which is just a statement of the conservation of energy. Therefore,

$$\frac{1}{2}m\dot{r}^2 + \frac{1}{2}\frac{\ell^2}{mr^2} = E \quad , \tag{3.3}$$

where E is a constant. Equation (3.3) may be immediately integrated to give the time t as a function of r, which may be written as,

$$t = \int_{b}^{r} \frac{dr}{\sqrt{\frac{2}{m}(E - \frac{\ell^2}{2mr^2})}} \quad . \tag{3.4}$$

Equation (3.2) may also be integrated to give the angle θ as a function of time once r is known as a function of time from Equation (3.4). The equation for θ becomes,

$$\theta = \ell \int_{0}^{t} \frac{dt}{mr^2(t)} + \theta_o \quad .$$

The time may be eliminated from Equations (3.2) and (3.3) to yield a differential equation in r and θ. This may be done by writing Equation (3.2) as,

$$\ell dt = mr^2 d\theta \quad .$$

The time derivative may then be converted into a derivative with respect to θ since,

$$\frac{d}{dt} = \frac{\ell}{mr^2} \frac{d}{d\theta} \quad .$$

The operator d/dt may be applied to itself to give,

$$\frac{d^2}{dt^2} = \frac{\ell}{mr^2} \frac{d}{d\theta} (\frac{\ell}{mr^2} \frac{d}{d\theta}) \quad . \tag{3.5}$$

Equation (3.2) can be written as,

$$\ddot{mr} - \frac{\ell^2}{mr^3} = 0 \quad ,$$

which becomes, after using Equation (3.5),

$$\frac{\ell}{r^2}\frac{d}{d\theta}\left(\frac{\ell}{mr^2}\frac{dr}{d\theta}\right) - \frac{\ell^2}{mr^3} = 0 \quad . \tag{3.6}$$

Equation (3.6) may now be written as,

$$-2\frac{\ell^2}{mr^5}\left(\frac{dr}{d\theta}\right)^2 + \frac{\ell^2}{mr^4}\frac{d^2r}{d\theta^2} - \frac{\ell^2}{mr^3} = 0 \quad ,$$

which becomes, after making use of Equation (3.3) and some algebra,

$$-2\frac{\ell^2}{mr^5}\left(\frac{dr}{d\theta}\right)^2 + \frac{4E}{r} - \frac{2\ell^2}{mr^3} = 0 \quad . \tag{3.7}$$

Equation (3.7) may now be cast into the form,

$$\frac{dr}{d\theta} = r^2\sqrt{\frac{2mE}{\ell^2} - \frac{1}{r^2}} \quad ,$$

and finally becomes

$$\theta = \int_b^r \frac{dr}{r^2\sqrt{\frac{2mE}{\ell^2} - \frac{1}{r^2}}} \quad ,$$

where it will be assumed that at $t = 0$, $r = b$ and $\theta = 0$. This is easily integrated using the substitution $r = 1/x$. The solution becomes,

$$\theta = \sin^{-1}\frac{1}{b\sqrt{\frac{2mE}{\ell^2}}} - \sin^{-1}\frac{1}{r\sqrt{\frac{2mE}{\ell^2}}} \quad . \tag{3.8}$$

At the instant the particle is emitted the energy is,

$$E = \frac{1}{2}mV_{so}^2 + \frac{1}{2}mb^2\omega^2 \quad , \tag{3.9}$$

and the angular momentum is,

$$\ell = mb^2\omega \quad . \tag{3.10}$$

The solution may therefore be written as,

$$\theta = \sin^{-1}\frac{b^2\omega}{b\sqrt{V_{so}^2 + b^2\omega^2}} + \sin^{-1}\frac{b^2\omega}{r\sqrt{V_{so}^2 + b^2\omega^2}} \quad .$$

Referring to Figure (3.7) once more, the angles α and θ are related through the angle ωt by the expression,

$$\alpha = \omega t - \theta \quad . \tag{3.11}$$

Since the origin of the rotating frame is placed at the origin of the inertial frame the coordinate r is the same in both systems. The time t in Equation (3.9) can be expressed as a function of r through Equation (3.4) which becomes,

$$t = \int_b^r \frac{rdr}{\sqrt{\frac{2}{m}(Er^2 - \frac{\ell^2}{2m})}} \quad ,$$

the result of which is,

$$t = \frac{m}{2E}\left[\sqrt{\frac{2}{m}\left(Er^2 - \frac{\ell^2}{2m}\right)} - \sqrt{\frac{2}{m}\left(Eb^2 - \frac{\ell^2}{2m}\right)}\right] \quad .$$

After use is made of Equations (3.9) and (3.10), this equation becomes,

$$t = \frac{1}{(V_{so}^2 + b^2\omega^2)}\left[\sqrt{(V_{so}^2 + b^2\omega^2)r^2 - b^4\omega^2} - V_{so}b\right] \quad .$$

The expressions for t and θ may now be placed into Equation (3.11) so that α can be expressed in terms of r. Equation (3.11) therefore becomes,

$$\alpha = \frac{\omega}{(V_{so}^2 + b^2\omega^2)}\left[\sqrt{(V_{so}^2 + b^2\omega^2)r^2 - b^4\omega^2} - V_{so}b\right] -$$

$$\left[\sin^{-1}\frac{b^2\omega}{b\sqrt{V_{so}^2 + b^2\omega^2}} - \sin^{-1}\frac{b^2\omega}{r\sqrt{V_{so}^2 + b^2\omega^2}}\right] \quad . \qquad (3.12)$$

The Archimedes spiral equation for the interplanetary magnetic field most often encountered in the literature is, (e.g. Dessler, 1967),

$$r = \frac{V_s}{\omega}\alpha + b \quad . \qquad (3.13)$$

To see how Equation (3.12) is related to the Archimedes spiral given by Equation (3.13), suppose that the arcsin functions may be neglected and, in addition, let $b^2\omega^2 < V_{so}^2$. Equation (3.12) then becomes,

$$\alpha = \frac{\omega}{\sqrt{V_{so}^2 + b^2\omega^2}} r - \frac{\omega b}{(V_{so}^2 + b^2\omega^2)} V_{so} \quad .$$

Solving for r in this equation gives,

$$r = \frac{\sqrt{V_{so}^2 + b^2\omega^2}}{\omega} \alpha + \frac{bV_{so}}{\sqrt{V_{so}^2 + b^2\omega^2}} \quad .$$

If, now $b^2\omega^2 << V_{so}^2$, we see that

$$r = \frac{V_{so}}{\omega}\alpha + b \quad ,$$

which is just the Archimedes spiral of Equation (3.13).

It is of interest to determine the angle made by this spiral with respect to a radius from the sun at a distance r. Figure (3.8) shows that this angle ψ may be obtained through the following equation,

$$\tan\psi = \frac{r\dot{\alpha}}{\dot{r}} \quad . \tag{3.14}$$

Since $\alpha = \omega t - \theta$ then the time derivative of α in the inertial coordinate system becomes,

$$\dot{\alpha} = \omega - \dot{\theta} \quad ,$$

and multiplying through by the coordinate r gives,

$$r\dot{\alpha} = r\omega - r\dot{\theta} \quad . \tag{3.15}$$

From Equations (3.4) and (3.10) an expression for $r\dot{\theta}$ may be obtained,

Figure 3.8

Definition of the angle ψ.

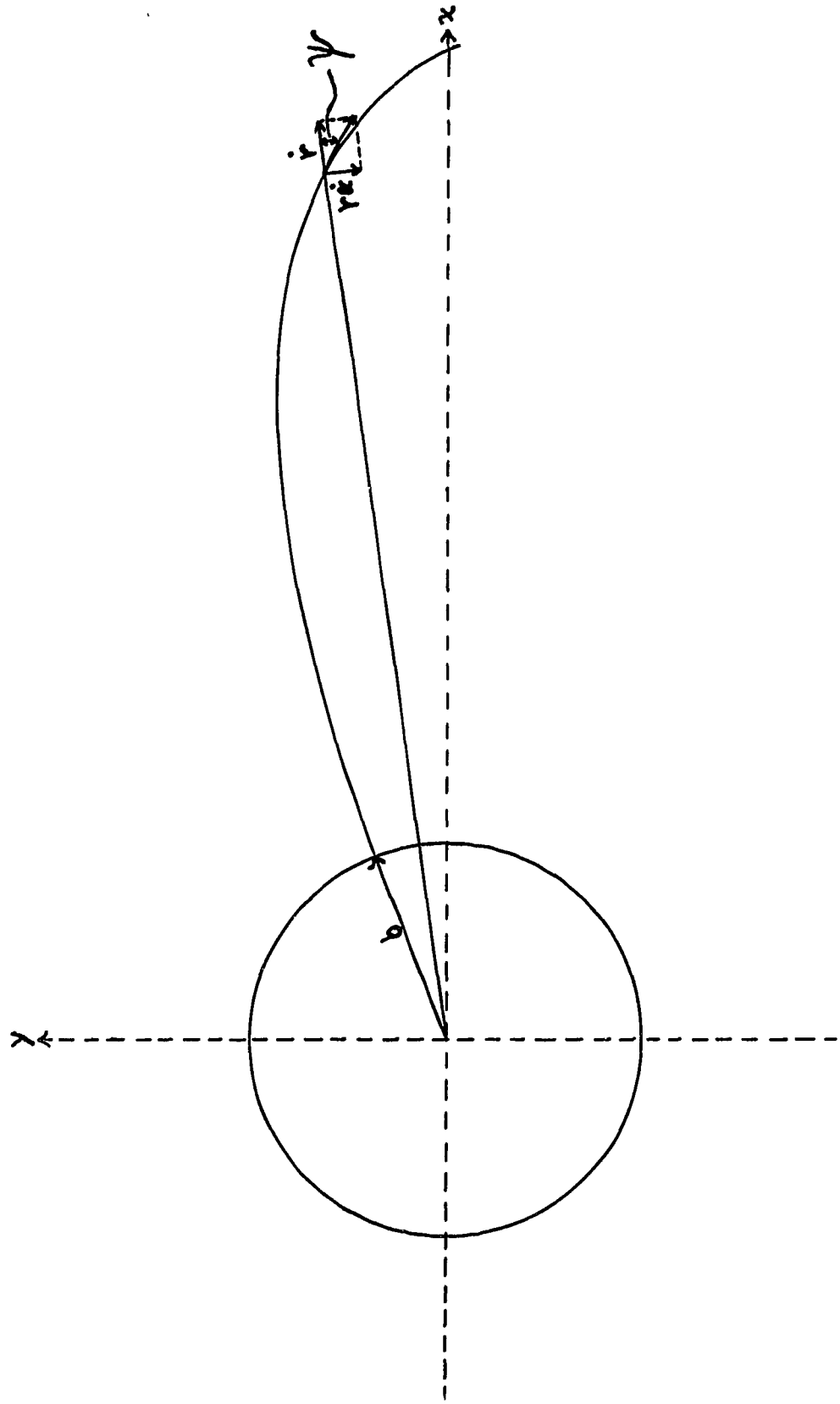
x
y
ρ

which is,

$$r\dot{\theta} = \frac{b^2\omega}{r} \quad .$$

Equation (3.15) therefore becomes,

$$r\dot{\alpha} = r\omega - \frac{b^2\omega}{r} \quad . \tag{3.16}$$

An expression for $\dot{r}$, obtained from Equations (3.3) and (3.9), is

$$\dot{r} = \left[V_{so}^2 + b^2\omega^2 - \frac{b^4\omega^2}{r^2}\right]^{\frac{1}{2}} \quad . \tag{3.17}$$

Equation (3.14) may now be expressed as,

$$\tan\psi = \frac{\omega\left[r - b\left(\frac{b}{r}\right)\right]}{\left[V_{so}^2 + b^2\omega^2\left(1 - \frac{b^2}{r^2}\right)\right]^{\frac{1}{2}}} \quad . \tag{3.18}$$

If $b < r$ then b^2/r^2 may be neglected in comparison with 1. Equation (3.18) then becomes,

$$\tan\psi = \frac{\omega\left[r - b\left(\frac{b}{r}\right)\right]}{\sqrt{V_{so}^2 + b^2\omega^2}} \quad .$$

If, in addition, $b^2\omega^2 << V_{so}^2$ then this equation becomes,

$$\tan\psi = \frac{\omega\left(r - b\left(\frac{b}{r}\right)\right)}{V_{so}} \quad ,$$

which is just Chapman's (1964, p.35) result. If b << r, then the equation reduces to

$$\tan\psi = \frac{\omega r}{V_{so}} \quad ,$$

as in Dessler's (1967) result. Figure (3.9) gives ψ as a function of V_{so} at 1 A.U. (astronomical unit, which is the mean radius of the earth's orbit about the sun) using Equation (3.18).

For a given magnetic field at the location of the emitting region on the sun, the components of the magnetic field in the interplanetary region can be determined. Let B_o represent the field at the emitting region and assume it to be drawn out from the sun radially in the sun's frame of reference as in the "frozen-in" field approximation in magnetohydrodynamics (Alfven, 1950).

The components of the interplanetary magnetic field can now be determined. In the inertial coordinate system, let B_r be the magnetic field component along r and B_α be the magnetic field component perpendicular to r in the $\hat{\alpha}$ direction. The total magnetic field can then be written as,

$$\vec{B}_t = B_r\hat{r} + B_\alpha\hat{\alpha} \quad . \tag{3.19}$$

Gauss' law gives

$$\frac{B_r}{B_{or}} = \left(\frac{b^2}{r^2}\right) \quad , \tag{3.20}$$

Figure 3.9

Values of ψ as a function of V_{SO} at 1A.U. using Equation (3.18).

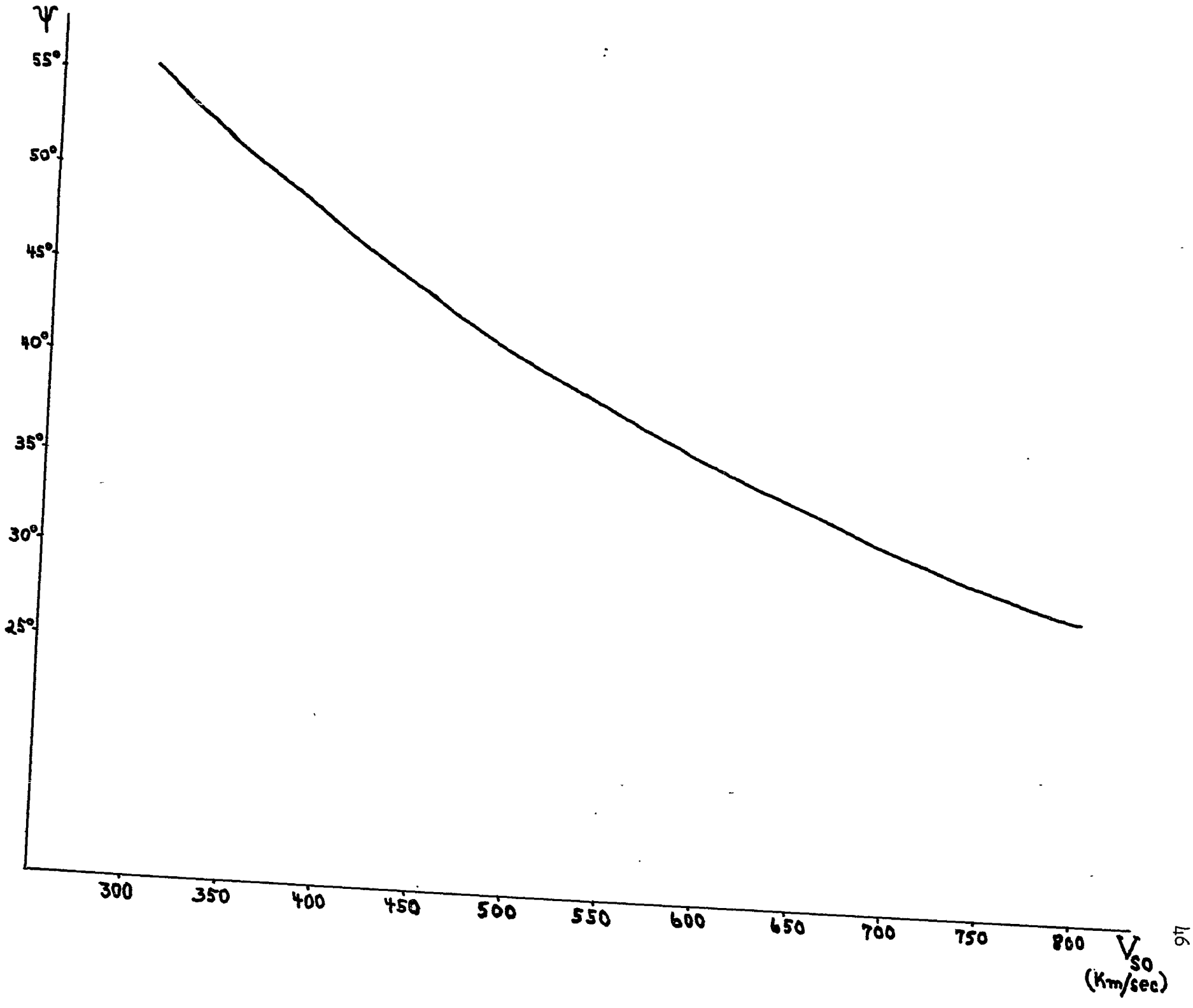
ψ
55°
50°
45°
40°
35°
30°
25°
300
350
400
450
500
550
600
650
700
750
800
V_{so}
(Km/sec)

where B_{or} is the component of B_o along $\hat{r}$ at $r = b$. This component is,

$$B_{or} = \frac{B_o V_{so}}{(V_{so}^2 + b^2\omega^2)^{\frac{1}{2}}} \quad , \tag{3.21}$$

allowing Equation (3.20) to be written as,

$$B_r = \frac{B_o V_{so}}{(V_{so}^2 + b^2\omega^2)^{\frac{1}{2}}} \left(\frac{b^2}{r^2}\right) \quad . \tag{3.22}$$

The component B_α may be determined from Equation (3.18) by noting that

$$\tan\psi = \frac{B_\alpha}{B_r} \quad . \tag{3.23}$$

This gives,

$$B_\alpha = B_r \frac{\omega\left(r - b\left(\frac{b}{r}\right)\right)}{\left(V_{so}^2 + b^2\omega^2\left[1 - \frac{b^2}{r^2}\right]\right)^{\frac{1}{2}}} \quad . \tag{3.24}$$

Combining Equations (3.22) and (3.24) yields,

$$B_\alpha = \frac{B_o V_{so}}{(V_{so}^2 + b^2\omega^2)^{\frac{1}{2}}} \frac{\omega\left(r - b\left(\frac{b}{r}\right)\right)}{\left(V_{so}^2 + b^2\omega^2\left(1 - \frac{b^2}{r^2}\right)\right)^{\frac{1}{2}}} \quad . \tag{3.25}$$

The magnitude of the total field may be expressed as,

$$B_t = \frac{B_o V_{so}}{(V_{so}^2 + b^2\omega^2)^{\frac{1}{2}}} \left|\frac{b^2}{r^2}\right| \left[1 + \frac{\left(\omega\left(r - b\left(\frac{b}{r}\right)\right)\right)^2}{V_{so}^2 + b^2\omega^2\left(1 - \frac{b^2}{r^2}\right)}\right]^{\frac{1}{2}} \quad . \qquad (3.26)$$

To see what value this equation predicts for the magnetic field at r = 1 A.U. $\equiv 1.5 \times 10^{13}$ cm., some typical values of the parameters are used. Let b = 1 $R_\odot \equiv 7 \times 10^{10}$ cm., and B_o = 1 gauss. Take $\omega = 2.9 \times 10^{-6}/_{sec}$ which corresponds to an equatorial sidereal period of 24.7 days, and let $V_{so} = 3 \times 10^7$ cm./sec. These parameters give for B_t a value of 3.7γ. The angle ψ may be determined from Figure (3.9), and turns out to be around 55^o. These values are all in agreement with the experimentally determined values in the solar wind.

CHAPTER 4

THE MAGNETOSPHERE

4.1 Early Predictions and Theoretical Determinations of the Boundary

Once the evidence for solar corpuscular radiation was made known, the question eventually arose as to what would happen to an advancing plasma cloud impinging on the magnetic field of a dipole. Chapman and Ferraro (1931) considered the advancing plasma cloud from the sun to be planar, rigid, and perfectly conducting, thereby allowing them to replace the cloud by an image dipole of the same strength. With this model they were able to determine the magnetic field distribution as a function of time on the earth side of the plasma cloud. This model provided an explanation of the sudden commencements of certain geomagnetic storms. They realized, however, that the portion of the cloud near the dipole would suffer retardation and as a result a magnetic cavity would be formed. The magnetic fields tangent to this plane just in front of the plasma cloud would be twice that of the tangential component of the dipole field of the earth at the plane.

The continual presence of the solar wind meant that this cavity should be a permanent feature of the earth's environment. Detailed calculations of the shape and position of the boundary between the geomagnetic dipole field and a steady solar wind plasma were carried out by many workers (Dungey, 1961; Parker, 1956; Cole and Huth, 1959; Zhigulev and Romishevskii, 1960; Beard, 1960, 1962; Ferraro, 1960; Hurley, 1961; Spreiter and Briggs, 1961, 1962;

Davis and Beard, 1962; Midgley and Davis, 1962, 1963; Slutz, 1962; Spreiter and Hyett, 1963; Mead and Beard, 1964) using various assumptions and techniques. Common to most of the analyses was the assumption that the magnetopause (i.e. the boundary between the confined geomagnetic field and the external solar wind plasma; see Fig.7.3) was stable in a steady solar wind and that a dynamical equilibrium existed across this boundary. The only kind of boundary compatible with the idea that the geomagnetic field completely excludes the interplanetary field and plasma is one which is a tangential discontinuity. Such a discontinuity requires that there be no mass flow across the boundary and that the normal component of the magnetic field be zero. The mathematical formulation of the free boundary problem for the shape of the magnetosphere was then reduced to the following equation:

$$\frac{|(\vec{B}(r,\theta))_b|^2}{8\pi} = K\rho V_{so}{}^2 \mathrm{Cos}^2\xi \quad , \tag{4.1}$$

where,

$$\vec{B}(r,\theta) = -AB_{eq.}\left(\frac{R_E}{r}\right)^3 (\hat{\theta}\mathrm{Sin}\theta + 2\hat{r}\mathrm{Cos}\theta) \tag{4.2}$$

in a coordinate system with the dipole in the negative Z direction and where r and θ are the usual spherical coordinates. The symbols ρ and V_{so} refer to the upstream values of the mass density and velocity of the solar wind respectively. The symbol R_E represents the radius of the earth and $B_{eq.}$ is the equatorial value of the magnetic field at the surface of the earth ($B_{eq.}$ = 0.312 gauss).

The symbol ξ is the angle between the normal to the boundary and the incident solar wind and will be a function of the shape of the boundary, ($\xi = f(r_b, \theta_b, \phi_b)$), and the orientation of the dipole with respect to the solar wind direction, thereby making Equation (4.1) a difficult non-linear differential equation (Davis and Beard, 1962). This, coupled with the codetermination of the boundary necessitates the use of numerical methods for the general solution. The constant K in Equation (4.1) can take on a maximum value of 2 for specular reflections and the constant A in Equation (4.2) has usually been taken to be 2 in the three-dimensional analyses.

The shape of the boundary found by such analyses was such that the part closest to the earth was in the sun's direction (assuming radial flow) and the rest of it flared out in the anti-solar direction enclosing the earth's magnetic field in something like a paraboloid (see Figure (7.3) in Chapter 7). Equations (4.1) and (4.2) will now be used to find the subsolar distance to the boundary when the dipole is perpendicular to the solar wind flow for typical values of the solar wind parameters. Equations (4.1) and (4.2), when combined, yield for r the following expression when $\theta = \pi/2$, A = 2, and K = 2:

$$r = \left(\frac{B_{eq.}^{\,2}}{4\pi\rho V_{so}^{\,2}} \right)^{1/6} , \qquad (4.3)$$

where r is now expressed in earth radii. Letting the number density of the solar wind be $10/cm^3$ and assuming it to be composed chiefly of ionized hydrogen flowing at a velocity of 300 km./sec.,

the distance from the earth to the boundary at the subsolar point becomes,

$$r \simeq 9.1 R_E \quad .$$

4.2 Experimental Confirmation of Magnetopause

The first identification of the magnetopause was reported by Sonett (1960) using the magnetometer data aboard the Pioneer I and Pioneer V satellites. He found that the field intensity was higher than that for the extrapolated earth dipole field up to $13R_E$ and thereafter the field intensity decreased more rapidly than r^{-3}. Explorer 12 made a number of passes through the magnetopause with the magnetometer clearly showing the boundary as reported by Cahill and Amazeen (1963). Inside the boundary the field was generally twice that due to the dipole field of the earth and just outside the boundary the field was variable in both magnitude and direction. They were able to identify the magnetopause as being a tangential discontinuity for most of the passes. There are five kinds of discontinuity for magnetohydrodynamic fluids of which the tangential discontinuity is just one. These are the tangential, contact, rotational, fast shock, and slow shock discontinuities. The boundary conditions for these discontinuities are outlined below (Spreiter et al., 1966; Spreiter et al., 1968; Spreiter and Alksne, 1969).

In the following let n and t refer to vector conponents normal and tangential to the discontinuity respectively. The quantity $|f|_1^2$ means the difference of the quantity f between regions

2 and 1 on either side of the discontinuity. The symbols v, B, ρ, and p stand for the usual quantities of fluid velocity, magnetic field intensity, mass density, and pressure (thermal and bulk) respectively.

The tangential discontinuity is represented by the following jump conditions:

$$\left\{\begin{array}{c} v_n = 0 \\ B_n = 0 \\ |\vec{v}_t|_1^2 \neq 0 \\ |\vec{B}_t|_1^2 \neq 0 \\ |\rho|_1^2 \neq 0 \\ |p + B^2/8\pi|_1^2 = 0 \end{array}\right\} . \tag{4.4}$$

The contact discontinuity is represented as:

$$\left\{\begin{array}{c} v_n = 0 \\ B_n \neq 0 \\ |\vec{v}|_1^2 = 0 \\ |\vec{B}|_1^2 = 0 \\ |p|_1^2 = 0 \\ |\rho|_1^2 = 0 \end{array}\right\} . \tag{4.5}$$

The rotational discontinuity is represented as:

$$
\left\{
\begin{array}{c}
v_n = \pm \dfrac{B_n}{(4\pi\rho)^{\frac{1}{2}}} \\
\\
\left|\vec{U}_t\right|_1^2 = \dfrac{\left|\vec{B}_t\right|_1^2}{(4\pi\rho)^{\frac{1}{2}}} \\
\\
\left|\rho\right|_1^2 = 0 \\
\left|p\right|_1^2 = 0 \\
\left|v_n\right|_1^2 = 0 \\
\left|v^2\right|_1^2 = 0 \\
\left|B^2\right|_1^2 = 0 \\
\left|B_n\right|_1^2 = 0
\end{array}
\right\} \qquad (4.6)
$$

The fast shock discontinuity is represented as:

$$
\left\{
\begin{array}{c}
v_n \neq 0 \\
\left|\rho\right|_1^2 > 0 \\
\left|p\right|_1^{2'} > 0 \\
\left|B_n\right|_1^2 = 0 \\
(\rho v_n)_{FAST} \geq (\rho v_n)_{ROT.} \\
\left|B_t\right|_1^2 > 0 \\
\left|B^2\right|_1^2 > 0
\end{array}
\right\} \qquad (4.7)
$$

The slow shock discontinuity is represented as:

$$\left\{\begin{array}{c} v_n \neq 0 \\ |\rho|_1^2 > 0 \\ |p|_1^2 > 0 \\ |B_n|_1^2 = 0 \\ (\rho v_n)_{ROT.} \geq (\rho v_n)_{SLOW} \\ |B_t|_1^2 < 0 \\ |B^2|_1^2 < 0 \end{array}\right\} \qquad (4.8)$$

Further evidence that the magnetopause is a tangential discontinuity has been given by Sonnerup and Cahill (1967, 1968), Fairfield (1967), Fairfield and Ness (1967), Cummings et al. (1968), and Cummings and Coleman (1968). The theoretical boundary shape and size has been verified by many other magnetometer and plasma experiments (Van Allen, 1959; Sonett et al., 1960; Coleman et al., 1960; Sonett, 1962; Bonetti et al., 1963; Freeman et al., 1963; Heppner et al., 1963; Frank and Van Allen, 1964; Ness et al., 1964; Bridge et al., 1965; Holzer et al., 1966; Wolfe et al., 1966a, 1966b; Fairfield and Ness, 1967; Wolfe and McKibbin, 1968). For a typical subsolar distance of 10 R_E from earth to the magnetopause a distance of 13 R_E is typical of the cross-sectional radius of the magnetosphere in a plane perpendicular to the sun-earth line. The typical thickness of the magnetopause is approximately 100 km. (Heppner et al., 1967).

4.3 The Standing Shock Wave and the Transition Region

Before the exact nature of the interplanetary medium was known, Gold (1959) theorized that a standing shock wave structure should exist upstream from the earth toward the sun due to the highly supersonic wind. More quantitative predictions about such a shock structure were made by Axford (1962), Kellogg (1962),

and Spreiter and Jones (1963). The latter calculated the size and shape of the shock using the equatorial trace of the magnetopause by Beard (1960) and by rotating this trace about the axis of symmetry obtained the size and shape of the blunt object they were to use in their gas dynamic theory. That such a shock should exist is due to the fact that the solar wind speed is much greater than the maximum velocity of a weak disturbance, which is just

$$v = \left(V_S^2 + V_A^2\right)^{\frac{1}{2}} \tag{4.9}$$

for an ideal ionized gas (Kulikovskiy and Lyubimov, 1965). The symbols V_S and V_A represent the sound speed and Alfven speed respectively in the ideal ionized gas. They are given by the following equations (Spreiter et al., 1968):

$$V_S = \left(\frac{\gamma RT}{\mu}\right)^{\frac{1}{2}} \tag{4.10}$$

$$V_A = \left(\frac{B^2}{4\pi\rho}\right)^{\frac{1}{2}} , \tag{4.11}$$

where γ is the ratio of specific heats, μ is the nondimensional mean molecular weight ($\mu = 16$ for atomic oxygen), R is the gas constant, T is the absolute temperature, B is the magnetic field intensity, and ρ is the mass density. By taking typical values of the solar wind parameters at 1A.U., the speed of propagation of a weak disturbance can be determined and compared with the stream speed. The following values of the parameters are used:

$\gamma = 5/3$ for monatomic gases with three degrees of freedom

$R = 8.3 \times 10^{7}$ ergs/gm K

$\mu = 1/2$ for fully ionized hydrogen

$T = 10^{5}\ ^{o}K$

$B = 5 \times 10^{-5}$ gauss

$\rho = 1.67 \times 10^{-23}$ gm.

The speed of the weak disturbance becomes: $v \simeq 60$ km./sec. The solar wind speeds have never been measured to be much below 280 km./sec. and there is some theoretical justification for never observing solar wind speeds less than 100 km./sec. (Dessler, 1967). Therefore a detached standing shock wave is expected upstream from the magnetopause as long as a solar wind is blowing.

The standing shock which may best be described as a fast shock discontinuity has been detected by many magnetometer and plasma experiments (Van Allen, 1959; Sonett et al., 1960; Coleman et al., 1960; Sonett, 1962; Bonetti et al., 1963; Freeman et al., 1963; Heppner et al., 1963; Frank and Van Allen, 1964; Ness et al., 1964; Sonett et al., 1964; Bridge et al., 1965; Wolfe et al., 1966a, 1966b; Fairfield and Ness, 1967; Burlaga and Ogilvie, 1968; Wolfe and McKibbin, 1968). The shape and size was found to generally agree with the predictions of Axford (1962),

Kellogg (1962), and Spreiter and Jones (1963). The thickness of the shock has generally been measured to be less than about 300 km. Some disagreement has arisen about the shock's thickness (Wolfe et al., 1966a; Bernstein et al., 1964) but recent measurements (Burlaga and Ogilvie, 1968) seem to favor the more well-defined thin shock.

The theoretical characteristics of the flow between the shock and the magnetopause has been studied by Spreiter et al. (1966), Dryer and Faye-Petersen (1966), and Dryer and Heckman (1967). Spreiter et al. (1966) use the magnetohydrodynamic equations and the shape of the boundary obtained by rotating the equatorial trace of the approximate solution given by Spreiter and Briggs (1961, 1962). They approximate the magnetohydrodynamic equations by noting that for large Alfven Mach numbers $\left[M_A = \frac{V_{SO}}{(B^2/4\pi\rho)^{\frac{1}{2}}}\right]$ and low values of $\vec{B}$ these equations reduce to the gasdynamic equations. Once the velocity field has been determined the magnetic field may be found by assuming the fluid to be perfectly conducting thereby allowing the frozen-in field equations to be used. These equations depend only upon $\vec{B}$ and $\vec{U}$, and since $\vec{U}$ has already been calculated the magnetic field intensity, $\vec{B}$, may be determined everywhere in the magnetosheath (which is the region between the shock and magnetopause) for any orientation of the interplanetary magnetic field. The configuration of the magnetosheath magnetic field determined in this way has been verified by the magnetometer experiments of Fairfield (1967), Fairfield and Ness (1967), Kaufmann (1967), and Wolfe and McKibbin (1968). The velocity stream lines in the magnetosheath have also been verified

by Ness et al. (1966a), and Burlaga and Ogilvie (1968). Detailed comparisons of the theoretical characteristics in the magnetosheath have been given by Spreiter and Alksne (1968) from data of Pioneer 6. Excellent agreement is obtained. The thermal anisotropies in the solar wind mentioned in Chapter 3 have been found by Hundhausen et al. (1967b) to be instantaneously aligned with the interplanetary magnetic field directions. The existence of the shock, however, provides for a randomization of the solar wind flow after passage through the shock boundary as observed by Bridge et al. (1965) and Argo et al. (1967), and are consistent with the fluid description of the flow past the magnetosphere.

Magnetohydrodynamic flows past the magnetosphere have been studied with the interplanetary magnetic field perpendicular and parallel to the flow respectively by Lees (1965), and Dryer and Faye-Petersen (1966). Walters (1964) also considered the interplanetary magnetic field in his analysis of the magnetohydrodynamic jump conditions across a fast shock discontinuity and predicted that the axis of symmetry of the bow shock and magnetopause boundaries was not directed into the solar wind but was tilted toward the west or clockwise (looking down on the ecliptic plane) by a few degrees. This is due to the tendency of the interplanetary magnetic field to line up with the Archimedes spiral angle. As already pointed out the interplanetary magnetic field at the orbit of the earth is neither parallel nor perpendicular to the solar wind flow. This prediction has been verified by Gosling et al. (1967a) and Hundhausen et al. (1969), and represents another phenomenon capable of being explained by the fluid theory.

The plasma density, temperature, and magnetic field intensity are found to increase after passage through the shock while the bulk stream speed decreases. The reasons for a collisionless gas to behave so much like a fluid are not to be found at the present time. There are many other interesting and incompletely understood phenomena occurring in the interplanetary medium, the magnetosheath, and within the magnetosphere itself. The works of Hess (1968), Carovillano et al. (1968), and Williams and Mead (1969) are recommended for recent surveys.

CHAPTER 5

MAGNETOHYDRODYNAMIC EQUATIONS

The thicknesses of the shock and magnetopause are very small with respect to the dimensions of the magnetosphere. This, coupled with the presence of a tangential discontinuity at the magnetopause and the successes of the fluid theories provide motivation for analysis of instability conditions at the magnetopause using the equations of magnetohydrodynamics.

Following Kulikovskiy and Lyubimov (1965) the basic equations of magnetohydrodynamics will now be given. A fundamental starting point is the assumption of Ohm's Law which may be written as,

$$\vec{J} = \sigma\left(\vec{E} + \frac{\vec{v} \times \vec{B}}{c}\right) + \rho_e \vec{v} \quad , \tag{5.1}$$

where $\vec{J}$ is the current density, σ is the conductivity, $\vec{E}$ and $\vec{B}$ are the electric and magnetic field intensities respectively, c is the speed of light, ρ_e is the excess charge density, and $\vec{v}$ is the velocity of the fluid element.

Maxwell's equations in the Gaussian system of units are,

$$\vec{\nabla} \times \vec{B} = \frac{4\pi}{c}\vec{J} + \frac{1}{c}\frac{\partial \vec{E}}{\partial t} \quad , \tag{5.2}$$

$$\vec{\nabla} \times \vec{E} = -\frac{1}{c}\frac{\partial \vec{B}}{\partial t} \quad , \tag{5.3}$$

$$\vec{\nabla} \cdot \vec{E} = 4\pi\rho_e \quad , \tag{5.4}$$

$$\vec{\nabla}\cdot\vec{B} = 0 \quad , \tag{5.5}$$

and are also fundamental to magnetohydrodynamics.

The current density, $\vec{J}$, given by Equation (5.1) is substituted into Equation (5.2) giving,

$$\vec{\nabla}\times\vec{B} = \frac{4\pi}{c}\left[\sigma\left(\vec{E} + \frac{1}{c}\vec{v}\times\vec{B}\right) + \rho_e\vec{v}\right] + \frac{1}{c}\frac{\partial\vec{E}}{\partial t} \quad . \tag{5.6}$$

The relative orders of magnitude for each of the terms in this equation may be estimated by giving the characteristic values of the quantities involved and are written below:

$$\left\{\begin{array}{ccc} \vec{\nabla}\times\vec{B} \sim \frac{B}{L} & , & \frac{4\pi\sigma\vec{E}}{c} \sim \frac{\sigma E}{c} \quad , \\ \frac{4\pi\sigma}{c^2}\vec{v}\times\vec{B} \sim \frac{\sigma VB}{c^2} & , & \frac{4\pi\rho_e\vec{v}}{c} \sim \frac{EV}{cL} \quad , \quad \frac{1}{c}\frac{\partial\vec{E}}{\partial t} \sim \frac{E}{ct} \end{array}\right\} \quad . \tag{5.7}$$

If the conductivity, σ, is such that the inequalities,

$$\frac{1}{\sigma t} << 1 \quad , \quad \frac{V}{\sigma L} << 1 \quad , \tag{5.8}$$

hold, then the terms $\frac{1}{c}\frac{\partial\vec{E}}{\partial t}$ and $\frac{4\pi\rho_e\vec{v}}{c}$ can be neglected in comparison with $\frac{4\pi\sigma\vec{E}}{c}$. For the interplanetary plasma at 1A.U., $\sigma \sim 10^{14}$/sec. (Alfven and Falthammar, 1963), $v \sim 10^7$cm./sec., $L \sim 10^7$cm., and $t \sim 2$ sec. For these values, the inequalities (5.8) easily hold. Equation (5.6) can therefore be written as,

$$\vec{\nabla}\times\vec{B} = \frac{4\pi\sigma}{c}\left(\vec{E} + \frac{1}{c}\vec{v}\times\vec{B}\right) \quad ,$$

or,

$$\vec{E} = \frac{1}{c}\left[\frac{c^2}{4\pi\sigma}\vec{\nabla}\times\vec{B} - \vec{v}\times\vec{B}\right] \quad . \tag{5.9}$$

This expression for $\vec{E}$ can now be substituted into Equation (5.3) to give,

$$\frac{\partial B}{\partial t} = \vec{\nabla}\times(\vec{v}\times\vec{B}) - \vec{\nabla}\times\left[\frac{c^2}{4\pi\sigma}\vec{\nabla}\times\vec{B}\right] \quad . \tag{5.10}$$

This equation is known as the induction equation and is basic to magnetohydrodynamics. The relative order of magnitude of the terms in the induction equation can be estimated for the interplanetary plasma. In terms of the characteristic values, the induction equation can be written as,

$$\frac{1}{t} \simeq \frac{V}{L} - \frac{c^2}{4\pi\sigma L^2} \quad ,$$

or

$$\frac{L}{Vt} \simeq 1 - \frac{c^2}{4\pi\sigma VL} \quad .$$

$\frac{L}{Vt} \sim 1$ for the interplanetary plasma at 1A.U. and the second term on the right side is very much less than unity. The magnetic Reynold's number, R_m, is defined as,

$$R_m \equiv \frac{4\pi\sigma VL}{c^2} \quad .$$

So, for large values of the magnetic Reynold's number, the second term on the right side of Equation (5.10) may be neglected, leaving,

$$\frac{\partial \vec{B}}{\partial t} = \vec{\nabla} \times (\vec{v} \times \vec{B}) \quad , \tag{5.11}$$

for the case of the solar wind flow past the magnetosphere.

The remaining basic equations of magnetohydrodynamics are statements of mass, momentum, and energy conservation in addition to an equation of state. These equations for an ideal gas are respectively:

$$\frac{\partial \rho}{\partial t} + \vec{\nabla} \cdot (\rho \vec{v}) = 0 \quad , \tag{5.12}$$

$$\frac{d}{dt}(\rho \vec{v}) = \vec{\nabla} \cdot \vec{p} + \rho_e \vec{E} + \frac{1}{c} (\vec{J} \times \vec{B}) \quad , \tag{5.13}$$

$$\frac{d}{dt}\left(\rho \varepsilon + \rho \frac{v^2}{2}\right) = - \vec{\nabla} \cdot \vec{q} + \vec{\nabla} \cdot (\vec{p} \cdot \vec{v}) + \vec{E} \cdot \vec{J} \quad , \tag{5.14}$$

$$p = \rho R T \quad , \tag{5.15}$$

where ρ is the mass density, $\overleftrightarrow{p}$ is the pressure tensor, $\vec{q}$ is the heat flux vector, and ε is the internal energy.

The pressure tensor is written in the form used in hydrodynamics:

$$\left(\overleftrightarrow{p}\right)_{ij} = - p \delta_{ij} + \tau_{ij} \quad , \tag{5.16}$$

where δ_{ij} is the Kronecker delta, p is the isotropic pressure,

and τ_{ij} is the viscous stress tensor. The viscous stress tensor is written as (Landau and Lifshitz, 1959),

$$\tau_{ij} = \eta\left(\frac{\partial v_i}{\partial x_j} + \frac{\partial v_j}{\partial x_i} - \frac{2}{3}\frac{\partial v_k}{\partial x_k}\delta_{ij}\right) + \zeta\frac{\partial v_k}{\partial x_k}\delta_{ij} \quad . \tag{5.17}$$

With the aid of Equation (5.9) it follows that,

$$E \leq \max\left|\frac{cB}{\sigma L}, \frac{v_B}{c}\right| \quad ,$$

and that,

$$\frac{1}{c}\frac{\partial \vec{E}}{\partial t} \leq \max\left|\frac{B}{\sigma L t}, \frac{v^2}{c^2}\frac{B}{L}\right| \quad ,$$

$$\frac{4\pi\rho_e v}{c} \leq \max\left|\frac{Bv}{\sigma L}, \frac{v^2}{c^2}\frac{B}{L}\right| \quad .$$

The relative sizes of the magnetic and electric forces in Equation (5.13) may now be estimated. These terms become,

$$\frac{1}{c}(\vec{J}\times\vec{B}) = \frac{1}{4\pi}(\vec{\nabla}\times\vec{B})\times\vec{B} \sim \frac{B^2}{L} \quad ,$$

$$\rho_e\vec{E} = \frac{1}{4\pi}\vec{E}(\vec{\nabla}\cdot\vec{E}) \sim \frac{E^2}{L} \sim \frac{B^2}{L}\max\left|\left(\frac{c}{\sigma L}\right)^2, \frac{v^2}{c^2}\right| = \frac{B^2}{L}\max\left|\frac{v}{\sigma L}\frac{1}{R_m}, \frac{v^2}{c^2}\right| \quad .$$

Since $\frac{v^2}{c^2} << 1$ and $R_m >> 1$, it turns out that,

$$E^2 << B^2$$

and the electric force in the equations of motion may be neglected

in comparison with the magnetic force. The Joule heat, $\vec{E}\cdot\vec{J}$ in Equation (5.14) may also be neglected following some similar arguments. With the added assumption of incompressibility the Equations (5.12)-(5.14) become:

$$(\vec{\nabla}\cdot\vec{v}) = 0 \quad , \tag{5.18}$$

$$\rho \frac{d\vec{v}}{dt} = \vec{\nabla}\cdot\overleftrightarrow{p} + \frac{1}{4\pi}(\vec{\nabla}\times\vec{B})\times\vec{B} \quad , \tag{5.19}$$

$$\rho \frac{d}{dt}\left(\varepsilon + \frac{v^2}{2}\right) = -\vec{\nabla}\cdot\vec{q} + \vec{\nabla}\cdot(\overleftrightarrow{p}\cdot\vec{v}) \quad . \tag{5.20}$$

Equation (5.20) may be written in the form,

$$\rho T \frac{ds}{dt} = -\vec{\nabla}\cdot\vec{q} + \Phi \quad , \tag{5.21}$$

where s is the entropy of the ideal gas and,

$$\Phi = \frac{1}{2}\tau_{ij}\left(\frac{\partial v_i}{\partial x_j} + \frac{\partial v_j}{\partial x_i}\right) \quad .$$

With the assumptions of low viscosity and no heat flux the magneto-hydrodynamic equations become:

$$\vec{\nabla}\cdot\vec{v} = 0 \quad , \tag{5.22}$$

$$\rho \frac{d\vec{v}}{dt} = -\vec{\nabla}p + \frac{1}{4\pi}(\vec{\nabla}\times\vec{B})\times\vec{B} \quad , \tag{5.23}$$

$$\frac{\partial\vec{B}}{\partial t} = \vec{\nabla}\times(\vec{v}\times\vec{B}) \quad . \tag{5.24}$$

CHAPTER 6

KELVIN-HELMHOLTZ INSTABILITY

6.1 Instability Condition

One of the most interesting regions of the earth's environment in space from the point of view of solar-terrestrial relationships is the boundary between the interplanetary medium and the geomagnetic field. Events occurring at this boundary are forerunners of events which take place in the ionosphere and at the surface of the earth. A better understanding of the magnetopause will therefore lead to a better understanding of the related processes in the ionosphere and the variations of the geomagnetic field at the surface of the earth.

The sides of the magnetosphere experience the magnetosheath plasma flowing nearly parallel to them in a manner analagous to a plane discontinuous velocity flow boundary. Following Chandrasekhar (1961), the conditions for stability of such an interface will be developed.

The following assumptions will be made: a planar surface; magnetohydrodynamic fluid behavior of the solar wind and the magnetospheric medium; no viscous forces; no gravitational forces; individual constant densities and velocities for each medium; magnetic fields parallel to the boundary imbedded within each medium; infinite conductivity for each medium; imcompressibility in each medium; infinitely thin boundary; and isotropic pressure. A Cartesian coordinate system is used with the fluid velocities directed along the X-direction and the Z-axis normal to the boundary.

With the above assumptions and the Maxwell equation,

$$\vec{\nabla}\times\vec{B} = \frac{4\pi}{C}\vec{J},$$

the force acting on a unit volume of fluid in C.G.S. units becomes:

$$\rho\frac{d\vec{U}}{dt} = -\vec{\nabla}p + \frac{1}{4\pi}(\vec{\nabla}\times\vec{B})\times\vec{B},$$

where ρ is the mass density, $\vec{U}$ is the velocity of the fluid element, p is the pressure, and $\vec{B}$ is the magnetic induction.

The induction equation may be obtained from the Maxwell equation,

$$\vec{\nabla}\times\vec{E} = -\frac{1}{C}\frac{\partial\vec{B}}{\partial t},$$

by replacing $\vec{E}$ by $-\frac{1}{C}(\vec{U}\times\vec{B})$, since the assumption of infinite conductivity reduces Ohm's Law to,

$$\vec{E} + \frac{1}{C}\vec{U}\times\vec{B} = 0.$$

Substituting this expression for $\vec{E}$ gives,

$$\frac{\partial\vec{B}}{\partial t} + (\vec{U}\cdot\vec{\nabla})\vec{B} = (\vec{B}\cdot\vec{\nabla})\vec{U}$$

after using a vector identity.

The three components of the force and induction equations, and the equation of incompressibility (i.e. $\vec{\nabla}\cdot\vec{U} = 0$), give seven

independent equations. If the velocity, magnetic field, and pressure are perturbed and are considered to vary according to the single Fourier component,

$$e^{i(k_x x + k_y y + \omega t)}$$

the equations may then be linearized and solved giving a dispersion relation for the surface waves.

The x, y, and z components of the force equation are, respectively,

$$\rho\frac{\partial U_x}{\partial t} + \rho\{U_x\frac{\partial}{\partial x} + U_y\frac{\partial}{\partial y} + U_z\frac{\partial}{\partial z}\}U_x - \frac{1}{4\pi}\{B_y(\frac{\partial}{\partial y}B_x - \frac{\partial}{\partial x}B_y) +$$

$$B_z(\frac{\partial}{\partial z}B_x - \frac{\partial}{\partial x}B_z)\} = -\frac{\partial}{\partial x}p \quad ,$$

$$\rho\frac{\partial U_y}{\partial t} + \rho\{U_x\frac{\partial}{\partial x} + U_y\frac{\partial}{\partial y} + U_z\frac{\partial}{\partial z}\}U_y - \frac{1}{4\pi}\{B_x(\frac{\partial}{\partial x}B_y - \frac{\partial}{\partial y}B_x) +$$

$$B_z(\frac{\partial}{\partial z}B_y - \frac{\partial}{\partial y}B_z)\} = -\frac{\partial}{\partial y}p \quad ,$$

$$\rho\frac{\partial U_z}{\partial t} + \rho\{U_x\frac{\partial}{\partial x} + U_y\frac{\partial}{\partial y} + U_z\frac{\partial}{\partial z}\}U_z - \frac{1}{4\pi}\{B_x(\frac{\partial}{\partial x}B_z - \frac{\partial}{\partial z}B_x) +$$

$$B_y(\frac{\partial}{\partial y}B_z - \frac{\partial}{\partial z}B_y)\} = -\frac{\partial}{\partial z}p \quad .$$

Similarly, the components of the induction equation may be written as,

$$\frac{\partial B_x}{\partial t} + (\vec{U}\cdot\vec{\nabla})B_x = (\vec{B}\cdot\vec{\nabla})U_x \quad ,$$

$$\frac{\partial B_y}{\partial t} + (\vec{U}\cdot\vec{\nabla})B_y = (\vec{B}\cdot\vec{\nabla})U_y \quad ,$$

$$\frac{\partial B_z}{\partial t} + (\vec{U}\cdot\vec{\nabla})B_z = (\vec{B}\cdot\vec{\nabla})U_z \quad .$$

The equation expressing incompressibility remains as,

$$\vec{\nabla}\cdot\vec{U} = 0.$$

When the perturbations,

$$(U_x, 0, 0) \rightarrow (U_x + u, v, w)$$

$$(B_x, B_y, 0) \rightarrow (B_x + b_x, B_y + b_y, b_z)$$

$$p \rightarrow p + \delta p,$$

are applied and the first order terms in the perturbed quantities u, v, w, b_x, b_y, b_z, and δp are retained and second and higher order terms are neglected, the equations become, in the order as they appeared in the preceding;

$$\rho\frac{\partial u}{\partial t} + \rho U_x\frac{\partial u}{\partial x} + \rho w\frac{\partial U}{\partial z} - \frac{1}{4\pi}B_y\left(\frac{\partial b_x}{\partial y} - \frac{\partial b_y}{\partial x}\right) = -\frac{\partial}{\partial x}\delta p,$$

$$\rho\frac{\partial v}{\partial t} + \rho U_x\frac{\partial v}{\partial x} - \frac{B_x}{4\pi}\left(\frac{\partial b_y}{\partial x} - \frac{\partial b_x}{\partial y}\right) = -\frac{\partial}{\partial y}\delta p,$$

$$\rho\frac{\partial w}{\partial t} + \rho U_x\frac{\partial w}{\partial x} - \frac{B_x}{4\pi}\left(\frac{\partial b_z}{\partial x} - \frac{\partial b_x}{\partial z}\right) - \frac{B_y}{4\pi}\left(\frac{\partial b_z}{\partial y} - \frac{\partial b_y}{\partial z}\right) = -\frac{\partial}{\partial z}\delta p,$$

$$\frac{\partial b_x}{\partial t} + U_x\frac{\partial b_x}{\partial x} = B_x\frac{\partial u}{\partial x} + b_z\frac{\partial U_x}{\partial z} + B_y\frac{\partial u}{\partial y},$$

$$\frac{\partial b_y}{\partial t} + U_x\frac{\partial b_y}{\partial x} = B_y\frac{\partial v}{\partial y} + B_x\frac{\partial v}{\partial x},$$

$$\frac{\partial b_z}{\partial t} + U_x\frac{\partial b_z}{\partial x} + B_x\frac{\partial w}{\partial x} + B_y\frac{\partial w}{\partial y},$$

$$\frac{\partial u}{\partial x} + \frac{\partial v}{\partial y} + \frac{\partial w}{\partial z} = 0.$$

Putting in the assumed form of the perturbations,

$e^{i(k_x x + k_y y + \omega t)}$, the equations become:

$$i\rho(\omega + k_x U_x)u + \rho w DU_x - \frac{B_y}{4\pi}(ik_y b_x - ik_x b_y) = -ik_x\delta p \qquad (6.1)$$

$$i\rho(\omega + k_x U_x)v - \frac{B_x}{4\pi}(ik_x b_y - ik_y b_x) = -ik_y\delta p \qquad (6.2)$$

$$i\rho(\omega + k_x U_x)w - \frac{B_x}{4\pi}(ik_x b_z - Db_x) - \frac{B_y}{4\pi}(ik_y b_z - Db_y) = -D\delta p \qquad (6.3)$$

$$i(\omega + k_x U_x)b_x = ik_x B_x u + b_z DU_x + ik_y B_y u \qquad (6.4)$$

$$i(\omega + k_x U_x)b_y = ik_y B_y v + ik_x B_x v \qquad (6.5)$$

$$i(\omega + k_x U_x)b_z = (ik_x B_x + ik_y B_y)w \qquad (6.6)$$

$$i(k_x u + k_y v) + Dw = 0 \qquad (6.7)$$

where $D \equiv \frac{d}{dz}$.

Using Equations (6.4), (6.5), and (6.6), the perturbations b_x, b_y, and b_z may be eliminated from Equations (6.1), (6.2), and (6.3). If $\phi = ik_x v - ik_y u$, these equations become:

$$i\rho(\omega + k_x U_x)u + \rho w DU_x - \left(\frac{B_y}{4\pi}\frac{k_x B_x + k_y B_y}{\omega + k_x U_x}\right)\left(\frac{k_y w}{\omega + k_x U_x} DU_x - \phi\right) = - ik_x p \quad , \tag{6.8}$$

$$i\rho(\omega + k_x U_x)v - \frac{B_x}{4\pi}\left(\frac{k_x B_x + k_y B_y}{\omega + k_x U_x}\right)\left(\phi - \frac{k_y w}{\omega + k_x U_x} DU_x\right) = - ik_y \delta p \quad , \tag{6.9}$$

$$i\rho(\omega + k_x U_x)w - \frac{ik_x B_x (k_x B_x + k_y B_y)}{4\pi(\omega + k_x U_x)} w + \frac{B_x D}{4\pi}\left(\left(\frac{k_x B_x + k_y B_y}{\omega + k_x U_x}\right)\left(u - i\frac{w}{\omega + k_x U_x} DU\right)\right) - \frac{k_y B_y (k_x B_x + k_y B_y)}{4\pi(\omega + k_x U_x)} w + \frac{B_y D}{4\pi}\left(\left(\frac{k_x B_x + k_y B_y}{\omega + k_x U_x}\right) v\right) = - D\delta p \quad . \tag{6.10}$$

Equations (6.8) and (6.9) may be combined, giving,

$$\left(\rho(\omega + k_x U_x) - \frac{(k_x B_x + k_y B_y)^2}{4\pi(\omega + k_x U_x)}\right)\phi = \frac{k_y w DU_x}{\omega + k_x U_x}\left(\rho(\omega + k_x U_x) - \frac{(k_x B_x + k_y B_y)^2}{4\pi(\omega + k_x U_x)}\right) ,$$

from which it is clear that

$$\phi = \frac{k_y w DU_x}{\omega + k_x U_x} \quad .$$

Using this expression for ϕ , Equations (6.8) and (6.9) may be recombined to give,

$$- \rho (ik_x U + ik_y v)(\omega + k_x U_x) - k_x \rho w DU_x = ik^2 \delta p,$$

where $k^2 = k_x^2 + k_y^2$. This equation finally becomes, after using Equation (6.7),

$$\rho (\omega + k_x U_x) Dw - \rho k_x w DU_x = ik^2 \delta p \quad . \tag{6.11}$$

The perturbation in pressure, δp, may now be eliminated from Equations (6.10) and (6.11) to give,

$$D\left[\rho (\omega + k_x U_x) Dw - \rho k_x w DU_x\right] = k^2 \rho (\omega + k_x U_x) w +$$

$$\frac{(k_x B_x + k_y B_y)^2}{4\pi} \left[D\left(\frac{Dw}{\omega + k_x U_x} \right) - \frac{k^2 w}{\omega + k_x U_x} \right] -$$

$$k_x \left[\frac{(k_x B_x + k_y B_y)^2}{4\pi} D\left(\frac{wDU}{(\omega + k_x U_x)^2} \right) \right] \quad . \tag{6.12}$$

This equation may now be applied to each region separately as depicted in Figure (6.1) to find the form of the perturbation w. Since the velocities are constant within each region, $DU_x = 0$. The equation then becomes,

Figure 6.1

Illustration of the coordinate system used for development of Kelvin-Helmholtz instability condition.

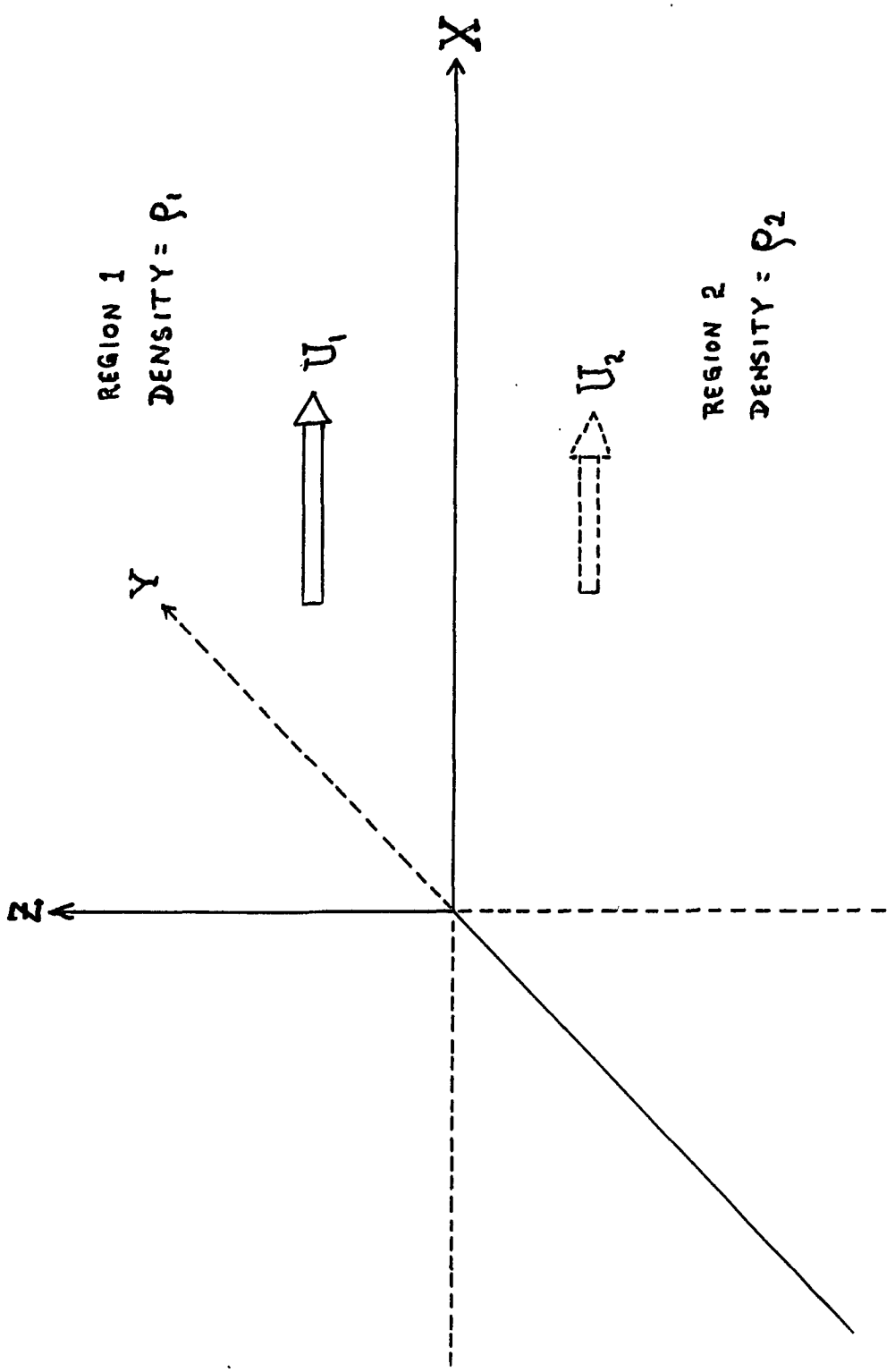
X
REGION 1
DENSITY = ρ_1
U_1
U_2
REGION 2
DENSITY = ρ_2
Y
Z

$$\left\{\rho\,(\omega + k_x U_x) - \frac{(k_x B_x + k_y B_y)^2}{4\pi(\omega + k_x U_x)}\right\}(D^2 - k^2)w = 0$$

or,

$$(D^2 - k^2)w = 0.$$

The solution may be written as,

$$w = Ae^{+kz} + Be^{-kz} .$$

The separate solutions in each region become,

$$w_1 = Be^{-kz} \qquad \text{for } z > 0$$

$$w_2 = Ae^{+kz} \qquad \text{for } z < 0 .$$

The quantity $\dfrac{w}{(\omega + k_x U_x)i}$ must be continuous across the surface because of the following consideration. If the equation of the interface, after the perturbation is applied, is to remain single-valued, then w may be related to the height of the interface above the initial planar surface. Let δz represent the deviation from the initial planar interface as shown in Figure (6.2). The relation between z and w is simply

$$w = \frac{d}{dt}\delta z \quad ,$$

Figure 6.2

Illustration of the definition of δ_z.

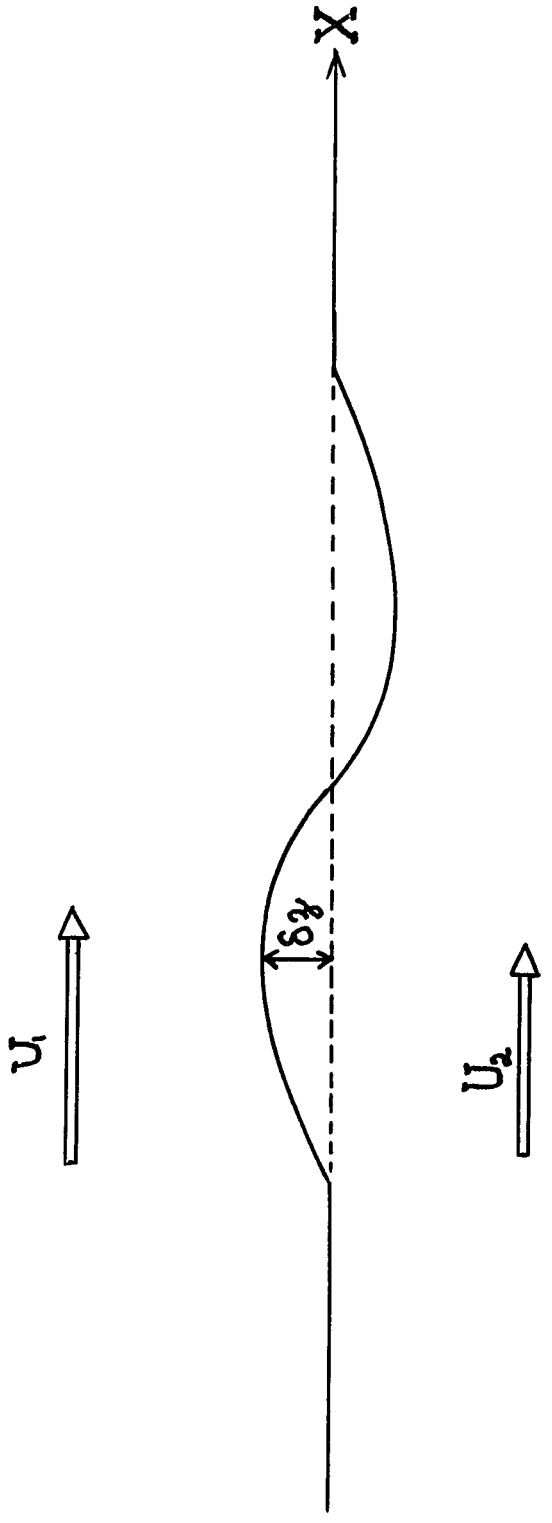
X
δz
U1
U2

where $\frac{d}{dt}$ is the full convective derivative. This relation can then be expressed as,

$$w = \frac{\partial}{\partial t}\delta z + U_x \frac{\partial}{\partial x}\delta z \quad ,$$

and when δz is considered to take part in the perturbation, the derivatives of δz may then be taken. The equation then becomes,

$$w = i(\omega + k_x U_x)\delta z \quad .$$

If δz is to be continuous and single-valued, then $\frac{w}{i(\omega + k_x U_x)}$ must also possess these qualities. The solutions for each region may then be written as,

$$w_1 = c_1(\omega + k_x U_1)e^{-kz} \qquad \text{for } z > 0$$

$$w_2 = c_2(\omega + k_x U_2)e^{+kz} \qquad \text{for } z < 0 \quad .$$

Now that w has been obtained in each region, Equation (6.12) may be integrated across the interface from $-\varepsilon$ to $+\varepsilon$ where the limit as ε approaches zero of the integral will be taken. Certain quantities in the integral will be continuous across the interface while others are discontinuous. Let f be a continuous function across the interface as shown in Figure (6.3). Integrals like the following will be zero:

$$\lim_{\varepsilon \to 0} \int_{-\varepsilon}^{+\varepsilon} f \, dz$$

Figure 6.3

Integration of a continuous function f between $-\varepsilon$ and $+\varepsilon$.

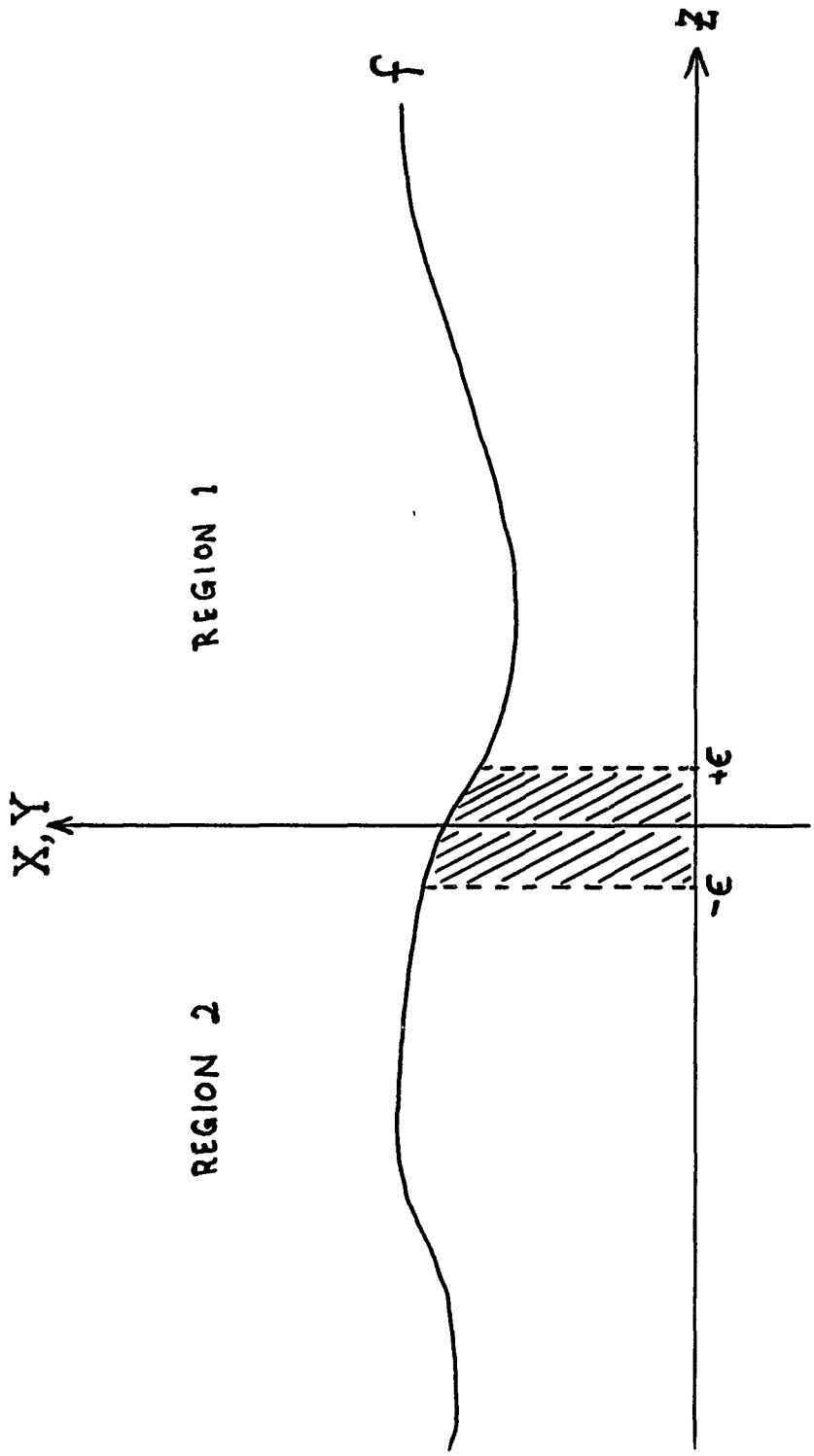
f
Z
REGION 1
X, Y
+ε
-ε
REGION 2

$$\lim_{\varepsilon \to 0} \int_{-\varepsilon}^{+\varepsilon} \frac{df}{dz}\, dz = \lim_{\varepsilon \to 0} \left[f \right]_{-\varepsilon}^{+\varepsilon} \quad .$$

If g is used now to represent a discontinuous function across the interface as shown in Figure (6.4) then the following integral is zero;

$$\lim_{\varepsilon \to 0} \int_{-\varepsilon}^{+\varepsilon} g\, dz \quad ,$$

but the next integral is not zero and represents the difference between the function's value on either side of the interface,

$$\lim_{\varepsilon \to 0} \int_{-\varepsilon}^{+\varepsilon} \frac{dg}{dz}\, dz = \lim_{\varepsilon \to 0} \left[g \right]_{-\varepsilon}^{+\varepsilon} = g_1 - g_2 \quad .$$

Keeping the above considerations in mind, the result of integrating Equation (6.12) is

$$\left[\rho (\omega + k_x U_x) Dw \right]_2^1 = \left[\frac{(k_x B_x + k_y B_y)^2}{4\pi} \frac{Dw}{(\omega + k_x U_x)} \right]_2^1 \quad ,$$

which becomes

$$\rho_1 (\omega + k_x U_1) Dw_1 - \rho_2 (\omega + k_x U_2) Dw_2 = \frac{(k_x B_{1x} + k_y B_{1y})^2}{4\pi} \frac{Dw_1}{(\omega + k_x U_1)} -$$

$$\frac{(k_x B_{1x} + k_y B_{1y})^2}{4\pi} \frac{Dw_1}{(\omega + k_x U_2)} \quad . \qquad (6.13)$$

At a particular x, y coordinate the deviation of the interface from the original position in one region is just the

Figure 6.4

Integration of a discontinuous function g between $-\varepsilon$ and $+\varepsilon$.

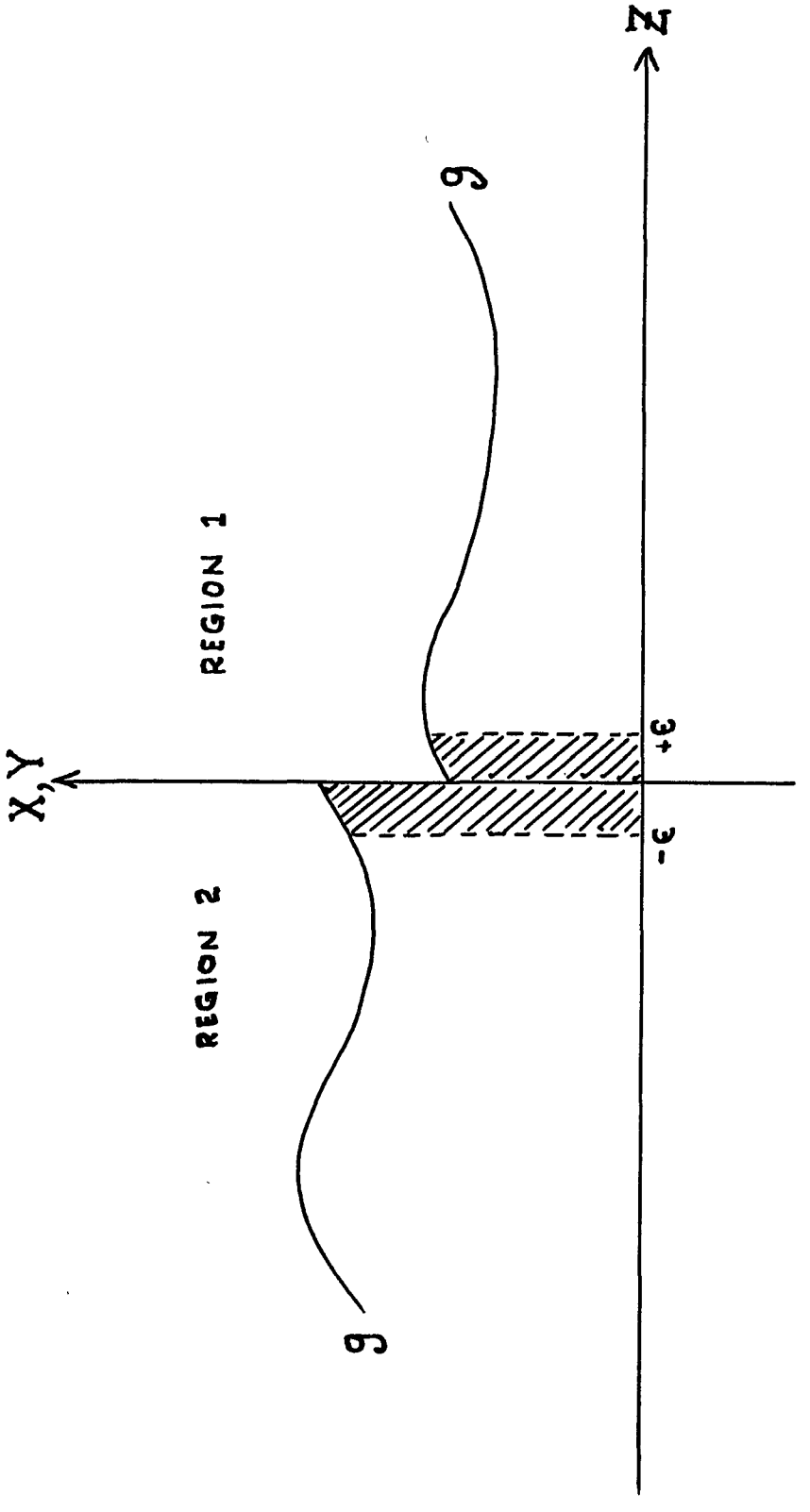
Z
g
REGION 1
+ε
X, Y
-ε
REGION 2
g

negative of that deviation in the other region. The w's in each region are,

$$w_1 = c_1(\omega + k_x U_1)e^{-k\delta z}$$

$$w_2 = c_2(\omega + k_x U_2)e^{-k\delta z} \quad ,$$

if a positive δz is considered. It is also known that $\frac{w}{i(\omega + k_x U_x)}$ is continuous so that

$$\frac{w_1}{i(\omega + k_x U_1)} = \frac{w_2}{i(\omega + k_x U_2)} \quad ,$$

therefore $c_1 = c_2 \equiv c$. The w's in each region now become,

$$w_1 = c(\omega + k_x U_1)e^{-kz}$$

$$w_2 = c(\omega + k_x U_2)e^{+kz}$$

and

$$Dw_1 = - kc(\omega + k_x U_1)e^{-kz}$$

$$Dw_2 = + kc(\omega + k_x U_2)e^{+kz} \quad .$$

The last two equations may now be substituted into Equation (6.13), however, the exponential dependence will vanish since the limit as ε goes to zero was taken. When this is done, the following

equation is obtained:

$$\rho_1(\omega + k_x U_1)^2 + \rho_2(\omega + k_x U_2)^2 - \frac{1}{4\pi}(\vec{k}\cdot\vec{B}_1)^2 + (\vec{k}\cdot\vec{B}_2)^2 = 0 \quad ,$$

where $\vec{k}\cdot\vec{B} = k_x B_x + k_y B_y$. This quadratic equation in ω may be put into the form,

$$(\rho_1 + \rho_2)\omega^2 + 2\left(\rho_1(k_x U_1) + \rho_2(k_x U_2)\right)\omega + \rho_1 k_x^2 U_1^2 + \rho_2 k_x^2 U_2^2 -$$

$$\frac{1}{4\pi}\left((\vec{k}\cdot\vec{B}_1)^2 + (\vec{k}\cdot\vec{B}_2)^2\right) = 0 \quad .$$

The frequency ω may now be solved for in terms of the other parameters. The solution is,

$$\omega = \frac{-2(\rho_1 k_x U_1 + \rho_2 k_x U_2)}{2(\rho_1 + \rho_2)} \pm$$

$$\frac{\sqrt{4(\rho_1 k_x U_1 + \rho_2 k_x U_2)^2 - 4(\rho_1 + \rho_2)\left(\rho_1 k_x^2 U_1^2 + \rho_2 k_x^2 U_2^2 - \frac{1}{4\pi}\left((\vec{k}\cdot\vec{B}_1)^2 + (\vec{k}\cdot\vec{B}_2)^2\right)\right)}}{2(\rho_1 + \rho_2)} \qquad (6.14)$$

If ω should ever be complex, then the surface waves will grow in amplitude exponentially. The conditions under which this instability occurs may be examined by looking at the quantity under the square root. When this quantity is less than zero, then a condition for instability of the interface will have been found. After some manipulation, the condition for instability becomes,

$$(U_1 - U_2)^2 > \frac{\rho_1 + \rho_2}{\rho_1\rho_2} \frac{}{4\pi k_x^2} \left[(\vec{k}\cdot\vec{B}_1)^2 + (\vec{k}\cdot\vec{B}_2)^2 \right] \quad . \tag{6.15}$$

The most likely orientation of the wave vector $\vec{k}$ will be along the x axis since the fluid velocity is in that direction. With this in mind the inequality (6.15) may be expressed as,

$$(U_1 - U_2)^2 > \frac{(\rho_1 + \rho_2)}{4\pi\rho_1\rho_2} \left[B_1^2 \cos^2\psi_1 + B_2^2 \cos^2\psi_2 \right] \quad ,$$

where ψ_1 and ψ_2 are defined in Figure (6.5).

This inequality may now be applied to the magnetopause where the subscript S refers to the magnetosheath and the subscript M refers to the magnetospheric medium. Let the coordinate system be fixed with respect to the magnetospheric medium which means that $U_2 = 0$. For given values of the magnetic field B in either medium, the magnetopause will be more stable when the magnetic fields are lined up parallel to the solar stream flow, because then the cosine terms assume their largest values. In this case the tension of the magnetic fields tend to inhibit any growing waves on the surface whose wave vector is directed along with the solar stream velocity. The higher the solar stream velocity is, the greater will the tendency be for instability. Without the magnetic field, stability is impossible.

The angle between the solar stream flow and the magnetospheric magnetic field varies from place to place on the magnetopause and also varies through the course of the day at any one particular place. Some regions of the magnetopause are therefore more susceptible to this instability than others. In addition

Figure 6.5

Definition of the angles Ψ_1 and Ψ_2.

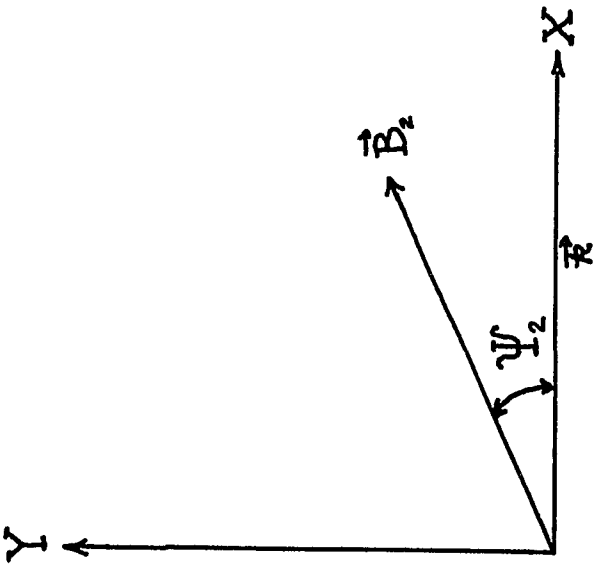
X
$\vec{B}_2$
$\vec{k}$
ψ_2
Y

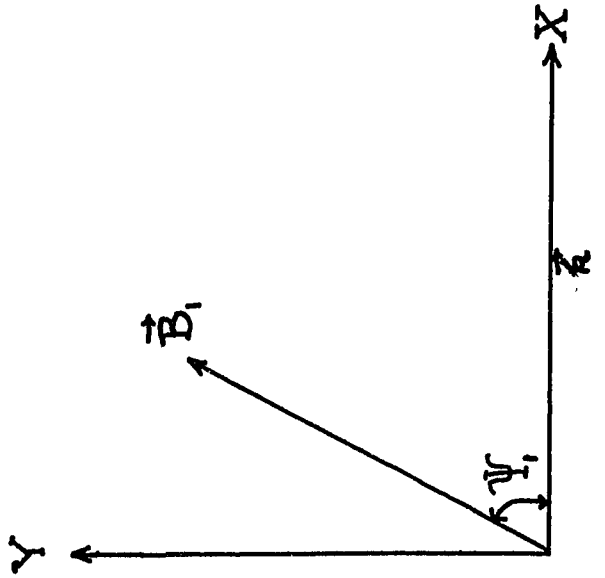
X
$\vec{B}_1$
$\vec{k}$
ψ_1
Y

to the above considerations there is a variation of this angle throughout the year for a particular time of the day at a specific region of the magnetopause.

6.2 Growth Rate of the Instability

The growth rate of the instability may be determined from Equation (6.14). The imaginary part of the frequency ω can be written as,

$$\omega_i = \frac{k_x}{(\rho_S + \rho_M)} \left\{ \rho_S \rho_M U^2 - \frac{(\rho_S + \rho_M)}{4\pi} (B_S^2 \cos^2\Psi_S + B_M^2 \cos^2\Psi_M) \right\}^{\frac{1}{2}} . \tag{6.16}$$

If the densities are equal on either side of the boundary, Equation (6.16) becomes,

$$\omega_i = k_x \left\{ \frac{U^2}{4} - \frac{1}{8\pi\rho} (B_S^2 \cos^2\Psi_S + B_M^2 \cos^2\Psi_M) \right\}^{\frac{1}{2}} . \tag{6.17}$$

The growth rate is proportional to, $\omega_i e^{\omega i t}$.

The waves will grow to e times their initial amplitude in a time given by $1/\omega_i$. This characteristic growth time may be written as,

$$t_g = \frac{\lambda}{2\pi \left\{ \frac{U^2}{4} - \frac{1}{8\pi\rho} (B_S^2 \cos^2\Psi_S + B_M^2 \cos^2\Psi_M) \right\}^{\frac{1}{2}}} . \tag{6.18}$$

If the quantity under the square root in (6.18) is denoted by I_x, the instability excess, the equation becomes,

$$t_g = \frac{\lambda}{2\pi I_x^{\frac{1}{2}}} \quad . \tag{6.19}$$

For a wavelength of 1000 km. and an instability excess of 1 km./sec., the characteristic growth time is approximately 160 seconds.

CHAPTER 7

THE CAUSE OF THE SEMIANNUAL VARIATION OF GEOMAGNETIC ACTIVITY

7.1 The Axial-Equinoctial Controversy

The semiannual variation of geomagnetic activity is a well established phenomenon, having maxima near the equinoxes and minima near the solstices. There have been two views as to the cause of this semiannual variation.

Cortie's (1912) "axial" hypothesis explained that the geomagnetic variation was associated with changes of the earth's heliographic latitude (maximum north heliographic latitude of $7^{\circ}.2$ on September 7 and maximum south heliographic latitude of $7^{\circ}.2$ on March 6). At the times of these maxima the earth would be more favorably situated with respect to the solar streams coming from the active regions between 10 and 20 degrees north and south heliographic latitude, thereby resulting in increased geomagnetic activity at these times. The axial hypothesis depends basically upon two things: that the solar streams cause geomagnetic activity, and that the solar streams emitted radially are not diffused very much in the interplanetary medium by the time they get to the orbit of the earth. Figure (7.1) illustrates how the earth intercepts a greater intensity of the solar streams on September 7 and March 6 than it would on December 8 and June 7. The intensity of the solar streams is taken to have maxima at 15° north and south heliographic latitudes in Figure (7.1).

Figure 7.1

Axial hypothesis: Illustrating the positions of the earth relative to solar streams at times of maximum and minimum heliographic latitude.

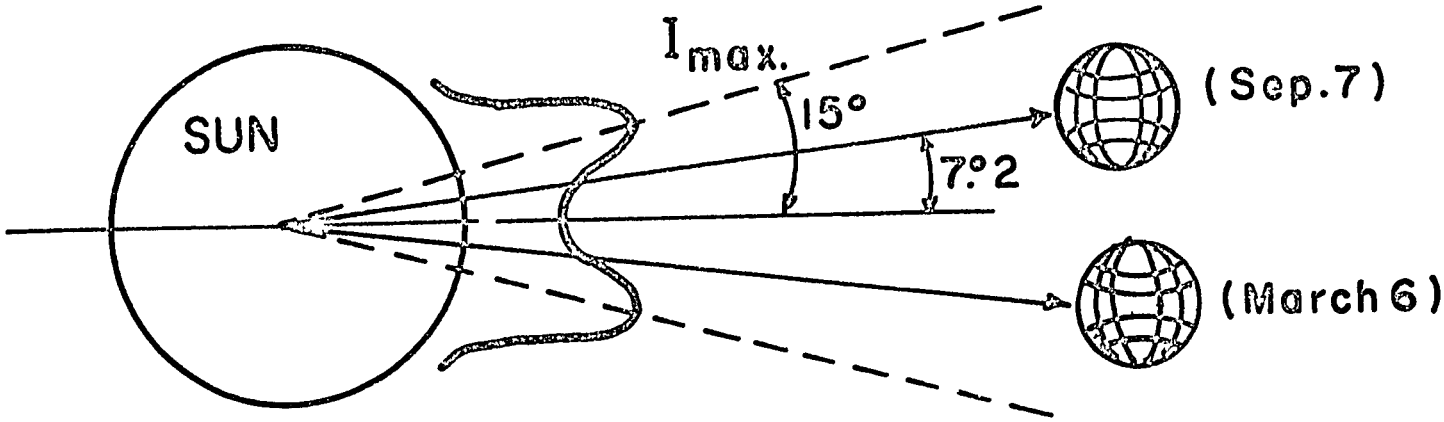
SUN
$I_{max.}$
15°
7°.2
(Sep.7)
(March 6)

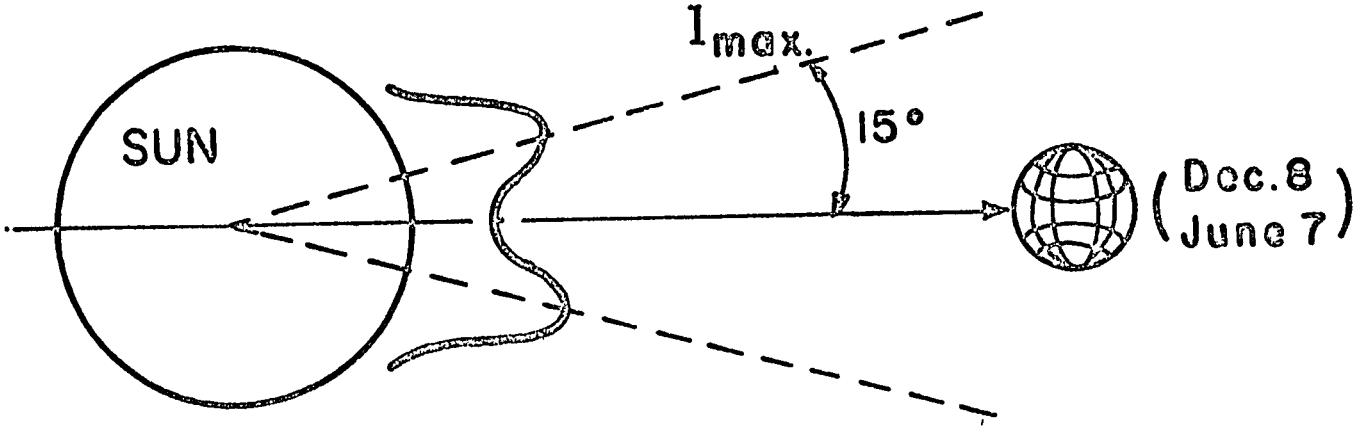
SUN
$I_{max.}$
15°
(Dec.8
June 7)

Bartels' (1932) and McIntosh's (1959) "equinoctial" hypothesis on the other hand attributes the semiannual variation to the change of the tilt of the dipole axis, the times of greater activity occurring when the dipole is perpendicular to the solar wind flow. The maximum activity occurs, therefore, twice yearly at the equinoxes. The physical mechanism is not specified. Figure (7.2) illustrates the dipole positions at the equinoxes and solstices.

There has been a continuing controversy over the correct explanation of the semiannual variation of geomagnetic activity, since the nature of the geomagnetic data makes it difficult to identify the dates of the maxima. Some authors (Priester and Cattani, 1962; Currie, 1966) have favored the axial hypothesis while others (Bartels, 1932, 1963; Meyer, 1966; Roosen, 1966; Shapiro, 1969) have favored the equinoctial hypothesis. Mishin et al. (1961) and Mishina (1967) invoke a more complicated interplay of several factors in explaining their geomagnetic analyses.

The lack of a physical mechanism to adequately explain the cause of the semiannual variation has been the major problem. A knowledge of the mechanism will identify the parameters responsible for the phenomenon and therefore make possible the understanding of the semiannual variation of geomagnetic activity.

7.2 The Kelvin-Helmholtz Hypothesis

It will be shown that the variations of Kelvin-Helmholtz instability at the boundary of the magnetosphere are due to the seasonal changes of the orientation of the earth's magnetic dipole

Figure 7.2

Equinoctial hypothesis: Illustrating the tilt of the dipole axis at the equinoxes and solstices.

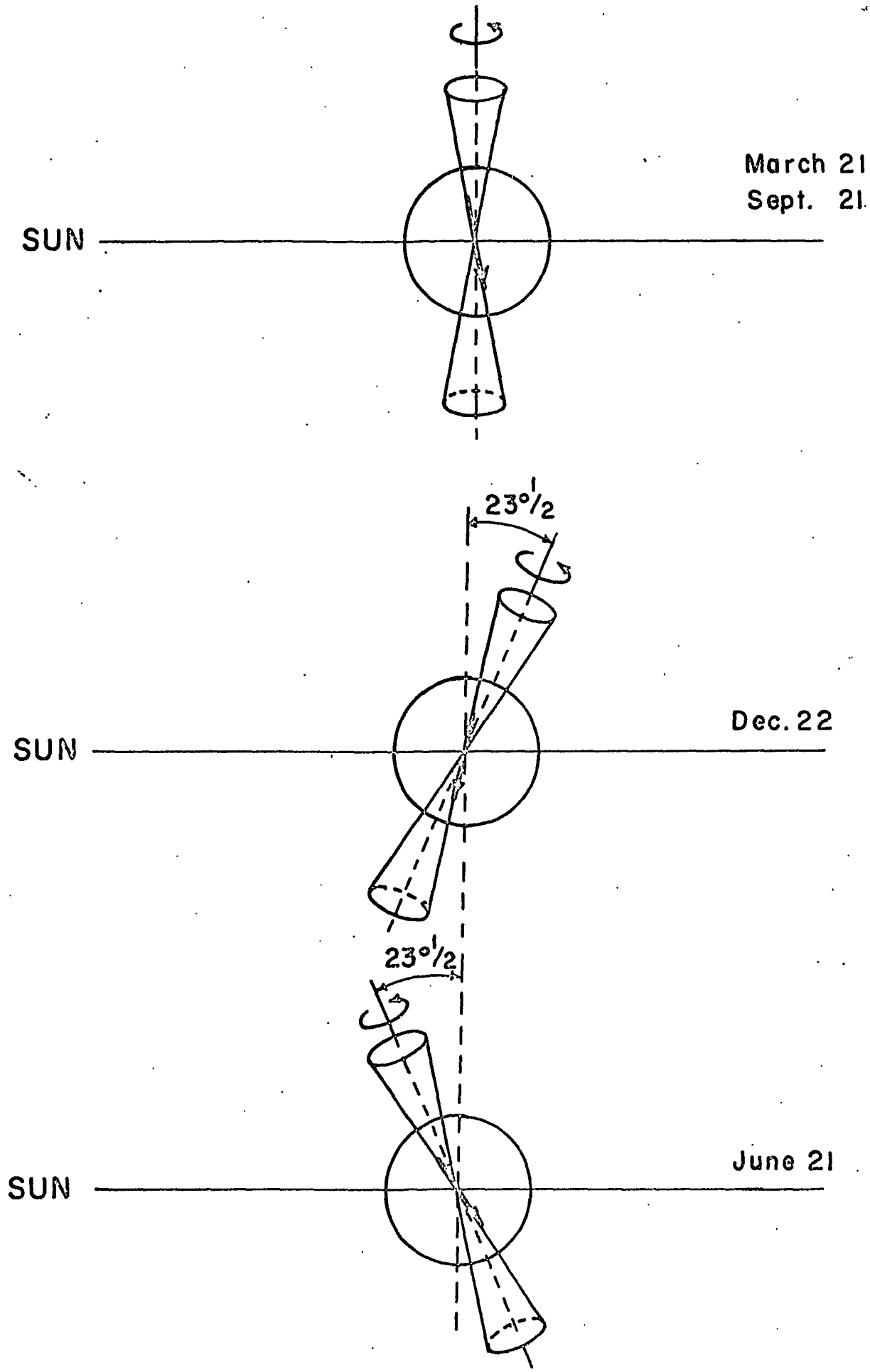
March 21
Sept. 21
SUN
23°½
Dec. 22
SUN
23°½
June 21
SUN

with respect to the solar wind flow. It is suggested that instabilities generated at the magnetopause will initiate the geomagnetic disturbance detected by surface magnetic observatories as the semiannual variation of magnetic disturbance.

Frictional or viscous-like interactions between the solar wind and the magnetosphere have been studied quantitatively by Axford (1964) and Parker (1965) based on a sound wave refraction mechanism and based on particle scattering by inhomogeneities of the magnetic field respectively. The Kelvin-Helmholtz phenomenon could possibly be the process extablishing the initial conditions in both cases.

The seasonal distribution of magnetospheric substorms may well contribute to the semiannual variation of geomagnetic activity. Akasofu (1968) cites 10 theories (see page 224) that have been suggested to explain the magnetospheric substorm. In two of these theories, Kelvin-Helmholtz instability might again serve as the intermediary between the solar wind and geomagnetic disturbance. It should not be assumed that the Kelvin-Helmholtz mechanism is exclusive, but rather in competition with other disturbance phenomena.

A number of important contributions to the Kelvin-Helmholtz instability problem have been made by Axford (1960, 1962, 1964), Sen (1963, 1964), Fejer (1963, 1964), Southwood (1968), and Talwar (1964, 1965). For a good review of this subject see Dungey (1968) and Gerwin (1968). The instability criterion developed in the preceding chapter may be applied to the magnetopause giving,

$$U^2 > \frac{\rho_S + \rho_M}{4\pi\rho_S\rho_M}\left[B_M^2 \cos^2\Psi_S + B_M^2 \cos^2\Psi_M\right] \quad .$$

Recalling the considerations of the previous chapter, the presence of parallel components of magnetic field with respect to the solar wind stream at the boundary create a stabilizing influence. If the magnetic fields were either non-existent or perpendicular to the solar stream a situation of complete instability would result for wave vectors along $\vec{U}$. Parallel components of magnetic fields therefore have a stabilizing influence on the boundary. The angle Ψ_M is a function of three quantities: the point on the magnetopause, the time of year, and the time of day. Some regions of the magnetopause are therefore more susceptible to this instability than others, and, in addition, they exhibit a time variation.

It is clear from the Kelvin-Helmholtz inequality that interplanetary fields will contribute to variations of instability. However, since seasonal variations of the interplanetary field have not been observed, any interplanetary field influence on a semiannual variation of instability will be averaged out, when considering several years of data. Short-term variations of the interplanetary magnetic field and their influences on geomagnetic activity, as observed by Fairfield (1968), Schatten and Wilcox (1967) and Wilcox et al. (1967) and explained in terms of interconnection between interplanetary and geomagnetic field lines in the manner of Dungey (1961) are by no means excluded by the

present discussion.

The association of the semiannual variation of geomagnetic activity with the seasonal variations of the angle Ψ_M in the Kelvin-Helmholtz theory will now be made. A sketch of the magnetosphere of the earth is shown in Figure (7.3). The Y - Z plane cuts a dawn-dusk cross-section through the flanks of the magnetosphere and passes through the center of the earth which is at the origin of the coordinate system. The solar wind is in the X-direction. The dipole is shown here to be along the Z-axis and perpendicular to the solar wind. This particular orientation of the dipole with respect to the solar wind will occur twice a day during the periods that the earth's rotation axis is perpendicular to the solar wind, i.e. during the equinoxes. An appropriate rotation of this coordinate system about the X-axis (solar wind direction) can always be made so that the dipole is contained in the X - Z plane and the X - Y plane intersects the magnetopause along the flanks.

Figure (7.4) is a cross-sectional view of the magnetosphere in the X - Y plane looking in the negative Z direction for the orientation of the dipole of Figure (7.3). Inside the magnetopause all along the dawn and dusk flanks the geomagnetic field lines are directed outward, or in the positive Z-direction. A local coordinate system X', Y', Z' (X' in the streaming direction, Y' perpendicular to the magnetopause, Z' = Z) may be placed anywhere along the dawn and dusk flanks. Such a coordinate system is shown at the dusk flank in Figure (7.4).

Figure 7.3

Sketch of the magnetosphere with Y - Z plane through the flanks.

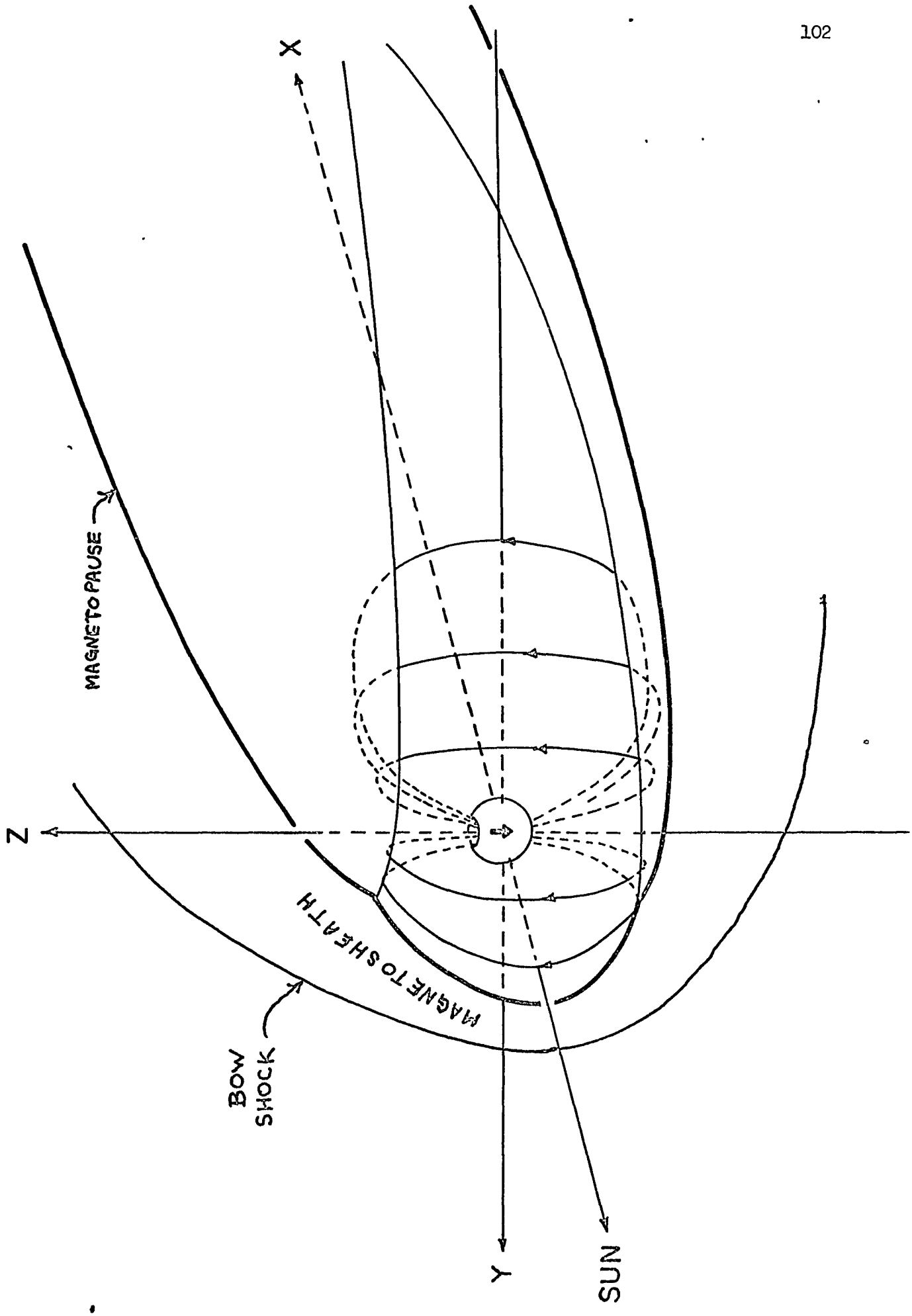
X
MAGNETOPAUSE
Z
MAGNETOSHEATH
BOW
SHOCK
Y
SUN

Figure 7.4

Sectional view of the magnetosphere in the X - Y plane with local coordinate system at the dusk flank.

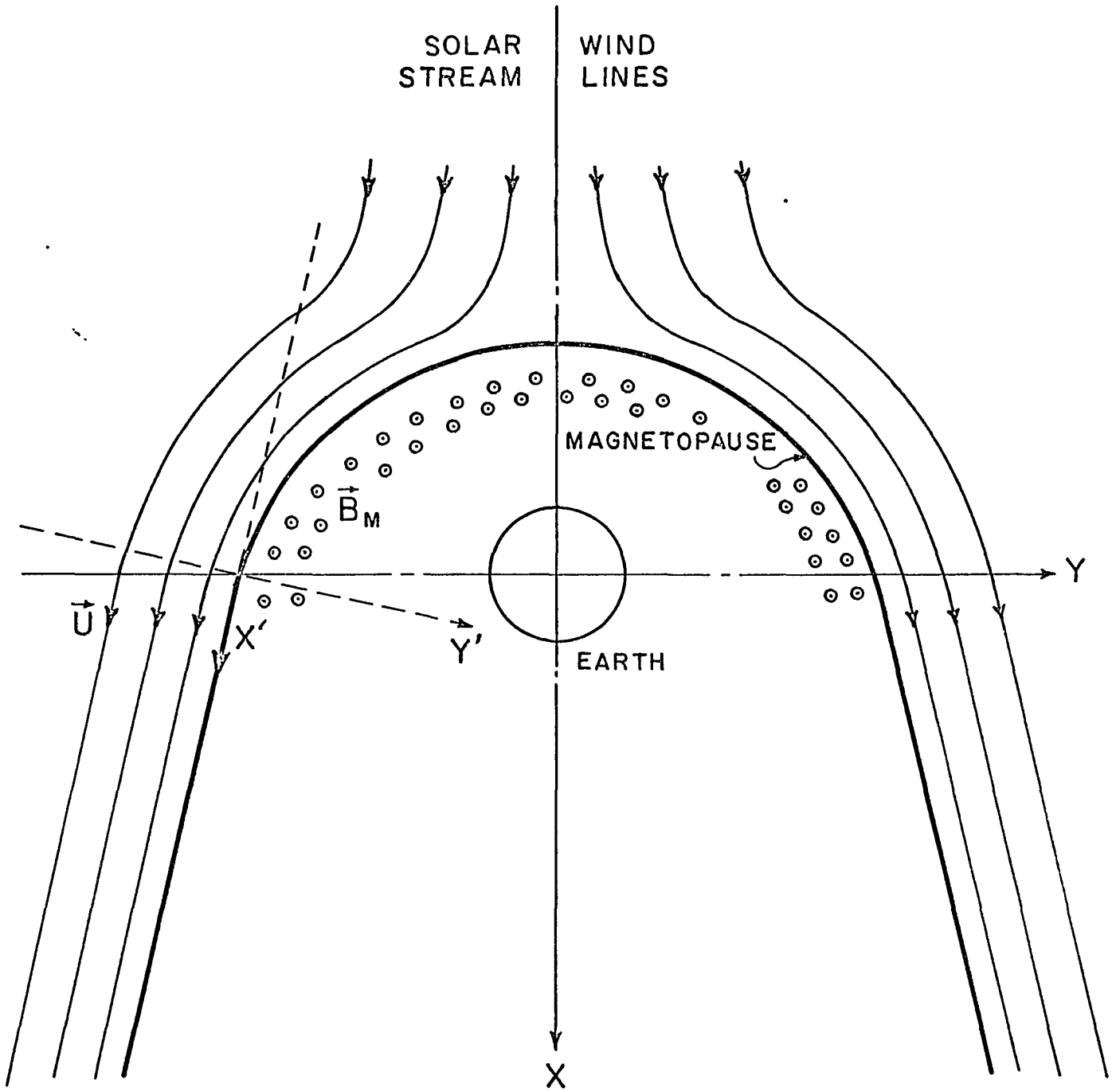
SOLAR
STREAM
WIND
LINES
MAGNETOPAUSE
$\vec{B}_M$
Y
$\vec{U}$
X'
Y'
EARTH
X

Clearly the angle $\Psi_M = 90^\circ$ at the flanks, and the inequality becomes

$$U^2 > \frac{\rho_S + \rho_M}{4\pi\rho_S\rho_M} B^2_S \cos^2\Psi_S$$

favoring instability. This value of Ψ_M occurs at 1030 and 2230 UT (sunrise and sunset at the north geomagnetic pole respectively). For this case, it is apparent that magnetospheric field lines cannot exert stabilizing influences in the $\vec{U}$ direction.

The least unstable situation at the flanks during the equinoxes occurs when $\Psi_M = 78.^\circ5$, or $101.^\circ5$. These values of Ψ_M occur at 0430 and 1630 UT (midnight and noon at the north geomagnetic pole respectively). The condition for instability now becomes,

$$U^2 > \frac{\rho_S + \rho_M}{4\pi\rho_S\rho_M}\left[B_S^2 \cos^2\Psi_S + 0.0397\, B_M^2\right] \quad .$$

Obviously, the components of field lines along $\vec{U}$ are a stabilizing influence in this case.

For the most unstable situation at the winter and summer solstices Ψ_M is 78° and 102° respectively, the former angle occurring at 1630 UT and the latter occurring at 0430 UT. The inequality can then be written as,

$$U^2 > \frac{\rho_S + \rho_M}{4\pi\rho_S\rho_M}\left[B_S^2 \cos^2\Psi_S + 0.0431 B_M^2\right] \quad .$$

The most unstable configuration at the solstices nearly corresponds to the most stable configuration at the equinoxes.

The least unstable configuration during the winter and summer solstices occurs when Ψ_M is 55° and 125° respectively, the former angle occurring at 0430 UT and the latter occurring at 1630 UT. The instability condition then becomes,

$$U^2 > \frac{\rho_S + \rho_M}{4\pi\rho_S\rho_M}\left[B_S^2 \cos^2\Psi_S + 0.329\, B_M^2\right] \quad .$$

There are other regions where the solar streaming is perpendicular to the geomagnetic field. However, these regions are exclusively at the front of the magnetosphere where the low value of solar streaming, as well as the absence of any seasonal dependence in this vicinity serve to exclude it from the present discussion.

Figure (7.5) displays the stable and unstable regions of U^2 plotted against Ψ_M alone. The values of Ψ_M during the equinoxes can correspond to unstable conditions with relatively lower values of U than at the solstices. If the other quantities in the inequality have no significant seasonal dependence, then the instability at the flanks is dependent solely upon the angle between the dipole and the sun-earth line as in the equinoctial hypothesis. However, any seasonal changes in the intensity of the solar streams (as suggested by the axial hypothesis) will have their Kelvin-Helmholtz effects. These have not been observed.

7.3 Prediction of Kelvin-Helmholtz Hypothesis

Figure 7.5

Stable and unstable regions of U^2 plotted against Ψ_m.

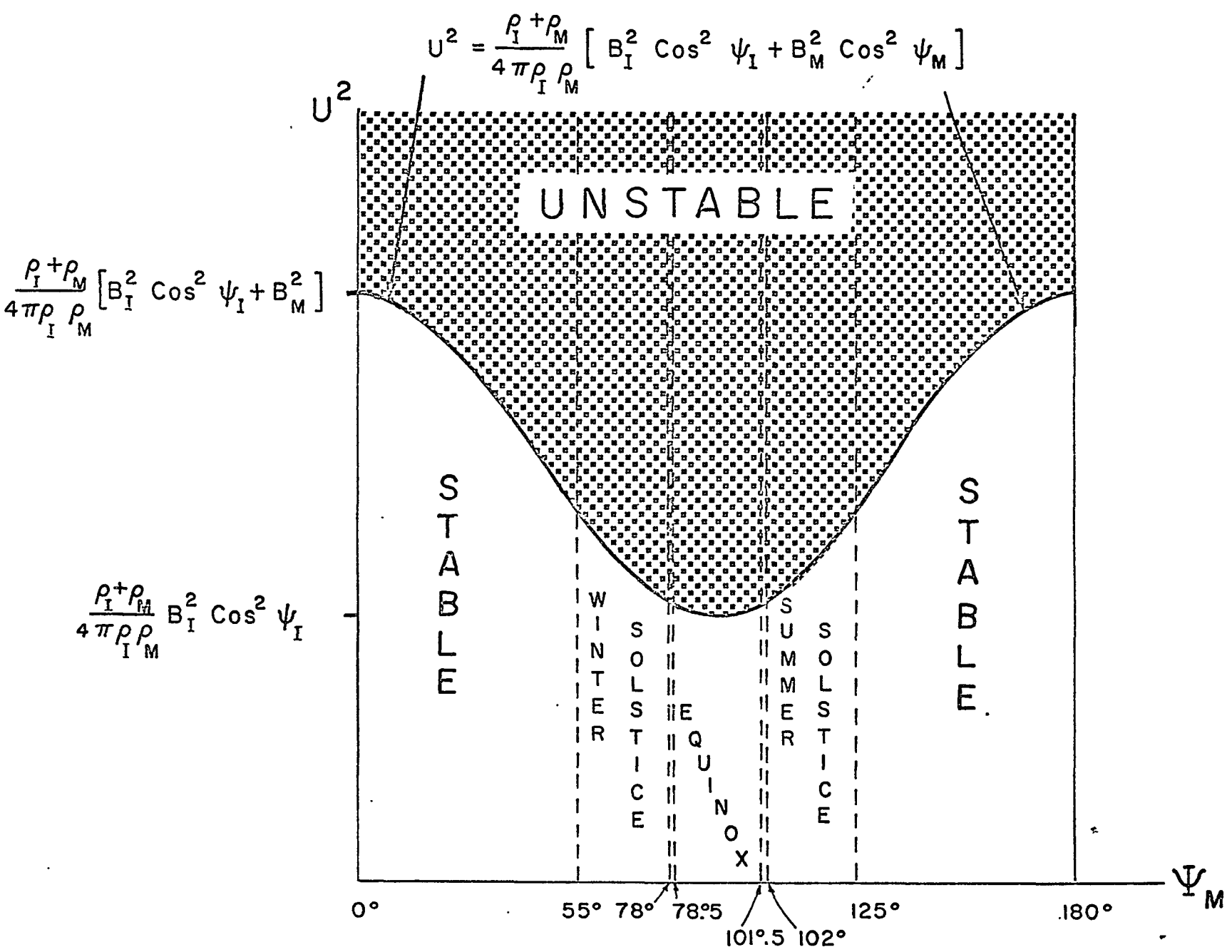
$U^2 = \frac{\rho_I + \rho_M}{4\pi\rho_I\rho_M}\left[B_I^2 \cos^2\psi_I + B_M^2 \cos^2\psi_M\right]$
U^2
UNSTABLE
$\frac{\rho_I+\rho_M}{4\pi\rho_I\rho_M}\left[B_I^2 \cos^2\psi_I + B_M^2\right]$
$\frac{\rho_I+\rho_M}{4\pi\rho_I\rho_M} B_I^2 \cos^2\psi_I$
STABLE
STABLE
WINTER SOLSTICE
EQUINOX
SUMER SOLSTICE
Ψ_M
0°
55°
78°
78°5
101°.5
102°
125°
180°

The parameters of the solar wind are known to be quite variable. These spatial variations in the solar wind are convected through the bow shock and pass through the magnetosheath. At any given time these parameters may change so as to alter the relative magnitudes of the left and right-hand sides of the instability condition. When the magnetospheric term is small, the probability for instability to occur will be high since the chances would be greater for the parameters to take on favorable values. If the magnetospheric term is large the probability for instability to occur would be correspondingly low. The times of the maximum and minimum probabilities for instability are seasonally dependent and may be determined from the instability condition as in Table 1, where the abbreviations D and S_t refer to the density factor and interplanetary term respectively. Therefore, if the instability of the magnetopause is geomagnetically effective, then the Kelvin-Helmholtz explanation predicts a universal time variation of geomagnetic activity. Illustrative plots of the probability of instability as a function of UT are shown in Figure (7.6) for the December solstice, the equinoxes, and the June solstice. We have assumed here that the probability of instability is approximately a linear function of the difference between the left-hand side and the right-hand side of the instability condition. It is pointed out that the flanks have the highest probability of instability at the equinoxes and in addition have a smaller diurnal variation than the solstices. The expected diurnal

TABLE 1.

Diurnal variation of Kelvin-Helmholtz Instability

Equinoxes	Summer Solstice	Winter Solstice
Max = 1030, 2230 UT $\Psi_M = 90^\circ, 90^\circ$ $U^2 > D\left(S_t\right)$	Max = 0430 UT $\Psi_M = 102^\circ$ $U^2 > D\left(S_t + 0.04\ B_M^2\right)$	Max = 1630 UT $\Psi_M = 78^\circ$ $U^2 > D\left(S_t + 0.04\ B_M^2\right)$
Min = 0430, 1630 UT $\Psi_M = 78^\circ.5, 101^\circ.5$ $U^2 > D\left(S_t + 0.04\ B_M^2\right)$	Min = 1630 UT $\Psi_M = 125^\circ$ $U^2 > D\left(S_t + 0.33\ B_M^2\right)$	Min = 0430 UT $\Psi_M = 55^\circ$ $U^2 > D\left(S_t + 0.33\ B_M^2\right)$

Figure 7.6

Illustrative plot of universal time variation of Kelvin-Helmholtz instability.

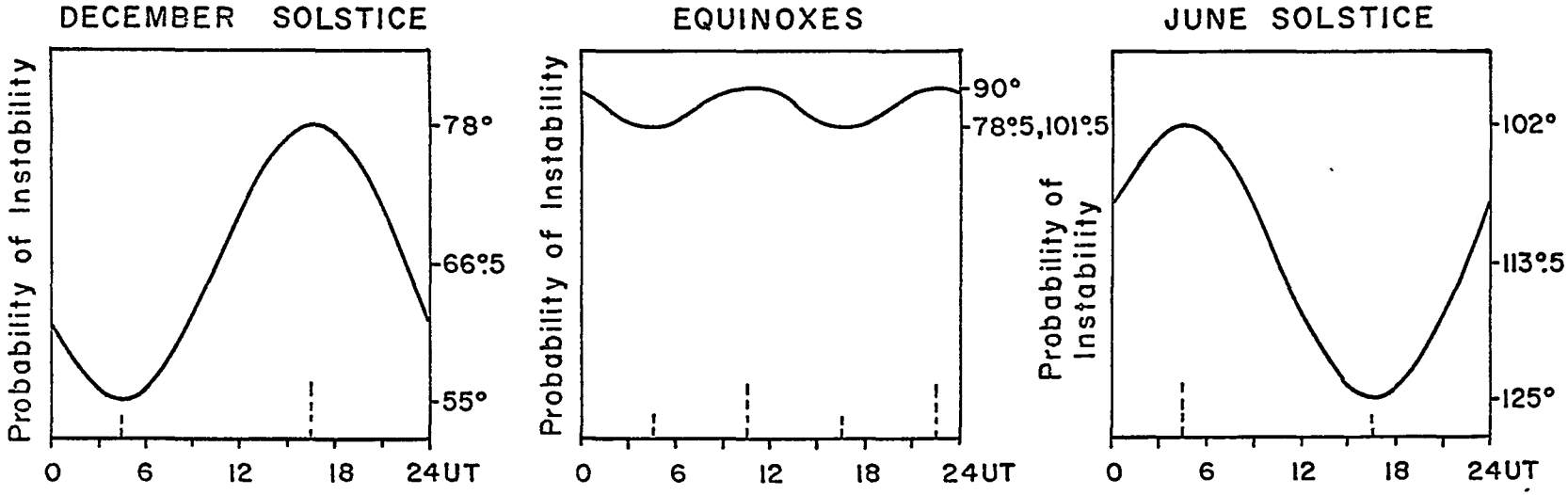
DECEMBER SOLSTICE
EQUINOXES
JUNE SOLSTICE
Probability of Instability
Probability of Instability
Probability of Instability
78°
66°5
55°
90°
78°5,101°5
102°
113°5
125°
0
6
12
18
24UT
0
6
12
18
24UT
0
6
12
18
24UT

variation at the solstices is approximately seven times greater than at the equinoxes, and the maximum probability of instability at the solstices is approximately equal to the minimum probability of instability at the equinoxes, as seen in Table 1 and shown in Figure (7.6). The ordinate of Figure (7.7a) is an illustrative plot of the difference between the probability of instability at the June solstice and the probability of instability at the December solstice but is labelled as the difference between the expected disturbances (Δ DISTURBANCE) at these times. Figure (7.8a) presents a similar illustrative plot but the ordinate now represents the differences between the sums of the expected disturbances at the equinoxes and the sums of the expected disturbances at the solstices. The phase and amplitude of the predicted curves of Figures (7.7a) and (7.8a) are confirmed by several analyses of available geomagnetic data.

7.4 Data Analysis and Confirmation of Kelvin-Helmholtz Hypothesis

The universal time variation predicted by the Kelvin-Helmholtz hypothesis should be revealed in the geomagnetic data on the removal of the local time effect. The changes of geomagnetic activity with local time are well known and have little seasonal variability. Therefore, the removal of the local time variation may be simply accomplished by taking differences between seasons. The June minus December difference leads to the doubling of the predicted variation and is illustrated in Figure (7.7a). The maximum occurs at 0430 UT and the minimum at 1630 UT. The difference between March and September would obviously eliminate

both the predicted effect and the local time variation. Therefore, the sum of the equinoxes minus the sum of the solstices is calculated resulting in a doubling of the predicted equinoctial variation seen in Figure (7.8a). Maxima occur at 1030 and 2230 UT and minima at 0430 and 1630 UT.

Figures (7.7) and (7.8) indicate the comparison of the predicted variation with several analyses of geomagnetic activity. Figures (7.7b) and (7.8b) present the indicated differences of the average daily variation of the K index of 12 observatories during 1950-1955 on selected days of K_p sum $>$ 20 reported by McIntosh (1959). Using data from all stations the average value of K is obtained separately for the months of June, December, March and September for each 3-hour interval of universal time over the indicated interval of years. The eight 3-hour intervals are then averaged for each of these months to obtain the average monthly K. The difference between the monthly average and the individual 3-hour monthly averages gives the 3-hour deviations from the mean for each month. This method is applied in determining Figures (7.7) and (7.8). Figures (7.7c) and (7.8c) present the indicated differences of the average daily variation of Mayaud's index (a_m) computed for 16 stations for 3 selected years (1959, 1961, 1964) including only 3-hourly intervals with $K_p \geq 2o$ (Mayaud 1967). Mayaud's a_m index is derived from his K_m index in the same manner as a_p is derived from K_p. The index K_m is formed from the K indices of 10 stations in the north and 6 stations in the south between 45°

Figure 7.7

Predicted June minus December univeral time variation of geomagnetic disturbance compared with data analyses of (b) McIntosh (c) Mayaud and (d) Nicholson and Wulf.

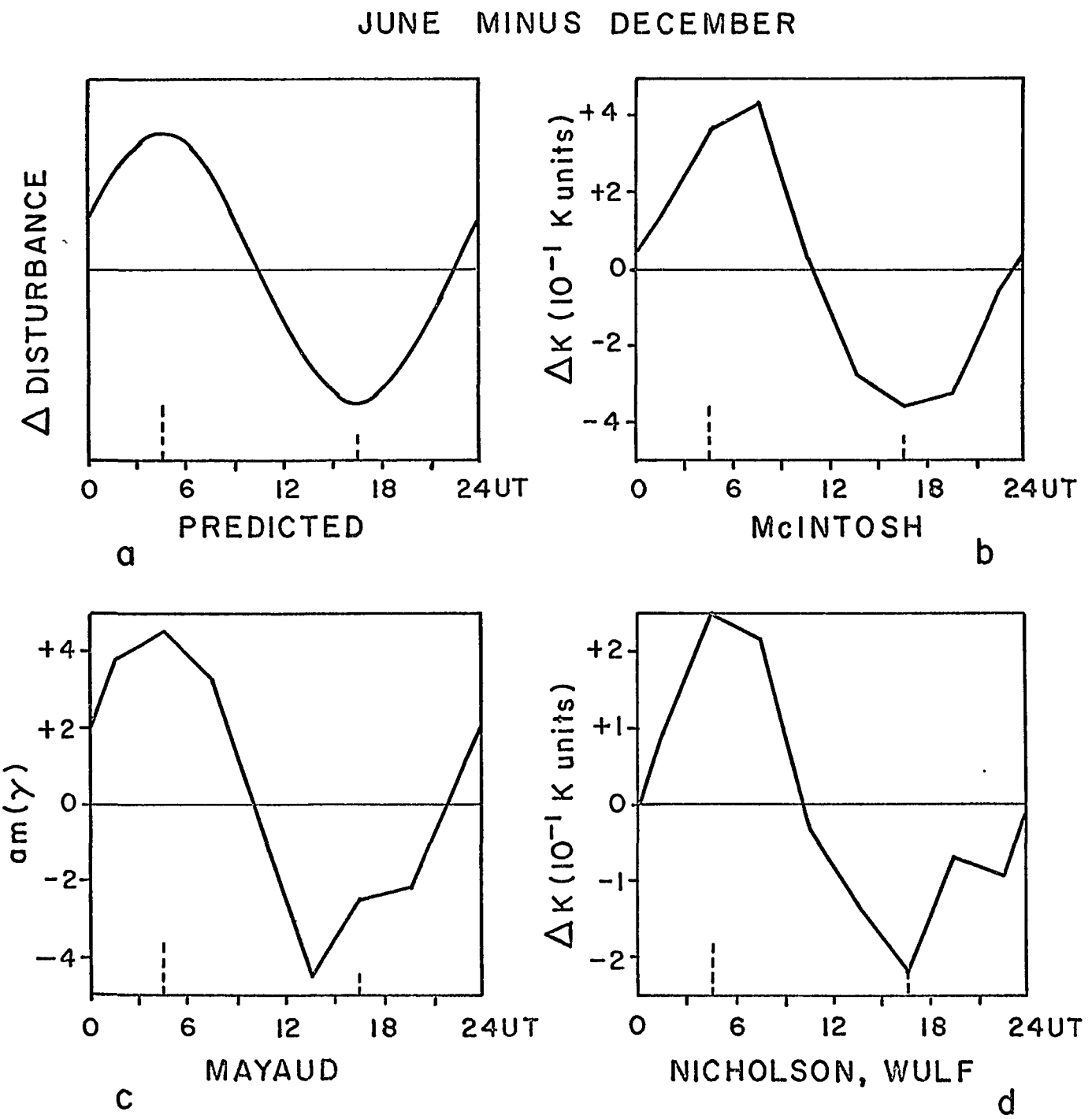
JUNE MINUS DECEMBER
Δ DISTURBANCE
0
6
12
18
24UT
PREDICTED
a
ΔK (10⁻¹ K units)
+4
+2
0
-2
-4
0
6
12
18
24UT
McINTOSH
b
am(γ)
+4
+2
0
-2
-4
0
6
12
18
24UT
MAYAUD
c
ΔK (10⁻¹ K units)
+2
+1
0
-1
-2
0
6
12
18
24UT
NICHOLSON, WULF
d

Figure 7.8

Predicted equinoxes minus solstices universal time variation of geomagnetic disturbance compared with data analyses of (b) McIntosh (c) Mayaud and (d) Nicholson and Wulf.

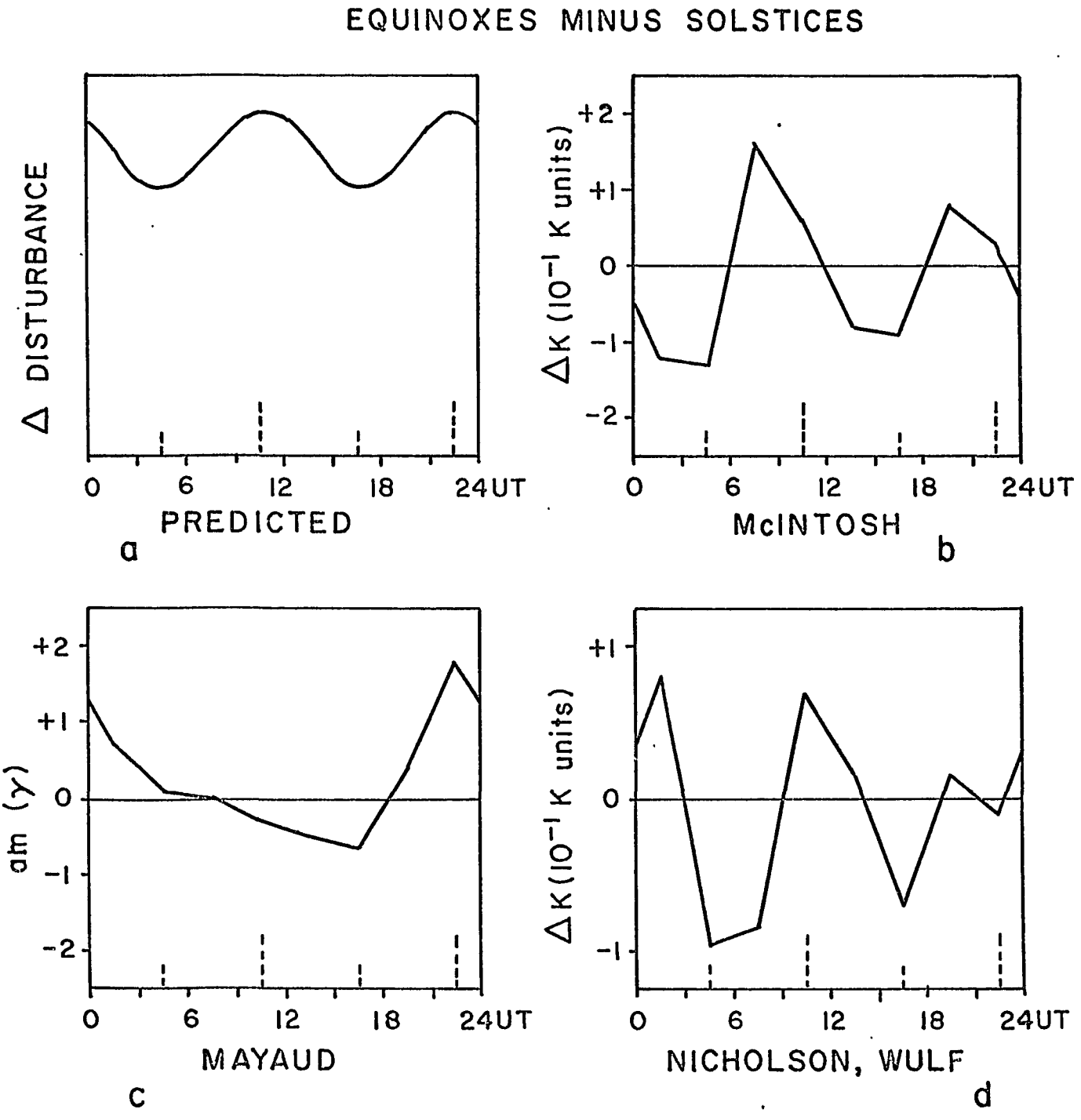
EQUINOXES MINUS SOLSTICES
Δ DISTURBANCE
0
6
12
18
24UT
PREDICTED
a
ΔK (10⁻¹ K units)
+2
+1
0
-1
-2
McINTOSH
b
am (γ)
MAYAUD
c
NICHOLSON, WULF
d

and 55° geomagnetic latitude, after certain modifications are made so that a_m is representative of an equivalent amplitude in the unit γ. Mayaud's June solstice consists of the months May, June, July, and August while his December solstice consists of the months November, December, January, and February. Mayaud's equinoxes consist of the months March, April, September, and October. Figures (7.7d) and (7.8d) present the indicated differences of the average daily variation of the K index for 6 observatories including all days of 1940-1946 calculated by Nicholson and Wulf (1955). These curves were formed from Nicholson and Wulf's (1955) individual monthly curves (June, December, March, and September) of the mean deviation of average K values as a function of UT. An excellent verification of the predicted phase is obtained. The relative amplitudes are confirmed, however, they are not quite as high as the predicted 7 to 1 ratio.

In order to verify further the Kelvin-Helmholtz mechanism, supported by the geomagnetic analysis of others, the data from 4 observatories closer to the auroral zone are studied: Murmansk (63.5N, 126.2E), Wellen (61.8N, 237.1E), Kerguelen (56.5S, 127.8E), Maquarie Island (60.7S, 243.0E), where geomagnetic coordinates are indicated. The K-indices analyzed are taken from three weeks before to three weeks after the key dates of the equinoxes and solstices from December 1, 1959 to October 12, 1964. The indices are linearized as in the method of Bartels by forming a_k, the equivalent amplitude, for each station and then converting these into the range in γ. These values are averaged over each pair

of stations in the north and in the south during the indicated time interval at each season for each 3-hour period of UT. The indicated differences of a_k are then taken and plotted in Figures (7.9a) and (7.9c), where June and December refer to the solstices. Composites for all four stations are shown in Figures (7.9b) and (7.9d). Figure (7.10) displays the same data in the unit γ and very little difference is found between this figure and Figure (7.9). As before, the phase verification is excellent, and in addition, the relative amplitudes are now closer to the predicted for the near auroral stations. Using all stations in Figure (7.9) a ratio of 6 to 1 is found while Figure (7.10) shows this ratio to be 5.5 to 1.

Analysis of the K-indices from 8 polar-cap observatories are performed for the same time period and, as expected, reveal no seasonal Kelvin-Helmholtz effect. It is clear that the polar cap represents quite a different regime of geomagnetic activity.

Figure 7.9

Variation of geomagnetic activity with universal time for 2 stations in the north and 2 stations in the south for June minus December, and equinoxes minus solstices, including composites in the unit a_k.

JUNE MINUS DECEMBER

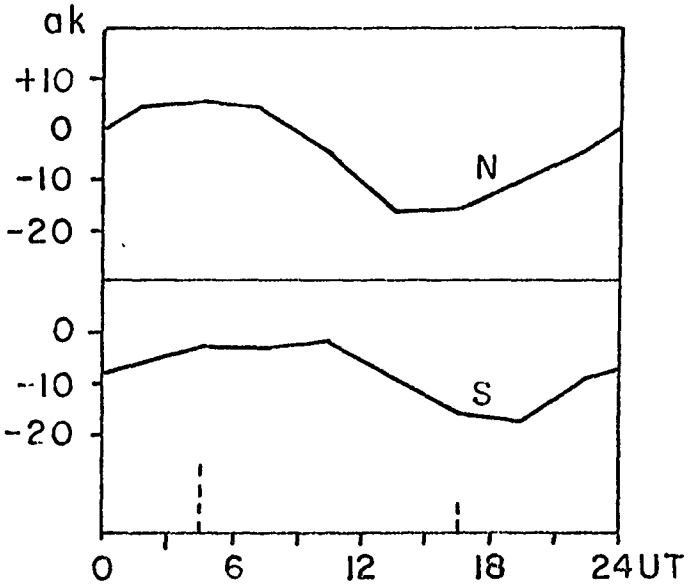

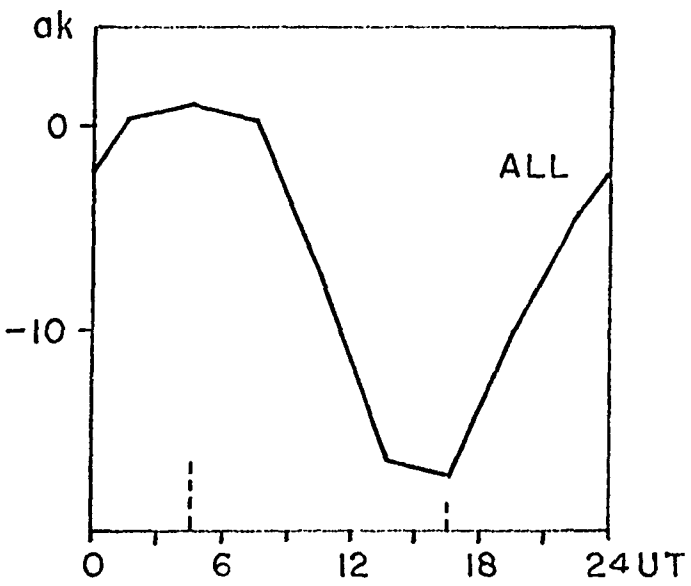

EQUINOXES MINUS SOLSTICES

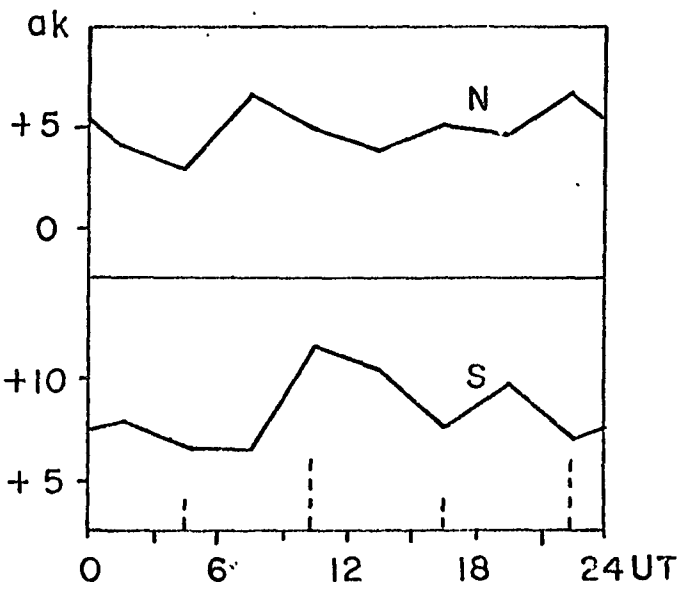

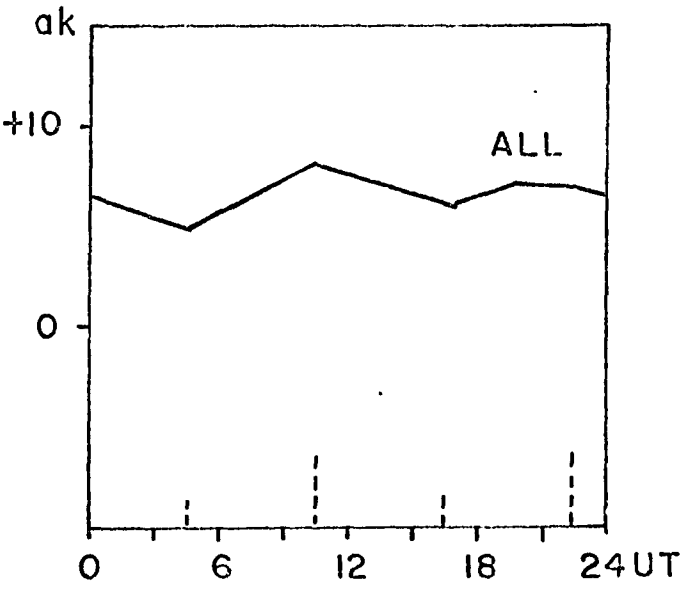

Figure 7.10

Variation of geomagnetic activity with universal time for 2 stations in the north and 2 stations in the south for June minus December, and equinoxes minus solstices, including composites in the unit γ.

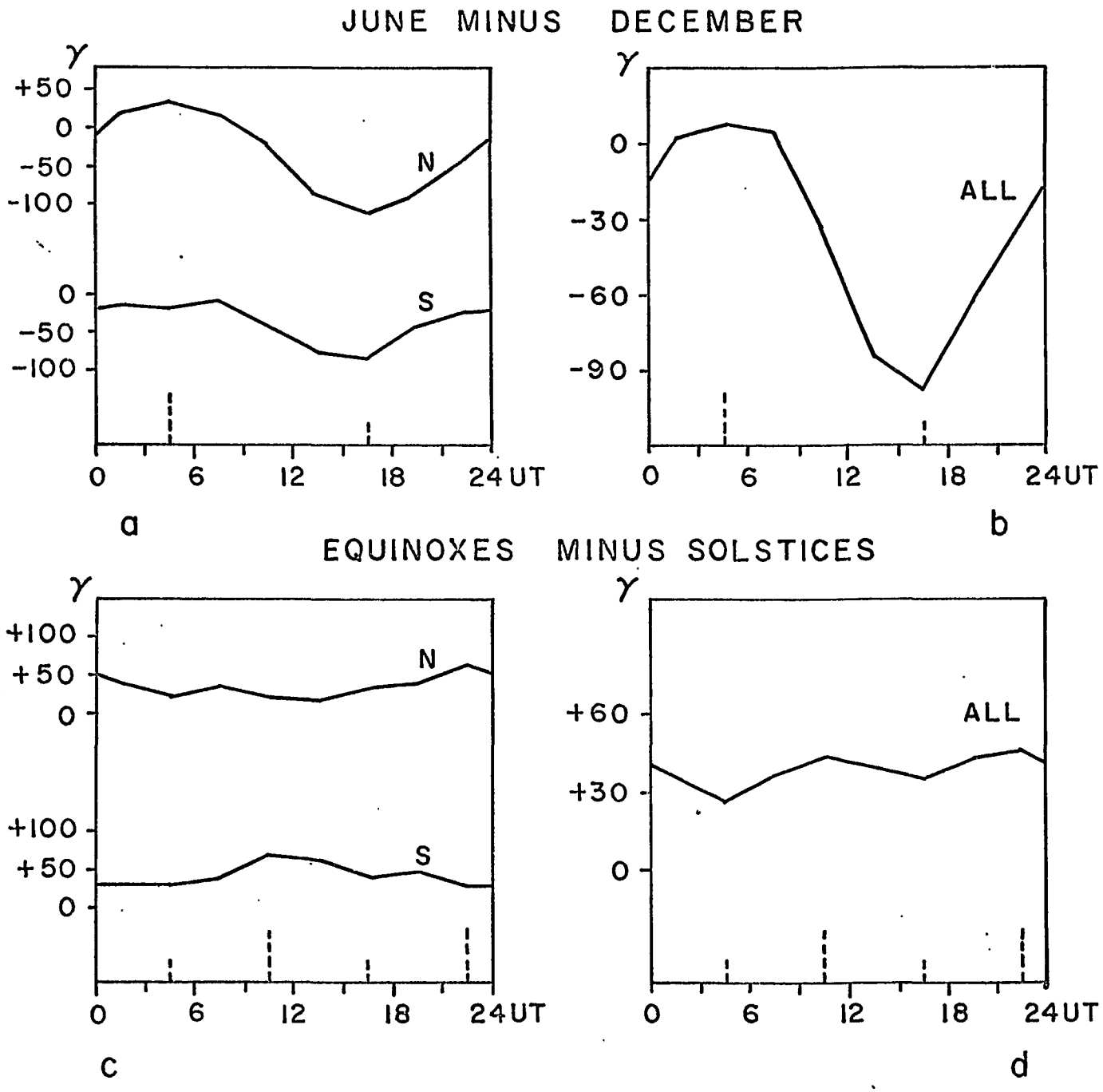
JUNE MINUS DECEMBER
γ
+50
0
-50
-100
N
0
-50
-100
S
0
6
12
18
24UT
a
γ
0
-30
-60
-90
ALL
0
6
12
18
24UT
b
EQUINOXES MINUS SOLSTICES
γ
+100
+50
0
N
+100
+50
0
S
0
6
12
18
24UT
c
γ
+60
+30
0
ALL
0
6
12
18
24UT
d

CHAPTER 8

ANALYSIS OF SATELLITE DATA

8.1 Illustrative Quantitative Estimate of the Kelvin-Helmholtz Instability Criterion

Estimates of the magnitudes of the left and right hand sides of the instability criterion will be made for disturbed and quiet conditions of the magnetosphere. Explorer 34 data are used for five crossings of the magnetosphere boundary.

The crossings occurred at the following times with geomagnetic disturbance measured by K_p:

CROSSING 1	13 September 1967	2124UT	(K_p = 3o)
CROSSING 2	14 September 1967	0618UT	(K_p = 3o)
CROSSING 3	9 October 1967	2145UT	(K_p = 5+)
CROSSING 4	18 November 1967	0940UT	(K_p = 1-)
CROSSING 5	30 November 1967	1950UT	(K_p = 4+)

Each crossing supplied magnetic field measurements on either side of the magnetopause. Reliable plasma data were available only outside the bow shock. Since the first, third, and fifth crossings were inbound, the hourly average values of solar wind speed (U_∞) and number density (n_∞) are measured just before the satellite entered the bow shock. The second and fourth crossings were outbound so that the hourly average values of solar wind speed and number density measured are those obtained just after the satellite passed through the bow shock. Table 2 lists these measured parameters. The magnetic field measurements (in γ) and satellite position (in earth radii) at the crossing

TABLE 2

MEASURED VALUES OF THE PARAMETERS

CROSSING	K_p	$B_s(\gamma)$	θ_s	ϕ_s	$B_M(\gamma)$	θ_M	ϕ_M	X_{SE}	Y_{SE}	Z_{SE}	R_{SE}	U_∞(km./sec.)	n_∞(cm.$^{-3}$)
1	3o	40	-20°	270°	40	15°	180°	9.30	-1.00	5.55	10.87	563	3.7
2	3o	40	10°	310°	45	0°	315°	6.96	0.21	-6.17	9.30	539	2.3
3	5+	40	20°	120°	65	0°	135°	5.42	-3.26	5.33	8.27	466	1.5
4	1-	15	-45°	210°	30	20°	240°	5.07	-12.71	-7.40	15.56	382	2.0
5	4+	40	0°	50°	55	0°	50°	1.35	-7.50	5.97	9.68	422	5.4

point are given in solar ecliptic coordinates (Ness et al., 1964). (see Figure (8.3)).

The measured parameters are not in a form which could be used in the instability condition. In particular, the values of the solar wind stream speed (U) and mass densities (ρ_S, ρ_M) are needed at the satellite crossing point. These values may be obtained by using Spreiter et al.'s (1968) gasdynamic curves (e.g. for a free-stream Mach number equal to 5). They display contours of the ratio of magnetosheath to free-stream values of these quantities for the dayside magnetosheath. The free-stream values (U_∞ and n_∞) determine the stream speed and the mass density at the crossing point. The magnetosphere mass density is assumed to be the same as the magnetosheath mass density in the absence of interior plasma measurements.

The direction of the solar streaming at the satellite crossing point must be found so that the components of the magnetic fields in this direction may be determined. The direction of the solar streaming is uniquely determined by the intersection of the plane containing the satellite crossing point and the sun-earth line and the plane formed by the magnetosheath and magnetospheric magnetic fields at the crossing point. The quantities $B_S Cos\Psi_S$ and $B_M Cos\Psi_M$ are then found. The magnetic fields for the fifth-crossing are in the same direction so that no unique plane is defined by them. A plane was picked so that it is consistent with the general shape of the magnetosphere at this crossing point and contains the magnetic fields. The

unit vector normal to this plane has the following solar ecliptic coordinates: $\theta_n = 40°$, $\Phi_n = 140°$. Section 8.3 contains the equations used for the determination of the quantities $B_S \cos\Psi_S$ and $B_M \cos\Psi_M$.

Table 3 contains the calculated values of the parameters to be used in the instability condition for all five crossings. It is found that the instability condition is fulfilled for the second crossong point while it is not fulfilled for the other crossing points. The fact that the instability condition is not fulfilled for the fourth crossing point is consistent with the period being a quiet one. Application of the gasdynamic curves of Spreiter et al. (1968) and some assumptions concerning the magnetic fields (see Section 8.4) to determine conditions at the flanks are displayed in Table 4. Tables 3 and 4 reveal that the magnetopause is always in a condition bordering on instability of the kind described by the Kelvin-Helmholtz mechanism. The values of the left and right hand sides of the instability condition are near each other (most within an order of magnitude) at the crossing points and even closer to each other when the parameters are extrapolated to the flanks. The fact that the instability condition does not appear to work for all the times of the crossings could be due to a number of uncertainties associated with the way the parameters have been determined. In addition, the measure used to determine geomagnetic activity, K_p, is a three-hour index and a crossing could occur before conditions become disturbed. A more comprehensive study of the boundary during quiet and disturbed times is necessary and will be done as soon as data becomes available.

8.2 The Kelvin-Helmholtz Instability Condition and the Sector Structure of the Interplanetary Medium

An attempt is made here to construct a predicted curve of geo-

TABLE 3

CALCULATED VALUES OF THE PARAMETERS AT THE CROSSING POINTS

CROSSING	1 (K_p = 3o)	2 (K_p = 3o)	3 (K_p = 5+)	4 (K_p = 1-)	5 (K_p = 4+)
$U(10^7 cm./sec.)$	1.7	2.16	2.1	2.29	2.74
$\rho_S=\rho_M(10^{-24} gm./cm.^3)$	21.3	12.3	7.51	7.68	17.1
$B_S Cos\Psi_S(10^{-5} gauss)$	-1.68	-7.09	18.5	8.39	-34.2
$B_M Cos\Psi_M(10^{-5} gauss)$	34.8	-16.3	51.5	21.2	-47.4
$U^2(10^{14} cm.^2/sec.^2)$	2.9	4.66	4.4	5.25	7.5
RIGHT HAND SIDE $(10^{14} gauss^2 cm.^3/gm.)$	8.9	4.08	63.4	10.8	31.6
INSTABILITY CONDITION FULFILLED	NO	YES	NO	NO	NO

TABLE 4

CALCULATED VALUES OF THE PARAMETERS AT THE FLANKS AT THE TIMES OF THE CROSSINGS

CROSSING TO FLANK	1 (K_p = 3o)	2 (K_p = 3o)	3 (K_p = 5+)	4 (K_p = 1-)	5 (K_p = 4+)
$U(10^7 cm./sec.)$	3.97	3.78	3.28	2.68	2.95
$\rho_S=\rho_M(10^{-24} gm./cm.^3)$	9.74	6.15	4.02	5.33	14.4
$B_S Cos\Psi_S(10^{-5} gauss)$	~ 20	~ 20	~ 20	~ 10	~ 26.7
$B_M Cos\Psi_M(10^{-5} gauss)$	0	2.75	0.94	9.4	3.51
$U^2(10^{14} cm.^2/sec.^2)$	15.67	14.2	10.8	7.16	8.7
RIGHT HAND SIDE $(10^{14} gauss^2 cm.^3/gm.)$	6.49	10.55	15.8	5.63	8.0
INSTABILITY CONDITION FULFILLED	YES	YES	NO	YES	YES

magnetic disturbance as a function of day within the sector structure of Wilcox and Ness (1965) using their parameters and the Kelvin-Helmholtz instability condition at the flanks. Tables 5 and 6 give the free-stream values of the number density (n_∞), magnetic field intensity (B_∞), and solar wind speed (U_∞) for the 3-hour intervals of the days of the away and toward sectors obtained from the curves of Wilcox and Ness (1965) which are displayed in Chapter 3. The ratio of the bulk kinetic energy density (assuming only protons in the solar wind) to the magnetic field energy density has been calculated for the free-stream values and is also given in these tables. These free-stream values are converted to the values they would have at the flanks by using the gasdynamic curves (Mach 5) of Spreiter et al. (1968). The relationships between the free-stream values and the solar stream parameters at the flanks are:

$$n = 1.6n_\infty \quad ; \quad U = 0.7U_\infty \quad ; \quad B = 5B_\infty \quad .$$

These new values are displayed in Tables 7 and 8 for away and toward sectors and are used to calculate the left and right hand sides of the instability condition which are presented in Tables 9 and 10 where it has been assumed that $\Psi_S = 0^\circ$ and $\Psi_M = 90^\circ$. The difference between the left hand side and right hand side of the instability condition (DIFFERENCE) is also given in these tables and plotted in Figures (8.1) and (8.2) for the away and toward sectors respectively. This difference is assumed to be proportional to the probability of instability at the flanks and therefore proportional to geomagnetic disturbance.

Acomparison between these curves and the curves

TABLE 5

SOLAR WIND PARAMETERS FOR AWAY SECTORS OF WILCOX AND NESS, 1965

Days of Sector Structure	3 Hour Interval	n_∞ cm^{-3}	$U_\infty(10^7$ cm./sec)	$B_\infty(10^{-5}$ gauss)	β_∞
1	1	16.9	3.06	2.7	227.7
	2	26.0	3.31	2.5	478.0
	3	26.0	3.31	2.5	478.0
	4	31.5	3.26		
	5	31.5	3.26		
	6	39.4	3.26		
	7	39.4	3.26		
	8	35.6	3.26		
2	1	35.6	3.26		
	2	18.1	3.50	6.45	55.9
	3	18.1	3.50	6.45	55.9
	4	11.3	4.10	6.3	50.2
	5	11.3	4.10	6.3	50.2
	6	9.0	4.26		
	7	9.0	4.26	6.55	39.9
	8	7.5	4.26	6.5	33.8
3	1	7.5	4.30	6.5	34.4
	2	8.1	4.26	6.55	35.9
	3	8.1	4.26	6.55	35.9
	4	6.1	4.25	6.2	30.1
	5	6.1	4.25	6.2	30.1
	6	6.1	4.26	5.85	33.9
	7	6.1	4.26	5.85	33.9
	8	5.6	4.28	5.4	36.9
4	1	5.6	4.28	5.4	36.9
	2	5.6	4.21	5.5	34.4
	3	5.6	4.21	5.5	34.4
	4	5.6	4.21	5.6	33.2
	5	5.6	4.21	5.6	33.2
	6	5.9	4.25	5.5	36.9
	7	6.1	4.25	5.5	38.2
	8	5.9	4.44	5.6	38.9
5	1	5.9	4.44	5.6	38.9
	2	4.7	4.94	5.2	44.5
	3	4.7	4.94	5.2	44.5
	4	5.2	4.36	4.5	51.2
	5	5.2	4.36	4.5	51.2
	6	4.8	3.75	3.3	65.0
	7	4.8	3.75	3.3	65.0
	8	6.6	3.53	3.2	84.2
6	1	6.6	3.53	3.2	84.2
	2	7.3	3.18	3.55	61.4
	3	7.3	3.18	3.55	61.4
	4	7.6	3.18	3.55	64.0
	5	7.6	3.18	3.55	64.0
	6	7.3	3.29	3.55	65.8
	7	7.3	3.29	3.6	63.9
	8	7.6	3.23	4.1	49.5

TABLE 5
Continued

Days of Sector Structure	3 Hour Interval	n_∞ $cm.^{-3}$	$U_\infty(10^7 cm./sec.)$	$B_\infty(10^{-5} gauss)$	β_∞
	1	7.6	3.23	4.1	49.5
	2	8.8	3.21	4.5	47.0
	3	8.8	3.21	4.5	47.0
7	4	10.0	3.06	5.0	39.3
	5	10.0	3.06	5.0	39.3
	6		2.93	4.6	
	7		2.93	4.6	
	8	11.8	2.81	4.3	52.8
	1	11.8	2.81	4.3	52.8
	2	12.5	2.81	4.4	53.5
	3	12.5	2.81	4.4	53.5
8	4	12.8	2.68	4.2	54.7
	5	12.8	2.68	4.2	54.7

TABLE 6

SOLAR WIND PARAMETERS FOR TOWARD SECTORS OF WILCOX AND NESS, 1965

Day of Sector Structure	3 Hour Interval	n_∞ cm^{-3}	$U_\infty(10^7 cm./sec.)$	$B_\infty(10^{-5} gauss)$	β_∞
1	1	11.8	2.87	6.05	27.8
	2	11.8	2.87	6.05	27.8
	3	11.8	2.87	6.05	27.8
	4	11.8	2.87	6.05	27.8
	5	14.4	3.02	5.9	39.7
	6	14.4	3.02	5.8	40.9
	7	15.0	3.73	6.4	53.4
	8	15.0	3.73	6.45	52.6
2	1	16.2	4.10	5.65	89.5
	2	16.2	4.10	5.65	89.5
	3	16.2	4.10	5.65	89.5
	4	16.2	4.10	5.65	89.5
	5	14.6	4.21	6.55	63.3
	6	14.6	4.21	6.5	64.2
	7	11.3	4.30	6.1	58.9
	8	11.3	4.30	6.1	58.9
3	1	10.0	4.44	6.0	57.4
	2	10.0	4.44	6.0	57.4
	3	10.0	4.44	6.0	57.4
	4	10.0	4.44	6.0	57.4
	5	7.3	4.69	5.3	60.0
	6	7.3	4.69	5.3	60.0
	7	6.5	4.44	4.8	58.3
	8	6.5	4.44	4.8	58.3
4	1	6.1	4.23	4.4	59.1
	2	6.1	4.23	4.4	59.1
	3	6.1	4.23	4.4	59.1
	4	6.1	4.23	4.4	59.1
	5	6.1	4.23	4.0	71.5
	6	6.1	4.23	4.0	71.5
	7	6.9	4.06	4.45	60.2
	8	6.9	4.06	4.45	60.2
5	1				
	2				
	3				
	4				
	5	9.1	3.03	4.4	45.3
	6	9.1	3.03	4.4	45.3
	7	7.9	3.00	3.7	54.5
	8	7.9	3.00	3.7	54.5
6	1	7.9	3.00	3.7	54.5
	2	7.9	3.00	3.7	54.5
	3	7.9	3.00	3.7	54.5
	4	7.9	3.00	3.7	54.5
	5	9.1	2.84	3.4	66.6
	6	9.1	2.84	3.4	66.6
	7	10.6	2.60	3.5	61.3
	8	10.6	2.60	3.5	61.3

TABLE 6
Continued

Day of Sector Structure	3 Hour Interval	n_∞ $cm.^{-3}$	$U_\infty(10^7 cm./sec.)$	$B_\infty(10^{-5} gauss)$	β_∞
7	1	9.1	2.84	3.55	61.1
	2	9.1	2.84	3.55	61.1
	3	9.1	2.84	3.55	61.1
	4	9.1	2.84	3.55	61.1
	5	10.6	2.81	3.65	65.9
	6	10.6	2.81	3.65	65.9
	7	15.3	2.65	3.65	84.6
	8	15.3	2.65	3.65	84.6
8	1	16.2	2.62	3.2	113.9
	2	16.2	2.62	3.2	113.9
	3	16.2	2.62	3.2	113.9
	4	16.2	2.62	3.2	113.9
	5	19.7	2.87		

TABLE 7

SOLAR STREAM PARAMETERS AT FLANKS FOR AWAY SECTORS

Day of Sector Structure	3 Hour Interval	n $cm.^{-3}$	U(10^7cm./sec.)	B(10^{-5}gauss)	β
	1	27.0	2.14	13.5	7.12
	2	41.6	2.32	12.5	15.03
	3	41.6	2.32	12.5	15.03
1	4	50.4	2.28		
	5	50.4	2.28		
	6	63.0	2.28		
	7	63.0	2.28		
	8	57.0	2.28		
	1	57.0	2.28		
	2	29.0	2.45	32.3	1.75
	3	29.0	2.45	32.3	1.75
2	4	18.1	2.87	31.5	1.58
	5	18.1	2.87	31.5	1.58
	6	14.4	2.98		
	7	14.4	2.98	32.8	1.25
	8	12.0	2.98	32.5	1.06
	1	12.0	3.01	32.5	1.08
	2	13.0	2.98	32.8	1.13
	3	13.0	2.98	32.8	1.13
3	4	9.8	2.98	31.0	0.95
	5	9.8	2.98	31.0	0.95
	6	9.8	2.98	29.3	1.06
	7	9.8	2.98	29.3	1.06
	8	9.0	3.00	27.0	1.17
	1	9.0	3.00	27.0	1.17
	2	9.0	2.95	27.5	1.09
	3	9.0	2.95	27.5	1.09
4	4	9.0	2.95	28.0	1.05
	5	9.0	2.95	28.0	1.05
	6	9.4	2.98	27.5	1.16
	7	9.8	2.98	27.5	1.21
	8	9.4	3.11	28.0	1.22
	1	9.4	3.11	28.0	1.22
	2	7.5	3.46	26.0	1.39
	3	7.5	3.46	26.0	1.39
5	4	8.3	3.05	22.5	1.60
	5	8.3	3.05	22.5	1.60
	6	7.7	2.63	16.5	2.05
	7	7.7	2.63	16.5	2.05
	8	10.6	2.47	16.0	2.65
	1	10.6	2.47	16.0	2.65
	2	11.7	2.23	17.8	1.93
	3	11.7	2.23	17.8	1.93
6	4	12.2	2.23	17.8	2.01
	5	12.2	2.23	17.8	2.01
	6	11.7	2.30	17.8	2.05
	7	11.7	2.30	18.0	2.00
	8	12.2	2.26	20.5	1.56

TABLE 7
Continued

Day of Sector Structure	3 Hour Interval	n $cm.^{-3}$	U(10^7 cm./sec.)	B(10^{-5} gauss)	β
	1	12.2	2.26	20.5	1.56
	2	14.1	2.25	22.5	1.48
	3	14.1	2.25	22.5	1.48
7	4	16.0	2.14	25.0	1.23
	5	16.0	2.14	25.0	1.23
	6		2.05	23.0	
	7		2.05	23.0	
	8	18.9	1.97	21.5	1.66
	1	18.9	1.97	21.5	1.66
	2	20.0	1.97	22.0	1.68
	3	20.0	1.97	22.0	1.68
8	4	20.5	1.88	21.0	1.72
	5	20.5	1.88	21.0	1.72

TABLE 8

SOLAR STREAM PARAMETERS AT FLANKS FOR TOWARD SECTORS

Day of Sector Structure	3 Hour Interval	n $cm.^{-3}$	U(10^7 gm./sec.)	B(10^{-5} gauss)	β
	1	18.9	2.01	30.3	0.87
	2	18.9	2.01	30.3	0.87
	3	18.9	2.01	30.3	0.87
1	4	18.9	2.01	30.3	0.87
	5	23.0	2.11	29.5	1.23
	6	23.0	2.11	29.0	1.28
	7	24.0	2.61	32.0	1.67
	8	24.0	2.61	32.3	1.64
	1	25.9	2.87	28.3	2.79
	2	25.9	2.87	28.3	2.79
	3	25.9	2.87	28.3	2.79
2	4	25.9	2.87	28.3	2.79
	5	23.4	2.95	32.8	1.99
	6	23.4	2.95	32.5	2.02
	7	18.1	3.01	30.5	1.85
	8	18.1	3.01	30.5	1.85
	1	16.0	3.11	30.0	1.80
	2	16.0	3.11	30.0	1.80
	3	16.0	3.11	30.0	1.80
3	4	16.0	3.11	30.0	1.80
	5	11.7	3.28	26.5	1.88
	6	11.7	3.28	26.5	1.88
	7	10.4	3.11	24.0	1.83
	8	10.4	3.11	24.0	1.83
	1	9.8	2.96	22.0	1.86
	2	9.8	2.96	22.0	1.86
	3	9.8	2.96	22.0	1.86
4	4	9.8	2.96	22.0	1.86
	5	9.8	2.96	20.0	2.25
	6	9.8	2.96	20.0	2.25
	7	11.0	2.84	22.3	1.87
	8	11.0	2.84	22.3	1.87
	1				
	2				
	3				
5	4				
	5	14.6	2.12	22.0	1.42
	6	14.6	2.12	22.0	1.42
	7	12.6	2.10	18.5	1.70
	8	12.6	2.10	18.5	1.70
	1	12.6	2.10	18.5	1.70
	2	12.6	2.10	18.5	1.70
	3	12.6	2.10	18.5	1.70
6	4	12.6	2.10	18.5	1.70
	5	14.6	1.99	17.0	2.10
	6	14.6	1.99	17.0	2.10
	7	17.0	1.82	17.5	1.93
	8	17.0	1.82	17.5	1.93

TABLE 8
Continued

Day of Sector Structure	3 Hour Interval	n $cm.^{-3}$	U(10^7 cm./sec.)	B(10^{-5} gauss)	β
7	1	14.6	1.99	17.8	1.91
	2	14.6	1.99	17.8	1.91
	3	14.6	1.99	17.8	1.91
	4	14.6	1.99	17.8	1.91
	5	17.0	1.97	18.3	2.07
	6	17.0	1.97	18.3	2.07
	7	24.5	1.86	18.3	2.65
	8	24.5	1.86	18.3	2.65
8	1	25.9	1.83	16.0	3.55
	2	25.9	1.83	16.0	3.55
	3	25.9	1.83	16.0	3.55
	4	25.9	1.83	16.0	3.55
	5	31.5	2.01		

TABLE 9

VALUES OF THE LEFT AND RIGHT HAND SIDES OF THE INSTABILITY CONDITION AND THEIR DIFFERENCE AT THE FLANKS FOR AWAY SECTORS

Day of Sector Structure	3 Hour Interval	U^2 (10^{14}cm.^{2}/sec.^{2})	$B^2/6.28\rho$ (10^{14}gauss^{2}cm.^{3}/gm.)	Difference
1	1	4.58	0.64	+3.94
	2	5.38	0.36	+5.02
	3	5.38	0.36	+5.02
	4			
	5			
	6			
	7			
	8			
2	1			
	2	6.00	3.43	+2.57
	3	6.00	3.43	+2.57
	4	8.24	5.23	+3.01
	5	8.24	5.23	+3.01
	6	8.88		
	7	8.88	7.12	+1.76
	8	8.88	8.39	+0.49
3	1	9.06	8.39	+0.67
	2	8.88	7.89	+0.99
	3	8.88	7.89	+0.99
	4	8.88	9.35	-0.47
	5	8.88	9.35	-0.47
	6	8.88	8.35	+0.53
	7	8.88	8.35	+0.53
	8	9.00	7.72	+1.28
4	1	9.00	7.72	+1.28
	2	8.70	8.01	+0.69
	3	8.70	8.01	+0.69
	4	8.70	8.31	+0.39
	5	8.70	8.31	+0.39
	6	8.88	7.67	+1.21
	7	8.88	7.36	+1.52
	8	9.67	7.95	+1.72
5	1	9.67	7.95	+1.72
	2	11.97	8.59	+3.38
	3	11.97	8.59	+3.38
	4	9.30	5.82	+3.58
	5	9.30	5.82	+3.58
	6	6.92	3.37	+3.55
	7	6.92	3.37	+3.55
	8	6.10	2.30	+3.80
6	1	6.10	2.30	+3.80
	2	4.97	2.58	+2.39
	3	4.97	2.58	+2.39
	4	4.97	2.48	+2.49
	5	4.97	2.48	+2.49
	6	5.29	2.58	+2.71
	7	5.29	2.64	+2.65
	8	5.11	3.28	+1.83

TABLE 9
Continued

Day of Sector Structure	3 Hour Interval	U^2 (10^{14} cm.^{2}/sec.^{2})	$B^2/6.28\rho$ (10^{14} gauss^{2}cm.^{3}/gm.)	Difference
	1	5.11	3.28	+1.83
	2	5.06	3.42	+1.64
	3	5.06	3.42	+1.64
7	4	4.58	3.72	+0.86
	5	4.58	3.72	+0.86
	6			
	7			
	8	3.88	2.33	+1.55
	1	3.88	2.33	+1.55
	2	3.88	2.31	+1.57
	3	3.88	2.31	+1.57
8	4	3.53	2.05	+1.48
	5	3.53	2.05	+1.48

TABLE 10

VALUES OF THE LEFT AND RIGHT HAND SIDES OF THE INSTABILITY CONDITION AND THEIR DIFFERENCE AT THE FLANKS FOR TOWARD SECTORS

Day of Sector Structure	3 Hour Interval	U^2 (10^{14}cm.^{2}/sec.^{2})	$B^2/6.28\rho$ (10^{14}gauss^{2}cm.^{3}/gm.)	Difference
1	1	4.04	4.63	-0.59
	2	4.04	4.63	-0.59
	3	4.04	4.63	-0.59
	4	4.04	4.63	-0.59
	5	4.45	3.61	+0.84
	6	4.45	3.49	+0.96
	7	6.81	4.07	+2.74
	8	6.81	4.14	+2.67
2	1	8.24	2.95	+5.29
	2	8.24	2.95	+5.29
	3	8.24	2.95	+5.29
	4	8.24	2.95	+5.29
	5	8.70	4.38	+4.32
	6	8.70	4.30	+4.40
	7	9.06	4.90	+4.16
	8	9.06	4.90	+4.16
3	1	9.67	5.36	+4.31
	2	9.67	5.36	+4.31
	3	9.67	5.36	+4.31
	4	9.67	5.36	+4.31
	5	10.76	5.72	+5.04
	6	10.76	5.72	+5.04
	7	9.67	5.28	+4.39
	8	9.67	5.28	+4.39
4	1	8.76	4.71	+4.05
	2	8.76	4.71	+4.05
	3	8.76	4.71	+4.05
	4	8.76	4.71	+4.05
	5	8.76	3.89	+4.87
	6	8.76	3.89	+4.87
	7	8.07	4.31	+3.76
	8	8.07	4.31	+3.76
5	1			
	2			
	3			
	4			
	5	4.49	3.16	+1.33
	6	4.49	3.16	+1.33
	7	4.41	2.59	+1.82
	8	4.41	2.59	+1.82
6	1	4.41	2.59	+1.82
	2	4.41	2.59	+1.82
	3	4.41	2.59	+1.82
	4	4.41	2.59	+1.82
	5	3.96	1.89	+2.07
	6	3.96	1.89	+2.07
	7	3.31	1.72	+1.59
	8	3.31	1.72	+1.59

TABLE 10
Continued

Day of Sector Structure	3 Hour Interval	U^2 (10^{14}cm.^{2}/sec.^{2})	$B^2/6.28\rho$ (10^{14}gauss^{2}cm.^{3}/gm.)	Difference
	1	3.96	2.07	+1.89
	2	3.96	2.07	+1.89
	3	3.96	2.07	+1.89
7	4	3.96	2.07	+1.89
	5	3.88	1.88	+2.00
	6	3.88	1.88	+2.00
	7	3.46	1.30	+2.16
	8	3.46	1.30	+2.16
	1	3.35	0.94	+2.41
	2	3.35	0.94	+2.41
	3	3.35	0.94	+2.41
8	4	3.35	0.94	+2.41

Figure 8.1

The difference between the left-hand side and right-hand side of the instability condition as a function of time within the away sectors

DIFFERENCE (10^{14} cm²/sec²)
5
4
3
2
1
1
2
3
4
5
6
7
8
DAYS IN SECTOR

Figure 8.2

The difference between the left-hand side and right-hand side of the instability condition as a function of time within the toward sectors

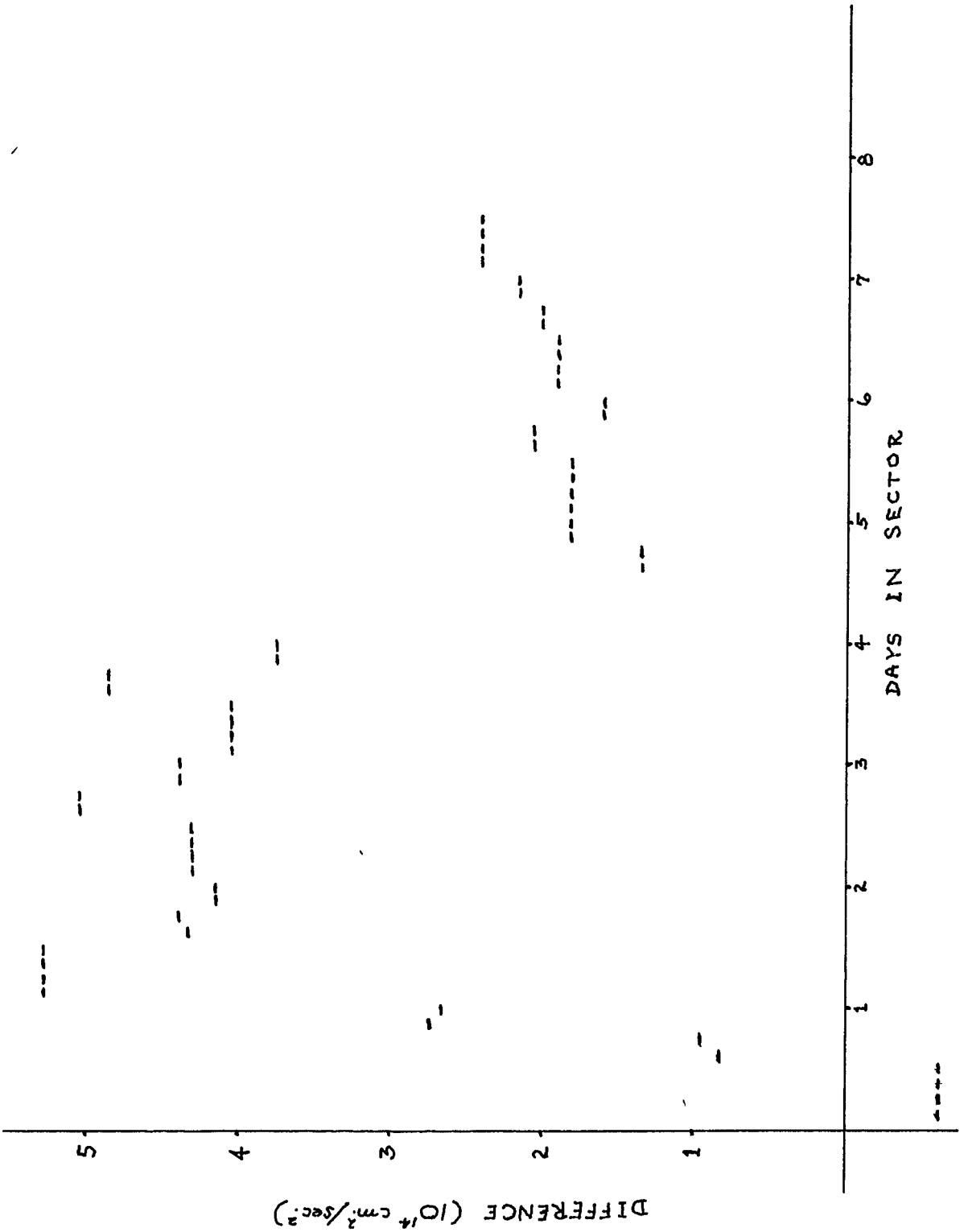
DIFFERENCE (10^{14} cm^2/sec^2)
5
4
3
2
1
1
2
3
4
5
6
7
8
DAYS IN SECTOR

displaying the K_p index as a function of day in the sector structure (Figures (3.5a) and (3.5b)) reveals that the toward sector prediction of Figure (8.2) has the general characteristics of the K_p index for these sectors while the away sector prediction of Figure (8.1) bears no resemblance to the K_p index in these sectors. Just why the analysis works for the toward sectors and not for the away sectors remains unclear at the present time. An argument is presented to explain this result but more work should be done to further identify the causes.

If the northern hemisphere of the sun was more active (as suggested by Wilcox (1968)) at the time of these sector structure measurements then an away sector would have southerly components while a toward sector would have northerly components. When the earth is in a toward sector there is little chance for the merging of interplanetary and magnetospheric magnetic fields (see section 9.3). Geomagnetic disturbances due to magnetic field line merging would therefore be absent in the toward sectors. This leaves the Kelvin-Helmholtz mechanism free to operate without the merging mechanism to cloud up the picture. Other disturbance phenomena may be present, however, but the Kelvin-Helmholtz mechanism apparently dominates in the toward sectors. When the earth is in an away sector it appears that the merging process dominates as an examination of Figures (3.2) and (3.5) reveals.

Appendix 1

8,3 Determination of $B_S Cos\Psi_S$ and $B_M Cos\Psi_M$

Define the radius vector from the center of the earth to the magnetopause crossing point in solar ecliptic coordinates (Figure (8.3)) to be

$$\vec{R}_{SE} = X_{SE}\hat{i} + Y_{SE}\hat{j} + Z_{SE}\hat{k} \quad ,$$

where $\hat{i}$, $\hat{j}$, and $\hat{k}$ are the unit vectors along the solar ecliptic axes.

The plane containing the magnetic field vectors and the solar stream velocity is defined by the following two equations:

$$(\vec{R}_{SE} \times \hat{i}) \cdot \vec{U} = 0 \qquad (8.1)$$

$$(\vec{B}_M \times \vec{B}_S) \cdot \vec{U} = 0 \quad . \qquad (8.2)$$

The solar stream velocity and magnetic fields may be written as,

$$\vec{U} = u\hat{i} + v\hat{j} + w\hat{k}$$

$$\vec{B}_M = B_{Mx}\hat{i} + B_{My}\hat{j} + B_{Mz}\hat{k}$$

$$\vec{B}_S = B_{Sx}\hat{i} + B_{Sy}\hat{j} + B_{Sz}\hat{k} \quad ,$$

where

Figure 8.3

The solar ecliptic coordinate system.

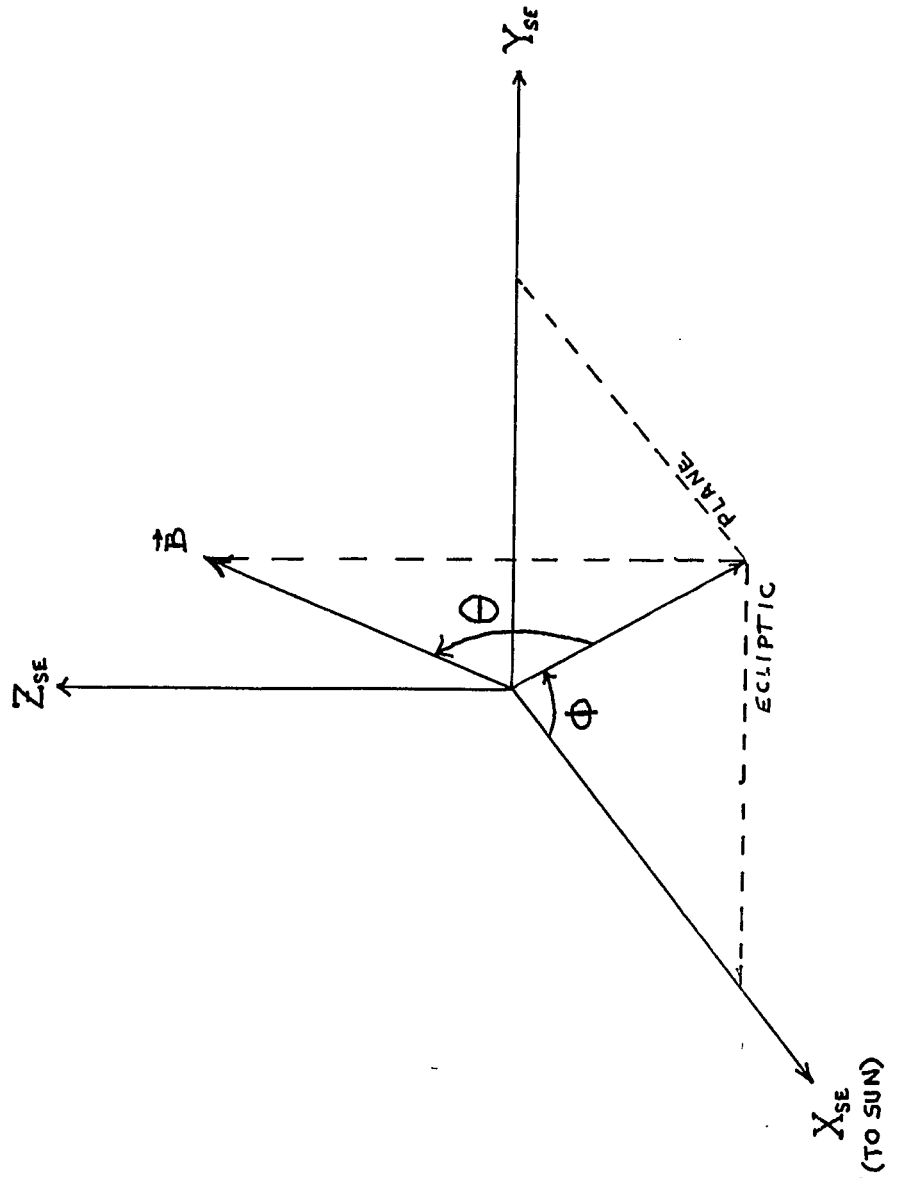
Y_{SE}
B
Z_{SE}
Θ
Φ
PLANE
ECLIPTIC
X_{SE}
(TO SUN)

$$|\vec{U}| = (u^2 + v^2 + w^2)^{\frac{1}{2}} \tag{8.3}$$

$$B_{Mx} = |\vec{B}_M| \cos\theta_M \cos\phi_M$$

$$B_{My} = |\vec{B}_M| \cos\theta_M \sin\phi_M$$

$$B_{Mz} = |\vec{B}_M| \sin\theta_M$$

$$B_{Sx} = |\vec{B}_S| \cos\theta_S \cos\phi_S$$

$$B_{Sy} = |\vec{B}_S| \cos\theta_S \sin\phi_S$$

$$B_{Sz} = |\vec{B}_S| \sin\theta_S \quad .$$

In component form, Equations (8.1) and (8.2) may then be written as,

$$wY_{SE} - vZ_{SE} = 0 \tag{8.4}$$

$$u(B_{My}B_{Sz} - B_{Mz}B_{Sy}) + v(B_{Mz}B_{Sx} - B_{Mx}B_{Sz})$$

$$+ w(B_{Mx}B_{Sy} - B_{My}B_{Sx}) = 0 \quad . \tag{8.5}$$

The individual components of the solar stream velocity may be found by simultaneously solving Equations (8.3), (8.4), and (8.5). The following relations,

$$|\vec{B}_M| \cos\Psi_M = \frac{\vec{U}\cdot\vec{B}_M}{|\vec{U}|}$$

$$|\vec{B}_S| \cos\Psi_S = \frac{\vec{U}\cdot\vec{B}_S}{|\vec{U}|}$$

are then determined.

Appendix 2

8.4 Assumptions Regarding the Magnetic Fields at the Flanks

CROSSING 1:

$|\vec{B}_M|$ at the flank is a factor of 3 less than $|\vec{B}_M|$ at this crossing point (Fairfield, 1968a) and at this time Ψ_M is likely to be 90°, so that $|\vec{B}_M| \cos\Psi_M = 0$. $|\vec{B}_S|$ at the flank is about a factor of 2 less than $|\vec{B}_S|$ at this crossing point (Alksne, 1967) and it is assumed that $\Psi_S = 0^\circ$.

CROSSING 2:

$|\vec{B}_M|$ at the flank is a factor of 55/18 less than $|\vec{B}_M|$ at this crossing point (Fairfield, 1968a) and at this time $\Psi_M \cong 79^\circ 15'$, so that $|\vec{B}_M| \cos\Psi_M = 2.75$. $|\vec{B}_S|$ at the flank is about a factor of 2 less than $|\vec{B}_S|$ at this crossing point (Alksne, 1967) and it is assumed that $\Psi_S = 0^\circ$.

CROSSING 3:

$|\vec{B}_M|$ at the flank is a factor of 40/18 less than $|\vec{B}_M|$ at this crossing point (Fairfield, 1968a) and at this time $\Psi_M \cong 88^\circ 11'$ so that $|\vec{B}_M| \cos\Psi_M = 0.935$. $|\vec{B}_S|$ at the flank is about a factor of 2 less than $|\vec{B}_S|$ at the crossing point (Alksne, 1967) and it is assumed that $\Psi_S = 0^\circ$.

CROSSING 4:

$|\vec{B}_M|$ at the flank is a factor of 3/2 less than $|\vec{B}_M|$

at this crossing point (Fairfield, 1968a) and at this time $\Psi_M \cong 62^\circ$ so that $|\vec{B}_M| \cos\Psi_M = 9.4'$. $|\vec{B}_S|$ at the flank is about a factor of 1.5 less than $|\vec{B}_S|$ at the crossing point (Alksne, 1967) and it is assumed that $\Psi_S = 0^\circ$.

CROSSING 5:

$|\vec{B}_M|$ at the flank is a factor of 22/18 less than $|\vec{B}_M|$ at this crossing point (Fairfield, 1968a) and at this time $\Psi_M \cong 73^\circ 48'$ so that $|\vec{B}_M| \cos\Psi_M = 3.51$. $|\vec{B}_S|$ at the flank is about a factor of 1.5 less than $|\vec{B}_S|$ at the crossing point (Alksne, 1967) and it is assumed that $\Psi_S = 0^\circ$.

CHAPTER 9

CONCLUDING REMARKS AND SUMMARY

9.1 Evidence for Waves on the Magnetopause

There have been numerous examples of motion of the magnetopause interpreted as surface waves from the data of magnetometer and plasma experiments aboard satellites (Judge and Coleman, 1962; Bonetti et al., 1963; Cahill, 1963; Heppner et al., 1963; Hirshberg, 1963; Rosser, 1963; Sonett, 1963; Freeman, 1964; Patel and Cahill, 1964; Heppner, 1965; Konradi and Kaufmann, 1965; Patel, 1965a; Patel, 1965b; Lin and Anderson, 1966; Cahill and Patel, 1967; Fairfield and Ness, 1967; Gosling et al., 1967a; Heppner et al., 1967; Patel et al., 1967; Anderson et al., 1968; Kaufmann and Konradi, 1969; Smith and Davis, 1970). Most of these waves have periods of 100 seconds or more and appear to have their wave vectors oriented along the streaming direction (Heppner et al., 1967). The amplitude determined from one set of data (Patel et al., 1967) appears to be about $1R_E$. Most of these measurements have been taken near the flanks of the magnetosphere. The very large amplitude waves detected by Kaufmann and Konradi (1969) are elongated along the north-south direction and move in the direction of the streaming magnetosheath plasma along the flanks of the magnetosphere. Some correlation has been found by these workers between the occurrence of these bumps or large scale nonuniformities and magnetogram records at auroral observatories. These waves seem to occur when the solar wind parameters undergo a change and larger amplitudes occur when the magnetosheath field

lines up with the magnetospheric field. They envision this change as occurring across a tangential discontinuity propagating with the solar wind.

9.2 Hydromagnetic Waves in the Magnetosphere and their Observation at the Surface of the Earth

Hydromagnetic waves have been observed in the magnetosphere (Dessler, 1958; Judge and Coleman, 1962; MacDonald, 1962; Sonett, 1963; Patel, 1965; Cummings et al., 1969) and ground records show circularly or eliptically polarized waves of the expected frequencies, assuming they were caused by the magnetopause waves (Jacobs and Sinno, 1960; Sugiura, 1961; Wilson and Sugiura, 1961; Sugiura and Wilson, 1964; Kokubun and Nagata, 1965; Atkinson and Watanabe, 1966; Wilson, 1966). The giant micropulsations show strong geomagnetically conjugate correlations and are well confined in longitude (Veldkamp, 1960; Nagata et al., 1963; Annexstad and Wilson, 1968). Their polarization is consistent with surface wave motions of the magnetopause. The left-handed polarization occurs on the dawn side and the right-handed polarization occurs on the dusk side. Micropulsations of all periods are generally confined to the day side of the earth and have maxima in the auroral zones. Their early morning maxima suggest strong wave motions along the dawn flank and a preference for left-handed circularly polarized hydromagnetic wave transmission. The latter has been theoretically demonstrated by Piddington (1955). Theoretical treatments of the transmission of hydromagnetic waves through the magnetosphere to the surface of the earth have been given by Prince and Bostick (1964),

Greifinger and Greifinger (1965), Field and Greifinger (1965, 1966), and Sen (1968a, 1968b). Resonant modes of oscillation of the magnetosphere have been studied by Radoski and Carovillano (1966), Radoski (1967), and Radoski and McClay (1967). The frequencies recorded at ground are theoretically capable of having been produced by hydromagnetic waves propagating through the magnetosphere from the magnetopause. The amplitudes of the magnetic variations on the ground are approximately the same as the amplitudes at the magnetopause (Patel, 1965). Dungey and Southwood (1969) have recently analyzed magnetomater data from Explorer 33 when it was below the magnetopause and find the polarizations to agree with those measured on the ground near dawn and dusk.

9.3 Open Versus Closed Magnetosphere

The question of whether or not the interplanetary magnetic field directly connects to the magnetospheric magnetic field has been a controversial one. Dungey (1958, 1961, 1963a, 1963b, 1968b) and Levy et al. (1964) have proposed that a southward component of the interplanetary magnetic field would merge with the magnetospheric magnetic field near the nose of the magnetosphere. As the solar wind carries this southwardly directed magnetic field past the magnetosphere, the dipole field lines passing through the polar caps are envisioned to be directly connected to the interplanetary magnetic field. Disconnection takes place in the tail. The rate of merging of these field lines at the nose of the magnetosphere would control the extent of geomagnetic storms.

The closed model of Dessler (1961, 1962, 1964, 1965) and Dessler and Walters (1964) portrays the entire magnetopause as a tangential discontinuity. The geomagnetic K_p index is thought of as being caused by the time rate of change of the total pressure of the solar wind at the boundary (Dessler and Fejer, 1963). Evidence for this has been given by Gosling et al. (1967b), Siscoe et al. (1968), and Burlaga and Ogilvie (1969) when sudden impulses and sudden commencements occur after the passage of sudden changes in the solar wind parameters.

The model of Reid and Sauer (1967) is a combination of the open and closed models. They envision a closed magnetosphere in the north and an open one in the south. This compromise, however, has been found to be untenable by Stolov (1969) by an examination of observed solar cosmic ray events by Mariners 2 and 4 and the subsequent effects in the polar caps.

The simultaneous observations of solar protons inside (Injun IV) and outside (Explorer 33) the magnetosphere has led Krimigis et al. (1967) to favor the Dungey model while Hakura (1967) and Williams and Bostrom (1969) support the Dessler model in their analyses of the access of solar protons in the polar cap regions by an apparent diffusion process.

Sonnerup and Cahill (1967, 1968) find that the rotational discontinuities have normal components of magnetic field intensity greater than 5γ and they occur during magnetic storms. They found further that the average value of K_p was 5 when rotational discontinuities existed while K_p = 3- when there were tangential

discontinuities.

Fairfield and Cahill (1966), Schatten and Wilcox (1967), and Fairfield (1968b) find that a southward component of the interplanetary magnetic field is generally more geomagnetically effective than a field with a northward component. Schatten and Wilcox (1967) also find that K_p is consistently higher in the away sectors (they point out that a higher velocity could be responsible for this in the away sector), which means, when Figure (3.6) is recalled, that a southward component would be expected. A toward sector would mean that northward components should be found. Lanzerotti (1968) finds that the strength of geomagnetic storms is proportional to the amount of time that the interplanetary magnetic field is southward. Magnetic merging seems to be an important process in the development of magnetic storms. Maguire and Carovillano (1968a, 1968b) and Carovillano and Maguire (1968) find that the interplanetary magnetic field contributes energy to geomagnetic storms when merging takes place at the magnetopause.

Ballif et al. (1967), Ballif and Jones (1967), and Ballif et al. (1969) find that transverse fluctuations of the interplanetary magnetic field are also important for producing geomagnetic disturbance. Other evidence that the changes and configuration of the interplanetary magnetic field are important has been given by Rostoker and Falthammar (1967) and Rostoker (1968).

The correlations between the interplanetary magnetic field, plasma density, solar wind velocity, and the daily sum

of the K_p index as the sector structures rotate past the earth have been pointed out in Chapter 3 and seem to be true also for the rising portion of the sunspot cycle (Wilcox and Colburn, 1969). It is therefore expected that the results of section 8.2 may also be true for this part of the solar cycle.

It appears that the magnetopause is not always a tangential discontinuity. Local instabilities at the boundary, as suggested here by the Kelvin-Helmholtz mechanism, will disrupt the tangential discontinuity in the form of growing, large amplitude waves along the flanks once the parameters take on favorable values for instability. If the interplanetary field has a component perpendicular to the plane of the ecliptic the angle Ψ_s in the instability condition will generally be larger at the flanks than normal since the plasma flow convects the magnetic field through the magnetosheath. This will clearly favor instability. Extreme Northward fields show a slight association with geomagnetic disturbance if the curves of Schatten and Wilcox (1967) and Wilcox et al. (1967) are examined closely. This effect has also been noticed by Patel el al. (1967), and is consistent with the Kelvin-Helmholtz mechanism. The stronger association with southward fields merely indicates that the merging mechanism could also be operating in concert with the Kelvin-Helmholtz mechanism.

The disruption of the magnetic field lines near the flanks has been indirectly observed by Williams (1967) and McDiarmid and Wilson (1968) through the observation of the lowering of the electron trapping boundary during magnetic storms and when the

angle between the dipole and the sun-earth line (i.e., Ψ_M) was 90°. The general picture is one in which the development of the instability produces large amplitude waves which get convected into the tail (Ness, 1965) of the magnetosphere carrying the magnetospheric field lines with them thereby resulting in a lowering of the trapping boundary. Parker (1967) envisions this as a peeling away of the outer layers of the magnetosphere along the flanks.

9.4 Summary

A derivation of the Archimedes spiral equation for particles emitted radially in the reference frame of the sun has been given. It reduces to the standard form of the Archimedes spiral equation when appropriate approximations are made. The structure of the interplanetary field is given which is based on the spiral equation developed here.

Following Chandrasekhar, an instability condition was developed for the magnetopause. It was then shown that Kelvin-Helmholtz instability along the flanks of the magnetosphere exhibits a semiannual variation with instability maxima at the equinoxes and instability minima at the solstices. The angle between the solar wind streaming and the magnetospheric magnetic field at the flanks has been shown to be the relevant parameter. The predicted behavior of the diurnal variation of geomagnetic activity on the basis of the Kelvin-Helmholtz mechanism is displayed by selected geomagnetic observatories just below the auroral regions by an analysis of their K indices. It was

expected that these auroral zone stations would display most strongly the effects of Kelvin-Helmholtz instability at the flanks of the magnetosphere. In addition, analysis of the parameters involved has shown that the instability condition is fulfilled at times of geomagnetic disturbance using data from Explorer 34. Also, an analysis of the sector structure of Wilcox and Ness (1965) has shown that the Kelvin-Helmholtz mechanism appears to dominate geomagnetic activity in the toward sectors for that period of time.

REFERENCES

Akasofu, S.-I., and S. Chapman, Geomagnetic storms and auroras, in Physics of Geomagnetic Phenomena, Volume II, p. 1113, edited by S. Matsushita, and W. H. Campbell, Academic Press, New York and London, 1967.

Akasofu, S.-I., Polar and Magnetospheric Substorms, D. Reidel Publishing Company, Dordrecht, Holland, 1968.

Alfven, H., Cosmical Electrodynamics, Oxford University Press (Clarendon), London and New York, 1950.

Alfven, H., and C.-G. Falthammar, Cosmical Electrodynamics, 2nd ed., Oxford University Press (Clarendon), London and New York, 1963.

Alksne, A. Y., The steady-state magnetic field in the transition region between the magnetosphere and the bow shock, Planetary Space Sci., 15, 239, 1967.

Anderson, K. A., J. H. Binsack, and D. H. Fairfield, Hydromagnetic disturbances of 3- to 15- minute period on the magnetopause and their relation to bow shock spikes, J. Geophys. Res., 73, 2371, 1968.

Annexstad, J. O., and C. R. Wilson, Characteristics of Pg Micropulsations at conjugate points, J. Geophys. Res., 73, 1805, 1968.

Argo, H. V., J. R. Asbridge, S. J. Bame, A. J. Hundhausen, and I. B. Strong, Observations of solar wind plasma changes across the bow shock, J. Geophys. Res., 72, 1989, 1967.

Atkinson, G., A theory of polar substorms, J. Geophys. Res., 71, 5157, 1966.

Atkinson, G., and T. Watanabe, Surface waves on the magnetospheric boundary as a possible origin of long period geomagnetic micropulsations, Earth Planetary Sci. Letters, 1, 89, 1966.

Axford, W. I., The stability of plane current-vortex sheets, Q. Journal Mech. and App. Math., 13, Part3, 314, 1960.

Axford, W. I., Note on a problem of magnetohydrodynamic stability, Canad. J. Phys., 40, 654, 1962a.

Axford, W. I., The interaction between the solar wind and the earth's magnetosphere, J. Geophys. Res., 67, 3791, 1962b.

Axford, W. I., Viscous interaction between the solar wind and the earth's magnetosphere, Planetary Space Sci., 12, 45, 1964.

Babcock, H. D., The sun's polar magnetic field, Astrophys. J., 130, 364, 1959.

Babcock, H. W., and W. D. Babcock, The sun's magnetic field, 1952-1954, Astrophys. J., 121, 349, 1955.

Ballif, J. R., and D. E. Jones, The magnetic morphology of solar streams and its relation to geomagnetic storms, J. Geophys. Res., 72, 5173, 1967.

Ballif, J. R., D. E. Jones, P. J Coleman, Jr., L. Davis, Jr., and E. J. Smith, Transverse fluctuations in the interplanetary magnetic field: a requisite for geomagnetic variability, J. Geophys. Res., 72, 4357, 1967.

Ballif, J. R., D. E. Jones, and P. J. Coleman, Jr., Further evidence on the correlation between transverse fluctuations in the interplanetary magnetic field and K_p, J. Geophys. Res., 74, 2289, 1969.

Barrington, R. E., and J. A. Fejer, Ionospheric noise and geomagnetic micropulsations, in Physics of the Earth's Upper Atmosphere, edited by C. O. Hines, I. Paghis, T. R. Hartz, and J. A. Fejer, p. 176, Prentice-Hall, Inc., Englewood Cliffs, New Jersey, 1965.

Bartels, J., Terrestrial-magnetic activity and its relations to solar phenomena, Terr. Magn., 37, 1, 1932.

Bartels, J., Geomagnetic and solar data, J. Geophys. Res., 54, 296, 1949.

Bartels, J., Geomagnetism, Part I, Annals of the IGY, Vol. IV, Parts IV-VII, 209, 1957.

Bartels, J., Discussion of time-variations of geomagnetic activity indices K_p and A_p, 1932-1961, Annales de Geophysique, 19, 1, 1963.

Bartels, J., N. H. Heck, and H. F. Johnston, The three-hour range index measuring geomagnetic activity, J. Geophys. Res., 44, 411, 1939.

Beard, D. B., The interaction of the terrestrial magnetic field with the solar corpuscular radiation, J. Geophys. Res., 65, 3559, 1960.

Beard, D. B., The interaction of the terrestrial magnetic field with the solar corpuscular radiation, 2, Second-order approximation, J. Geophys. Res., 67, 477, 1962.

Bell, B., Major flares and geomagnetic activity, Smithsonian Contr. Astrophys., 5, 69, 1961.

Bernstein, W., R. W. Fredricks, and F. L. Scarf, A model for a broad disordered transition between the solar wind and the magnetosphere, J. Geophys. Res., 69, 1201, 1964.

Biermann, L., Kometenschweife und solare Korpuskularstrahlung, Z. Astrophys., 29, 274, 1951.

Biermann, L., Physical processes in comet tails and their relation to solar activity, extrait des Mem. Soc. Roy. Sci. Liege Quatr. Ser., 13, 291, 1953.

Biermann, L., Solar corpuscular radiation and the interplanetary gas, Observatory, 77, 109, 1957.

Blevis, B. C., and W. C. Collins, Radio aurora, in Physics of the Earth's Upper Atmosphere, edited by C. O. Hines, I. Paghis, T. R. Hartz, and J. A. Fejer, p. 319, Prentice-Hall, Inc., Englewood Cliffs, New Jersey, 1965.

Bonetti, A., H. S. Bridge, A. J. Lazarus, B. Rossi, and F. Sherb, Explorer 10 plasma measurements, J. Geophys. Res., 68, 4017, 1963.

Bridge, H., J. A. Egidi, A. Lazarus, E. Lyon, and L. Jacobson, Preliminary results of plasma measurements on IMP-A, Space Res., 5, North Holland Publishing Co., 969, 1965.

Burlaga, L. F., and K. W. Ogilvie, Observations of the magnetosheath-solar wind boundary, J. Geophys. Res., 73, 6167, 1968.

Burlaga, L. F., and K. W. Ogilvie, Causes of sudden commencements and sudden impulses, J. Geophys. Res., 74, 2815, 1969.

Cahill, L. J., Jr., A study of the outer geomagnetic field, Space Res., 3, 324, 1963.

Cahill, L. J., Jr., and P. G. Amazeen, The boundary of the geomagnetic field, J. Geophys. Res., 68, 1835, 1963.

Cahill, L. J., Jr., and V. L. Patel, The boundary of the geomagnetic field, August to November, 1961, Planetary Space Sci., 15, 997, 1967.

Carovillano, R. L., J. F. McClay, and H. R. Radoski, editors, Physics of the Magnetosphere, D. Reidel Publishing Company, Dordrecht Holland, 1968.

Carovillano, R. L., and J. J. Maguire, Magnetic merging and the energy of geomagnetic disturbances, abstract, Trans. Am. Geophys. Union, 49, 276, 1968.

Chamberlain, J. W., Interplanetary gas, 2, Expansion of a model solar corona, Astrophys. J., 131, 47, 1960.

Chandrasekhar, S., Hydrodynamic and Hydromagnetic Stability, Oxford University Press (Clarendon), London and New York, 1961.

Chapman, S., Solar streams of corpuscles: their geometry, absorption of light, and penetration, Monthly Notices Roy. Astron. Soc., 89, 456, 1929.

Chapman, S., Solar Plasma, Geomagnetism, and Aurora, Gordon and Breach, New York, 1964.

Chapman, S., and J. Bartels, Geomagnetism, Oxford University Press (Clarendon), London, 1940.

Chapman, S., and V. C. A. Ferraro, A new theory of magnetic storms, Terr. Magn. Atmos. Elec., 36, 77, 1931.

Chapman, S., and V. C. A. Ferraro, A new theory of magnetic storms, Part II, The main phase, Terr. Magn. Atmos. Elec., 38, 79, 1933.

Cole, J. D., and J. H. Huth, Some interior problems of hydromagnetics, Phys. Fluids, 2, 624, 1959.

Coleman, P. J., Jr., L. Davis, Jr., E. J. Smith, and D. E. Jones, Variations in the polarity distribution of the interplanetary magnetic field, J. Geophys. Res., 71, 2831, 1966.

Coleman, P. J., Jr., L. Davis, Jr., E. J. Smith, and C. P. Sonett, Interplanetary magnetic fields: preliminary Mariner 2 observations, Science, 138, 1099 1962.

Coleman, P. J., Jr., L. Davis, and C. P. Sonett, Steady component of the interplanetary magnetic field: Pioneer V, Phys. Rev. Letters, 5, 43, 1960.

Coleman, P. J., Jr., C. P. Sonett, D. L. Judge, and E. J. Smith, Some preliminary results of the Pioneer 5 magnetometer experiment, J. Geophys. Res., 65, 1856, 1960.

Collins, W. C., and L. Herzberg, Solar activity and short-lived terrestrial effects (SID), in Physics of the Earth's Upper Atmosphere, edited by C. O. Hines, I. Paghis, T. R. Hartz, and J. A. Fejer, p. 198, Prentice-Hall, Inc., Englewood Cliffs, New Jersey, 1965.

Cortie, A. L., Sunspots and terrestrial magnetic phenomena, 1898-1911, Monthly Notices Roy. Astron. Soc., 73, 52, 1912.

Cummings, W. D., and P. J. Coleman, Jr., Magnetic fields in the magnetopause and vicinity at synchronous altitude, J. Geophys. Res., 73, 5699, 1968.

Cummings, W. D., A. W. Harris, and P. J. Coleman, Jr., Observations of the magnetopause and magnetosheath at 6.6R_E, Trans. Am. Geophys. Union, 49, 229, 1968.

Cummings, W. D., R. J. O'Sullivan, and P. J. Coleman, Jr., Standing Alfven waves in the magnetosphere, J. Geophys. Res., 74, 778, 1969.

Currie, R. G., The geomagnetic spectrum - 40 days to 5.5 years, J. Geophys. Res., 71, 4579, 1966.

Davis, L., Jr., and D. B. Beard, A correction to the approximate condition for locating the boundary between a magnetic field and a plasma, J. Geophys. Res., 67, 4505, 1962.

Dessler, A. J., Large amplitude hydromagnetic waves above the ionosphere, J. Geophys. Res., 63, 507, 1958.

Dessler, A. J., The stability of the interface between the solar wind and the geomagnetic field, J. Geophys. Res., 66, 3587, 1961.

Dessler, A. J., Further comments on stability of interface between solar wind and geomagnetic field, J. Geophys. Res., 67, 4892, 1962.

Dessler, A. J., Length of the magnetospheric tail, J. Geophys. Res., 69, 3913, 1964.

Dessler, A. J., Physical significance of inhomogeneities in polar cap absorption events, J. Geophys. Res., 70, 4305, 1965.

Dessler, A. J., Solar wind and interplanetary magnetic field, Rev. Geophys., 5, 1, 1967.

Dessler, A. J., and J. A. Fejer, Interpretation of K_p index and M-region geomagnetic storms, Planetary Space Sci., 11, 505, 1963.

Dessler, A. J., and G. K. Walters, Hydromagnetic coupling between solar wind and magnetosphere, Planetary Space Sci., 12, 227, 1964.

Dryer, M., and R. Faye-Petersen, The magnetogasdynamic boundary condition for a self-consistent solution to the closed magnetopause, AIAA J., 4, 246, 1966.

Dryer, M., and G. R. Heckman, On the hypersonic analogue as applied to planetary interaction with the solar plasma, Planetary Space Sci., 15, 515, 1967.

Dungey, J. W., Cosmic Electrodynamics, Cambridge University Press, New York and London, 1958.

Dungey, J. W., The steady state of the Chapman-Ferraro problem in two dimensions, J. Geophys. Res., 66, 1043, 1961.

Dungey, J. W., Interaction of solar plasma with the geomagnetic field, Planetary Space Sci., 10, 233, 1963a.

Dungey, J. W., Structure of the exosphere or adventures in velocity space, in Geophysics, the Earth's Environment, edited by C. DeWitt, J. Hieblot, and A. Lebeau, p. 505, Gordon and Breach, New York, 1963b.

Dungey, J. W., Waves and particles in the magnetosphere, in Physics of the Magnetosphere, edited by R. L. Carovillano, J. F. McClay, and H. R. Radoski, p. 218, D. Reidel Publishing Company, Dordrecht, Holland, 1968.

Dungey, J. W., The reconnection model of the magnetosphere, in Earth's Particles and Fields, edited by B. M. McCormac, Reinhold, N.Y., 1968b.

Dungey, J. W., and D. J. Southwood, Ultra low frequency waves in the magnetosphere, Imperial College of Science and Technology, University of London, preprint, August, 1969.

Ellison, M. A., Solar flares, Nature, 193, 532, 1962.

Fairfield, D. H., The ordered magnetic field of the magnetosheath, J. Geophys. Res., 72, 5865, 1967.

Fairfield, D. H., Average magnetic field configuration of the outer magnetosphere, J. Geophys. Res., 73, 7329, 1968a.

Fairfield, D. H., Polar magnetic disturbances and the interplanetary magnetic field, Space Res., 8, 107, 1968b.

Fairfield, D. H. and L. J. Cahill, Jr., Transition region magnetic field and polar magnetic disturbances, J. Geophys. Res., 71, 155, 1966.

Fairfield, D. H., and N. F. Ness, Magnetic field measurements with IMP2, J. Geophys. Res., 72, 2379, 1967.

Fejer, J. A., Hydromagnetic reflection and refraction at a fluid velocity discontinuity, Phys. Fluids, 6, 508, 1963.

Fejer, J. A., Hydromagnetic stability of a fluid velocity discontinuity between compressible fluids, Phys. Fluids, 7, 499, 1964.

Ferraro, V. C. A., An approximate method of estimating the size and shape of the stationary hollow carved out in a neutral ionized stream of corpuscles impinging on the geomagnetic field, J. Geophys. Res., 65, 3951, 1960.

Field, E. C., and C. Greifinger, Transmission of geomagnetic micropulsations through the ionosphere and lower exosphere, J. Geophys. Res., 70, 4885, 1965.

Field, E. C., and C. Greifinger, Equatorial transmission of geomagnetic micropulsations through the ionosphere and lower exosphere, J. Geophys. Res., 71, 3223, 1966.

Frank, L. A., and J. A. Van Allen, A survey of magnetospheric boundary phenomena, in Research in Geophysics, Vol. I: Sun, Upper Atmosphere, and Space, p. 161, edited by H. Odishaw, M.I.T. Press, Cambridge, Massachusetts, 1964.

Freeman, J. W., The morphology of the electron distribution in the outer radiation zone and near the magnetospheric boundry as observed by Explorer 12, J. Geophys. Res., 69, 1691, 1964.

Freeman, J. W., J. A. Van Allen, and L. J. Cahill, Explorer 12 observations of the magnetosphere boundary and the associated solar plasma on Sept. 13, 1961, J. Geophys. Res., 68, 2120, 1963.

Gerwin, R. A., Stability of the interface between two fluids in relative motion, Rev. Mod. Phys., 40, 652, 1968.

Gold, T., Magnetic field in the solar system, Nuovo Cimento, Suppl. (10) 13, 318, 1959.

Gosling, J. T., J. R. Asbridge, S. J. Bame, and I. B. Strong, Vela 2 measurements of the magnetopause and bow shock positions, J. Geophys. Res., 72, 101, 1967a.

Gosling, J. T., J. R., Asbridge, S. J. Bame, A. J. Hundhausen, and I. B. Strong, Discontinuities in the solar wind associated with sudden geomagnetic impulses and storm commencements, J. Geophys. Res., 72, 3357, 1967b.

Greifinger, C., and P. Greifinger, Transmission of micropulsations through the lower ionosphere, J. Geophys. Res., 70, 2217, 1965.

Gringauz, K. I., V. V. Bezrukikh, V. D. Ozerov, and R. Ye Rybchinskiy, Study of the interplanetary ionized gas, high energy electrons, and solar corpuscular radiation by means of three electrode traps for charged particles on the second Soviet cosmic rocket, Soviet Phys. Doklady, 5, 361, 1960.

Gringauz, K. I., V. V. Bezrukikh, S. M. Balandina, V. D. Ozerov, and R. E. Rybchinskiy, Direct observations of solar plasma streams at a distance of ~ 1,900,000 km. from the earth on Feb. 17, 1961, and simultaneous observations of the geomagnetic field, Space Res., 3, 602, 1963.

Gringauz, K. I., Some results of experiments in interplanetary space by means of charged particle traps on Soviet space probes, Space Res., 2, 539, 1961.

Hakura, Y. Entry of solar cosmic rays into the polar cap atmosphere, J. Geophys. Res., 72, 1461, 1967.

Hartz, T. R., Particle emissions from the disturbed sun, and the sun-earth environment, in Physics of the Earth's Upper Atmosphere, edited by C. O. Hines, I. Paghis, T. R. Hartz, and J. A. Fejer, p. 216, Prentice-Hall, Inc., Englewood Cliffs, New Jersey, 1965.

Heppner, J. P., Recent measurements of the magnetic field in the outer magnetosphere and boundary region, NASA-GSFC Preprint, X-612-65-490, 1965.

Heppner, J. P., N. F. Ness, T. L. Skillman, and C. S. Scearce, Explorer 10 magnetic field measurement, Space Res., 3, 553, 1963.

Heppner, J. P., M. Sugiura, T. L. Skillman, B. G. Ledley, and M. Campbell, OGO-A magnetic field observations, J. Geophys. Res., 72, 5417, 1967.

Hess, W. N., The Radiation Belt and Magnetosphere, Blaisdell Publishing Company, Waltham, Massachusetts, 1968.

Hines, C. O., I. Paghis, T. R. Hartz, and J. A. Fejer, editors Physics of the Earth's Upper Atmosphere, Prentice-Hall, Inc., Englewood Cliffs, New Jersey, 1965.

Hirshberg, J., Motions of the magnetospheric boundary and surface magnetic activity during the flight of Explorer 10, J. Geophys. Res., 68, 5917, 1963.

Holzer, R. E., M. G. McLeod, and E. J. Smith, Preliminary results from the Ogo 1 search coil magnetometer: boundary positions and magnetic noise spectra, J. Geophys. Res., 71, 1481, 1966.

Hultqvist, B., Auroras and polar substorms: Observations and theory, Rev. Geophys., 7, 129, 1969.

Hundhausen, A. J., J. R. Asbridge, S. J. Bame, and I. B. Strong, Vela satellite observations of solar wind ions, A preliminary report, J. Geophys. Res., 72, 87, 1967a.

Hundhausen, A. J., S. J. Bame, and N. F. Ness, Solar wind thermal anisotropies: Vela 3 and Imp 3, J. Geophys. Res., 72, 5265, 1967b.

Hundhausen, A. J., S. J. Bame, and J. R. Asbridge, Plasma flow pattern in the earth's magnetosheath, J. Geophys. Res., 74, 2799, 1969.

Hurley, J., Interaction of a streaming plasma with the magnetic field of a two-dimensional dipole, Phys. Fluids, 4, 854, 1961.

Jacobs, J. A., and K. Sinno, Occurrence frequency of geomagnetic micropulsations, Pc, J. Geophys. Res., 65, 107, 1960.

Judge, D. L., and P. J. Coleman, Jr., Observations of low-frequency hydromagnetic waves in the distant geomagnetic field: Explorer 6, J. Geophys. Res., 67, 5071, 1962.

Kaufmann, R. L., Shock observations with the Explorer 12 magnetometer, J. Geophys. Res., 72, 2323, 1967.

Kaufmann, R. L., and A. Konradi, Explorer 12 magnetopause observations: Large-scale nonuniform motion, J. Geophys. Res., 74, 3609, 1969.

Kellog, P. J., Flow of plasma around the earth, J. Geophys. Res., 67, 3805, 1962.

Kokubun, S., and T. Nagata, Geomagnetic pulsation Pc-5 in and near the auroral zones, Rept. Ionos. Space Res. Japan, 19, 158, 1965.

Konradi, A., and R. L. Kaufmann, Evidence for rapid motion of the outer boundary of the magnetosphere, J. Geophys. Res., 70, 1627, 1965.

Krimigis, S. M., J. A. Van Allen, and T. P. Armstrong, Simultaneous observations of solar protons inside and outside the magnetosphere, Phys. Rev. Letters, 18, 1204, 1967.

Kulikovskiy, A. G., and G. A. Lyubimov, Magnetohydrodynamics, Addison-Wesley Publishing Company, Inc., Reading, Massachusetts, 1965.

Landau, L. D., and E. M. Lifshitz, Fluid Mechanics, Addison-Wesley Publishing Company, Inc., Reading, Massachusetts, 1959.

Lanzerotti, L. J., Outer-zone electrons and the interplanetary magnetic fields during two geomagnetic storms, J. Geophys. Res., 73, 4388, 1968.

Lees, L., Interaction between the solar plasma wind and the geomagnetic cavity, AIAA J., 2, 1576, 1965.

Levy, R. H., H. E. Petschek, and G. L. Siscoe, Aerodynamic aspects of magnetospheric flow, AIAA, 2, 12, 1964.

Lin, R. P., and K. A. Anderson, Periodic modulation of energetic electron fluxes in the distant radiation zone, J. Geophys. Res., 71, 1827, 1966.

McDiarmid, I. B., and M. D. Wilson, Dependence of the high latitude electron (E > 35 kev) boundary on the orientation of the geomagnetic axis, J. Geophys. Res., 73, 7237, 1968.

McIntosh, D. H., On the annual variation of magnetic disturbance, Phil. Trans. Roy. Soc. London, A251, 525, 1959.

MacDonald, G. J. F., Spectrum of hydromagnetic waves in the exosphere, NASA-GSFC Preprint, TR R-143, 1962.

Maguire, J. J., and R. L. Carovillano, The contribution of the interplanetary field to the energy of a magnetic storm, abstract, Trans. Am. Geophys. Union, 49, 276, 1968a.

Maguire, J. J., and R. L. Carovillano, Effect of the interplanetary field on the energy of geomagnetic disturbances, J. Geophys. Res., 73, 3395, 1968b.

Matsushita, S., Geomagnetic disturbances and storms, in Physics of Geomagnetic Phenomena, Vol. II, p. 793, edited by S. Matsushita, and W. H. Campbell, Academic Press, New York and London, 1967.

Matsushita, S., and W. H. Campbell, editors, Physics of Geomagnetic Phenomena, 2 vols., Academic Press, New York, 1967.

Mayaud, P. N., Calcul Preliminaire d'indices K_m, K_n, et K_s ou a_m, a_n et a_s, mesures de l'activite magnetique a l'echelle mondiale et dans les hemispheres Nord et Sud, Annales de Geophysique, 23, 585, 1967.

Mead, G. D., and D. B. Beard, Shape of the geomagnetic field solar wind boundary, J. Geophys. Res., 69, 1169, 1964.

Meyer, J., A semiannual wave in the recurrence tendency of geomagnetic activity, J. Geophys. Res., 71, 2397, 1966.

Michel, F. C., K_p as a planetary index, J. Geophys. Res., 64, 1482, 1964.

Midgley, J. E., Perturbation of the geomagnetic field - a spherical harmonic expansion, J. Geophys. Res., 69, 1197, 1964.

Midgley, J. E., and L. Davis, Jr., Computation of the bounding surface of a dipole field in a plasma by a moment technique, J. Geophys. Res., 67, 499, 1962.

Midgley, J. E., and L. Davis, Jr., Calculation by a moment technique of the perturbation of the geomagnetic field by the solar wind, J. Geophys. Res., 68, 5111, 1963.

Mishin, V. M., G. P. Kalinovskaya, and N. A. Mishina, Annual variation of magnetic activity according to IGY data, Geomagnetism and Aeronomy, 1, 347, 1961.

Mishina, N. A., Semiannual variation of magnetic activity, Geomagnetism and Aeronomy, 7, 104, 1967.

Montalbetti, R., Optical aurora, in Physics of the Earth's Upper Atmosphere, edited by C. O. Hines, I. Paghis, T. R. Hartz, and J. A. Fejer, p. 299, Prentice-Hall, Inc., Englewood Cliffs, New Jersey, 1965.

Mustel, E. R., Results of a statistical study of geomagnetic disturbances for five cycles of solar activity, Soviet Astronomy, A. J., 5, 19, 1961.

Nagata, T., S. Kokubun, and T Sijima, Geomagnetically conjugate relationships of giant pulsations at Syowa Base, Antarctica, and Reykjavik, Iceland, J. Geophys. Res., 68, 4621, 1963.

Ness, N. F., The earth's magnetic tail, J. Geophys. Res., 70, 2989, 1965.

Ness, N. F., C. S. Scearce, and S. C. Cantarano, Preliminary results from Pioneer 6 magnetic field experiment, J. Geophys. Res., 71, 3305, 1966.

Ness, N. F., C. S. Scearce, and J. B. Seek, Initial results of the IMP magnetic field experiment, J. Geophys. Res., 69, 3531, 1964.

Neugebauer, M., and C. W. Snyder, The mission of Mariner 2: Preliminary observations, solar plasma experiment, Science, 138, 1095, 1962.

Nicholson, S. B., and O. R. Wulf, The diurnal variation of irregular geomagnetic fluctuations, J. Geophys. Res, 60, 389, 1955.

Paghis, I., Magnetic and Ionospheric Storms, in Physics of the Earth's Upper Atmosphere, edited by C. O. Hines, I. Paghis, T. R. Hartz, and J. A. Fejer, p. 271, Prentice-Hall, Inc., Englewood Cliffs, New Jersey, 1965.

Parker, E. N., On the geomagnetic storm effect, J. Geophys. Res., 61, 625, 1956.

Parker, E. N., Interaction of the solar wind with the geomagnetic field, Phys. Fluids, 1, 171, 1958a.

Parker, E. N., Dynamics of the interplanetary gas and magnetic field, Astrophys. J., 128, 664, 1958b.

Parker, E. N., Interplanetary Dynamical Processes, Interscience Publishers, John Wiley and Sons, New York and London, 1963.

Parker, E. N., Disturbance of the geomagnetic field by the solar wind, Physics of Geomagnetic Phenomena, edited by S. Matsushita and W. H. Campbell, p. 1153, Academic Press, New York, 1967.

Patel, V. L., Hydromagnetic waves of 3- to 30- minute periods in the magnetosphere (abstract), Trans. Am. Geophys. Union, 46, 114, 1965a.

Patel, V. L., Low-frequency hydromagnetic waves in the magnetosphere, Explorer 12, Planetary Space Sci., 13, 485, 1965b.

Patel, V. L., and L. J. Cahill, Jr., Evidence of hydromagnetic waves in the earth's magnetosphere and of their propagation to the earth's surface, Phys. Rev. Letters, 12, 213, 1964.

Patel, V. L., L. J. Cahill, and A. J. Dessler, Magnetosheath field, geomagnetic index a_p, and stability of magnetopause, J. Geophys. Res., 72, 426, 1967.

Piddington, J. H., Hydromagnetic waves in ionized gas, Monthly Notices Roy. Astron. Soc., 115, 671, 1955.

Price, A. T., A. Romana, and J. Veldkamp, Indices K and C, Rapid Variations, IAGA Bull., No. 12 r2, Geomagnetic Data 1963, published by International Union of Geodesy and Geophysics, Paris, 1966.

Priester, W., and D. Cattani, On the semiannual variation of geomagnetic activity and its relation to the solar corpuscular radiation, J. Atmos. Sci., 19, 121, 1962.

Roosen, J., The seasonal variation of geomagnetic disturbance amplitudes, Bull. Astron. Inst. Netherlands, 18, 295, 1966.

Prince, C. E., and F. X. Bostick, Jr., Ionospheric transmission of transversely propagated plane waves at micropulsation frequencies and theoretical power spectrums, J. Geophys. Res., 69, 3213, 1964.

Radoski, H. R., Introduction to geophysical magnetohydrodynamic resonances, Am. J. Phys. 35, 128, 1967.

Radoski, H. R., and R. L. Carovillano, Axisymmetric plasmasphere resonances: toroidal mode, Phys. Fluids, 9, 285, 1966.

Radoski, H. R., and J. F. McClay, The hydromagnetic toroidal resonance, J. Geophys. Res., 72, 4899, 1967.

Reid, G. C., Solar cosmic rays and the ionosphere, in Physics of the Earth's Upper Atmosphere, edited by C. O. Hines, I. Paghis, T. R. Hartz, and J. A. Fejer, p. 245, Prentice-Hall, Inc., Englewood Cliffs, New Jersey, 1965.

Reid, G. C., and H. H. Sauer, Evidence for nonuniformity of solar-proton precipitation over the polar caps, J. Geophys. Res., 72, 4383, 1967.

Rosser, W. G. V., Changes in the structure of the outer radiation zone associated with the magnetic storm of September 30, 1961, J. Geophys. Res., 68, 3131, 1963.

Rostoker, G., Relationship between the onset of a geomagnetic bay and the configuration of the interplanetary field, J. Geophys. Res., 73, 4382, 1968.

Rostoker, G., C.-G. Falthammar, Relationship between changes in the interplanetary magnetic field and variations in the magnetic field at the earth's surface, J. Geophys. Res., 72, 5853, 1967.

Schatten, K. H., and J. M. Wilcox, Response of the geomagnetic activity index K_p to the interplanetary magnetic field, J. Geophys. Res., 72, 5185, 1967.

Sen, A. K., Stability of hydromagnetic Kelvin-Helmholtz discontinuity, Phys. Fluids, 6, 1154, 1963.

Sen, A. K., Effect of compressibility on Kelvin-Helmholtz instability in a plasma, Phys. Fluids, 7, 1293, 1964.

Sen, A. K., A theory of geomagnetic micropulsations, I, J. Geomag. Geoelect., 20, 225, 1968a.

Sen, A. K., A theory of geomagnetic micropulsations, II, J. Geomag. Geoelect., 20, 245, 1968b.

Shapiro, R., The semiannual variation of geomagnetic disturbance and its modulation of shorter period variations, J. Geophys. Res., 74, 2356, 1969.

Siscoe, G. L., V. Formisano, and A. J. Lazarus, Relation between geomagnetic sudden impulses and solar wind pressure changes - an experimental investigation, J. Geophys. Res., 73, 4869, 1968.

Slutz, R. J., The shape of the geomagnetic field boundary under uniform external pressure, J. Geophys. Res., 67, 505, 1962.

Smith, E. J., and L. Davis, Jr., Magnetic measurements in the earth's magnetosphere and magnetosheath: Mariner 5, J. Geophys. Res., 75, 1233, 1970.

Snyder, C. W., M. Neugebauer, and U. R. Rao, The solar wind velocity and its correlation with cosmic-ray variations and with solar and geomagnetic activity, J. Geophys. Res., 68, 6361, 1963.

Sonett, C. P., Coupling of the solar wind and the exosphere, Phys.. Rev. Letters, 5, 46, 1960.

Sonett, C. P., Hyperwaves, shock-like phenomena in the outer exosphere, J. Phys. Soc. Japan, 17, Suppl. A-II, 528, 1962..

Sonett, C. P., The distant geomagnetic field, 5, Long-period oscillations, J. Geophys. Res., 68, 6371. 1963.

Sonett, C. P., D. S. Colburn, L. Davis, Jr., E. S. Smith, and P. J. Coleman, Jr., Evidence for a collision-free magnetohydrodynamic shock in interplanetary space, Phys. Rev. Letters, 13, 153, 1964.

Sonett, C. P., E. J. Smith, D. L. Judge, and P. J. Coleman, Jr., Current systems in the vestigial geomagnetic field: Explorer VI, Phys. Rev. Letters, 4, 161, 1960.

Sonnerup, B. U. O., and L. J. Cahill, Jr., Magnetopause structure and attitude from Explorer 12 observations, J. Geophys. Res., 72, 171, 1967.

Sonnerup, B. U. O., and L. J. Cahill, Jr., Explorer 12 observations of the magnetopause current layer, J. Geophys. Res., 73, 1757, 1968.

Southwood, D. J., The hydromagnetic stability of the magnetospheric boundary, Planetary Space Sci., 16, 587, 1968.

Spreiter, J. R., and A. Y. Alksne, Comparison of theoretical predictions of the flow and magnetic field exterior to the magnetosphere with the observations of Pioneer 6, Planetary Space Sci., 16, 971. 1968.

Spreiter, J. R., and A. Y. Alksne, Plasma flow around the magnetosphere, Rev. Geophys., 7, 11. 1969.

Spreiter, J. R., A. Y. Alksne, and A. L. Summers, External Aerodynamics of the magnetosphere, in Physics of the Magnetosphere, edited by R. L. Carovillano, J. F. McClay, and H. R. Radoski, p. 301, D. Reidel Publishing Company, Dordrecht, Holland, 1968.

Spreiter, J. R., and B. R. Briggs, Theoretical determination of the form of the hollow produced in the solar corpuscular stream by the interaction with the magnetic dipole field of the earth, NASA Preprint, TR R-120, 1961.

Spreiter, J. R., and B. R. Briggs, Theoretical determination of the form of the boundary of the solar corpuscular stream produced by interaction with the magnetic dipole field of the earth, J. Geophys. Res., 67, 37, 1962.

Spreiter, J. R., and B. J. Hyett, The effect of a uniform external pressure on the boundary of the geomagnetic field in a steady solar wind, J. Geophys. Res., 68, 1631, 1963.

Spreiter, J. R., and W. P. Jones, On the effect of a weak interplanetary magnetic field on the interaction between the solar wind and the geomagnetic field, J. Geophys. Res., 68, 3555, 1963.

Spreiter, J. R., A. L. Summers, and A. Y. Alksne, Hydromagnetic flow around the magnetosphere, Planetary Space Sci., 14, 223, 1966.

Stolov, H. L., Polar cap ionospheric response to solar cosmic ray events observed by Mariners 2 and 4, Proceedings Cospar Symposium on Solar Flares and Space Research, North-Holland, Amsterdam, 310, 1969.

Stormer, C., The Polar Aurora, Oxford University Press (Clarendon), London and New York, 1955.

Sugiura, M., Evidence of low-frequency hydromagnetic waves in the exosphere, J. Geophys. Res., 66, 4087, 1961.

Sugiura, M., and C. R. Wilson, Oscillation of the geomagnetic field lines and associated magnetic perturbations at conjugate points, J. Geophys. Res., 69, 1211, 1964.

Talwar, S. P.,Hydromagnetic stability of the magnetospheric boundary, J. Geophys. Res., 69, 2707, 1964.

Talwar, S. P., Kelvin-Helmholtz instability in an anisotropic plasma, Phys. Fluids, 8, 1295, 1965.

Van Allen, J. A., The geomagnetically trapped corpuscular radiation, J. Geophys. Res., 64, 1683, 1959.

Veldkamp, J., A giant geomagnetic pulsation, J. Atmos. Terr. Phys., 17, 320, 1960.

Volland, H., and J. Taubenheim, On the ionospheric current system of the geomagnetic solar flare effect (SFE), J. Atmos. Terr. Phys., 12, 258, 1958.

Walters, G. K., Effect of oblique interplanetary magnetic field on the shape and behavior of the magnetosphere, J. Geophys. Res., 69, 1769, 1964.

Wilcox, J. M., On a possible north-south asymmetry in the solar wind, Irish Astron. Soc., 7, 82, 1965.

Wilcox, J. M., The interplanetary magnetic field, Solar origin and terrestrial effects, Sp. Sci. Reviews, 8, 258, 1968.

Wilcox, J. M., and D. S. Colburn, Interplanetary sector structure in the rising portion of the sunspot cycle, J. Geophys. Res., 74, 2388, 1969.

Wilcox, J. M., and N. Ness, Solar source of the interplanetary sector structure, Solar Phys., 1. 437, 1967.

Wilcox, J. M., and N. F. Ness, Quasi-Stationary corotating structure in the interplanetary medium, J. Geophys. Res., 70, 5793, 1965.

Wilcox, J. M., K. H. Schatten, and N. F. Ness, Influence of interplanetary magnetic field and plasma on geomagnetic activity during quiet-sun conditions, J. Geophys. Res., 72, 19, 1967.

Williams, D. J., On the low-altitude trapped electron boundary collapse during magnetic storms, J. Geophys. Res., 72, 1644, 1967.

Williams, D. J., and C. O. Bostrom, Proton entry into the magnetosphere on May 26, 1967, J. Geophys. Res., 74, 3019, 1969.

Williams, D. J., and G. D. Mead, editors, Magnetospheric Physics, Proceedings of the symposium on the physics of the magnetosphere, Washington D. C., Sept. 3-13, American Geophysical Union, Washington, D. C., 1969.

Wilson, C. R., Conjugate three-dimensional polarization of high-latitude micropulsations from a hydromagnetic wave-ionospheric current model, J. Geophys. Res., 71, 3233, 1966.

Wilson, C. R., and M. Sugiura, Hydromagnetic interpretation of s.c.'s of magnetic storms, J. Geophys. Res., 66, 4097, 1961.

Wolfe, J. H., R. W. Silva, and M. A. Myers, Observations of the solar wind during the flight of IMP I, J. Geophys. Res. 71, 1319,1966a.

Wolfe, J. H., R. W. Silva, D. D. McKibbin, and R. H. Matson, The compositional, anisotropic and nonradial flow characteristics of the solar wind, J. Geophys. Res., 71, 3329, 1966b.

Wolfe, J. H., and D. D. McKibben, Pioneer 6 observations of a steady-state magnetosheath, Planetary Space Sci., 16, 953, 1968.

Wurm, K., Die Naturder Kometen, Mitteilungen Hamb. Sternw. in Bergedorf, 8, 57, 1943.

Zhigulev, V. N., and E. A. Romishevskii, Concerning the interaction of currents flowing in a conducting medium with the earth's magnetic field, Soviet Phys. "Doklady," 4, 859, 1960.

AUTOBIOGRAPHICAL STATEMENT

I was born and raised in New York City. I went to Iona College in New Rochelle on a scholarship and received the B.S. degree in physics in 1961. From there I went to the University of Pittsburgh on a teaching assistantship to do graduate work in physics. While there, I built a spark chamber for double scattering experiments at the cyclotron laboratory as a graduate research assistant. I received the M.S. degree in 1964 with a thesis entitled, "The Construction of a Thin Foil Spark Chamber." I entered the Ph.D. program in physics at The City College of the City University of New York in 1964. Since then I have held teaching and research assistantships in the Department of Physics at The City College. I have also held positions as adjunct instructor in physics at St. Peter's College in Jersey City and instructor in physics at Iona College. I am married and have a 3 year old son.